ETH zürich

ETH Library

Spatial characteristics of gridded Swiss temperature trends: local and large-scale influences

Master Thesis

Author(s):
Ceppi, Paulo

Publication date:
2009

Permanent link:
https://doi.org/10.3929/ethz-a-005989800

Rights / license:
In Copyright - Non-Commercial Use Permitted

This page was generated automatically upon download from the ETH Zurich Research Collection.
For more information, please consult the Terms of use.

Schweizerische Eidgenossenschaft
Confédération suisse
Confederazione Svizzera
Confederaziun svizra

Swiss Confederation

Federal Department of Home Affairs FDHA
Federal Office of Meteorology and Climatology
MeteoSwiss

ETH
Eidgenössische Technische Hochschule Zürich
Swiss Federal Institute of Technology Zurich

IAC*ETH*
Institute for Atmospheric and Climate Science

Master Thesis

Spatial characteristics of gridded Swiss temperature trends: local and large-scale influences

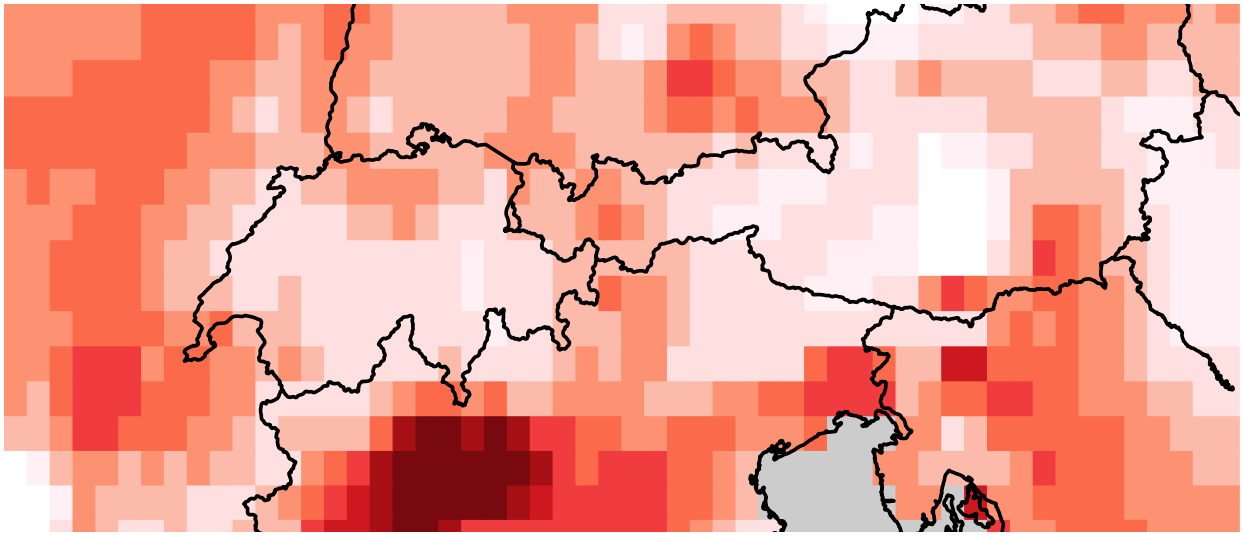

Submitted by

Paulo Ceppi

Supervised by

PD Dr. Christof Appenzeller
Dr. Simon C. Scherrer

December 2009

Abstract

Temperature is an essential variable in monitoring the impact of global climate change. Here we perform a detailed regional trend analysis of Swiss Alpine temperatures in the period 1959 to 2008 using a newly available gridded data set based on homogenised observations from 91 MeteoSwiss stations. The aim is to quantify possible large-scale and local-scale contributions to the local trends. It is shown that the yearly trends are all positive and highly significant, with an average warming rate of 0.35 °C/decade, consistent with results from earlier studies. The values show fairly little spatial variability, with 90% of all gridpoint trends between 0.30 and 0.39 °C/decade. This indicates that the warming in Switzerland has exceeded the NH extratropical mean trend by a factor of 1.6 over the last 50 years.

On a seasonal scale, the analysis also reveals overall positive temperature trends, but seasonal and spatial variability are pronounced. The weakest trends (mostly insignificant at the 5% level) are observed in autumn (SON, 0.17 °C/decade on average) and early summer features the strongest warming rates, peaking at 0.48 °C/decade in May-June-July. A pronounced altitude dependence is found from late summer to early winter (ASO to NDJ), where the trends decrease with elevation.

We investigate the impact of large-scale versus local-scale influences on seasonally-averaged temperatures using a regression model with atmospheric circulation patterns and northern hemispheric temperatures as explanatory variables. The analysis reveals that 45 (summer) to 80% (winter) of the interannual variability of Swiss gridpoint temperatures can be explained by large-scale influences. In spring, summer and autumn, a fraction of up to 20% of the temperature trends remains unexplained by the model. In spring, a positive trend anomaly close to the zero-degree isotherm is not detected by our model, while the largest unexplained trend magnitudes are found at low elevations in autumn and winter.

Our results suggest that snow-albedo feedback effects might be responsible for the unexplained 10% higher spring trends near the altitude of the zero degree isotherm and snow line. In autumn, the observed decrease in mist and fog frequency may be a key process explaining the 20% higher Swiss autumn temperature trends at low elevations. Changes in soil-atmosphere interactions could explain part of the difference between observed and modelled trends in summer. For the unexplained lower than modelled temperature trends in late winter at low altitudes the physical mechanisms remain to be determined.

Contents

1 Introduction **1**
- 1.1 Motivation . . . 1
- 1.2 Goals and structure of this thesis . . . 2

2 Data **5**
- 2.1 Swiss temperature data . . . 5
- 2.2 Northern hemispheric temperatures and geopotential height . . . 5
- 2.3 Snow depth data . . . 6

3 Methods **7**
- 3.1 Gridding . . . 7
- 3.2 Linear regression . . . 8
- 3.3 Trend analysis . . . 10
- 3.4 Principal component analysis . . . 10
- 3.5 Data fitting . . . 12

4 Temperature trends in Switzerland **15**
- 4.1 Yearly trends . . . 15
- 4.2 Seasonal trends . . . 15

5 Regression analysis of Swiss gridded temperatures **19**
- 5.1 Northern hemispheric warming corrected trends . . . 19
- 5.2 Regression model . . . 20
- 5.3 Influence of northern hemispheric temperatures . . . 22
- 5.4 Influence of large-scale circulation patterns . . . 22
- 5.5 Adjusted coefficient of determination . . . 26
- 5.6 Constructed temperature series . . . 26

6 Altitude dependence of temperature trends **31**
- 6.1 Vertical trend profiles . . . 31
- 6.2 Vertical trend anomalies . . . 33

7 Discussion **37**
- 7.1 Yearly and seasonal temperature trends . . . 37
  - 7.1.1 Magnitude of the trends . . . 37
  - 7.1.2 Spatial and temporal variability . . . 37
  - 7.1.3 Limitations of our analysis . . . 37
- 7.2 Regression analysis . . . 38
  - 7.2.1 Explanatory power of the regression model . . . 38
  - 7.2.2 Implications of the results . . . 39
  - 7.2.3 Overfitting . . . 39

7.3 Interpretation of the differences between NH warming corrected and constructed temperatures 40
7.4 Altitude dependence of temperature trends 41

8 Conclusions and recommendations for further research 43
8.1 Conclusions 43
8.2 Recommendations for further research 44

Bibliography 47

A Stations used in the gridding procedure 53

B Atmospheric circulation patterns and estimated temperature anomalies 57

C Time series of 500 hPa geopotential height PC scores 69

List of Figures

1.1 Time series of yearly temperature anomalies 1864-2008 (°C) with respect to the 1961-1990 reference period, averaged over 12 MeteoSwiss stations and based on homogenised data. Red and blue colors indicate positive and negative anomalies, respectively. The black line denotes the estimated linear trend. 2

1.2 Temperature trends (°C/decade) at Swiss stations in winter, spring, summer and autumn, based on seasonally-averaged homogenised temperatures. The stations are represented by red circles, with circle areas being proportional to the trend magnitude. Open circles denote insignificant trends at the 5% significance level. 3

2.1 *Left*: Histogram of the altitudinal distribution of gridpoints (grey) and stations (brown). The dark grey and brown horizontal bars denote the mean altitudes of gridpoints and stations, respectively. *Right*: Swiss topography and main geographical areas: Jura (about 10% of land area), Plateau (30%) and Alps (60%). Altitudes are given in meters above sea level. Open black circles denote temperature measurement stations which were used for gridding. The topography data was derived from a high-resolution (1/120°) global digital elevation map by nearest neighbour interpolation. 6

3.1 Gridded monthly temperature anomalies (°C) in March 2008 (left) and February 2009 (right). 8

3.2 Visualisation of the influence region of a fictitious, localised anomaly (arbitrary units) with four different values of the lambda parameter (see text). The anomaly is centered on a mountain peak (upper row) or in a valley (lower row). From Frei et al. (unpublished material). 8

3.3 PC loading patterns of seasonally-averaged 500 hPa geopotential height fields, multiplied by one standard deviation (m). The cumulative explained variance fraction is shown in the top right corner of each figure. From top to bottom: MAM, JJA, SON, DJF. 13

4.1 Swiss yearly temperature trends 1959-2008 (°C/decade). The open black circles represent the 91 measurement stations used for calculation of gridded temperature maps. All trends are highly significant. 16

4.2 Spatially-averaged yearly temperature anomalies from gridpoints (solid lines) and 12 representative MeteoSwiss stations (dashed lines). The values are yearly anomalies 1959-2008 (°C). The straight lines denote the trends estimated by linear regression. 17

4.3 Swiss seasonal temperature trends 1959-2008 (°C/decade). Hatched areas represent non-significant trends at the 5% level. 18

5.1 As in Fig. 4.3, but corrected for NH mean warming. See text for details. . . . 21
5.2 Anomalies of corrected gridpoint temperatures (in °C) corresponding to a positive anomaly of corrected NH temperatures by one standard deviation (0.52 °C). . . . 23
5.3 *Top*: PC loadings of 500 hPa seasonally-averaged geopotential height fields, multiplied by one standard deviation (m). The cumulative explained variance fraction (cf. Section 3.4) is given in the top right corner of each figure. *Bottom*: associated temperature anomalies for January-February-March (°C). Gridpoints where a particular PC was not kept in the model are represented in grey. . . . 24
5.4 Time series of the first 10 PCs of 500 hPa geopotential height fields over the North Atlantic and Europe. The dashed lines denote the estimated trends. Significant trends at the 5% level are marked in red. For other seasons, see Appendix C. . . . 25
5.5 Adjusted R-squared of the multiple linear regression model. . . . 26
5.6 Constructed temperature trends (°C/decade). Hatched areas represent non-significant trends at the 5% level. . . . 28
5.7 Difference between NH warming corrected and constructed trends (°C/decade). Note that the colour scale is different than in Fig. 5.6. . . . 29
5.8 Time series of spatially-averaged constructed temperature anomalies (°C). The NH warming corrected time series is represented by a dashed line. The brown line denotes the estimated linear trend function. Note that both corrected and constructed temperatures have the same linear trend. . . . 30

6.1 Vertical profiles of seasonal temperature trends. The grey dots denote the magnitude of observed, corrected temperature trends at individual gridpoints, while the vertical black curves represent LOESS fits of the corrected (solid) and constructed (dashed) trends. The thin horizontal black curves are estimated density distributions of the trends for 6 height classes of 500 m each (alternating grey and white bands). The zero-trend line is represented by a thin vertical grey line. . . . 32
6.2 Representation of the vertical trend anomalies in JJA. See text for more details. 33
6.3 Vertical trend anomalies of observed trends in °C/decade. The solid black lines denote estimated temperature isotherms, while the dashed grey lines represent isolines of 5, 30 and 100 cm snow depth. . . . 35
6.4 Vertical trend anomalies of constructed trends in °C/decade. See Fig. 6.3 for details. . . . 35
6.5 Vertical anomalies of trend differences (corrected minus constructed trends) in °C/decade. Note the slightly modified colour scale compared to Fig. 6.3. . 36

7.1 Histograms of the distribution of yearly trend magnitudes at gridpoints (grey bars) and 54 stations with full time series (brown shaded bars). The vertical bars denote the mean trend magnitudes for gridpoints and stations (dark grey and brown, respectively). . . . 38

A.1 Stations used in the gridding procedure. The numbers refer to Table A.1 below. 53

B.1 *Top*: PC loadings of 500 hPa seasonally-averaged geopotential height fields, multiplied by one standard deviation (m). *Bottom*: associated temperature anomalies in February-March-April (°C). Gridpoints where a particular PC was not kept in the model are represented in grey. See also Fig. 5.3. . . . 58
B.2 As in Fig. B.1 for MAM. . . . 59

B.3 As in Fig. B.1 for AMJ. 60
B.4 As in Fig. B.1 for MJJ. 61
B.5 As in Fig. B.1 for JJA. 62
B.6 As in Fig. B.1 for JAS. 63
B.7 As in Fig. B.1 for ASO. 64
B.8 As in Fig. B.1 for SON. 65
B.9 As in Fig. B.1 for OND. 66
B.10 As in Fig. B.1 for NDJ. 67
B.11 As in Fig. B.1 for DJF. 68

C.1 Time series of the first 10 PCs of 500 hPa geopotential height fields over the North Atlantic and Europe. The dashed lines denote the estimated trends. Significant trends at the 5% level are marked in red. See also Fig. 5.4. 69
C.2 As in Fig. C.1. 70
C.3 As in Fig. C.1. 71
C.4 As in Fig. C.1. 72
C.5 As in Fig. C.1. 73
C.6 As in Fig. C.1. 74

Chapter 1

Introduction

1.1 Motivation

During the 20th century, the effects of global warming have been observed worldwide in the form of positive temperature trends. On the global scale, mean surface temperatures have increased by 0.74 °C during the last century, while climate models predict even faster warming rates for the next decades. This increase in mean temperatures is expected to have substantial ecological, economic and societal impacts, and these effects will not be homogeneous across the globe; it is believed that coastal, mountain and high-latitude regions will be amongst the most affected areas (IPCC, 2007a).

The attribution of local warming trends to global climate change is made difficult by the large number of physical processes responsible for temperature variability. Recent European warming may have been driven by changes in a number of physical parameters, such as incoming shortwave radiation (Wild et al., 2005; Philipona et al., 2009), soil moisture (Fischer et al., 2007), fog occurrence frequency (Vautard et al., 2009) and atmospheric circulation patterns (Corti et al., 1999; van Oldenborgh et al., 2009a; Vautard and Yiou, 2009). The representation of such processes in current state-of-the-art global and regional climate models is still inaccurate, which leads to important discrepancies between model-based and observed trends (van Oldenborgh et al., 2009a) and will likely affect the prediction of future regional warming trends.

The physical processes described above are also likely to have an impact on the spatial distribution of surface temperature trends. This point, however, is still subject to much debate. In particular, the vertical dependence of tropospheric temperature trends is still uncertain. While most reanalyses and model predictions indicate an increase of warming effects with altitude in the mid-latitude lower to middle troposphere (see Fig. 10.7 in IPCC, 2007c, p. 765), studies based on observations yield less clear results, sometimes in contradiction with model-based analyses (e.g. Bradley et al., 2004; Pepin and Seidel, 2005; Appenzeller et al., 2008; Grant et al., 2008).

Many physical mechanisms can lead to an altitude dependence of temperature trends. It is widely accepted that specific weather patterns have different impacts on the vertical temperature distribution (lapse rate); this is particularly true for mid- and high-latitude continental regions during the cold season, where cold air pooling (settling of cold air near the surface under a temperature inversion) is a common phenomenon under given meteorological conditions (Hegerl and Wallace, 2002; Clements et al., 2003). Thus, changes in the frequency distribution of circulation patterns that impact mean lapse rates might lead to an altitude-dependent warming or cooling. Another important physical process involved in the altitude dependence of temperature trends (though mainly close to the surface) is the snow-albedo feedback. It has been speculated that observed decreases in snow pack in many mid-latitude

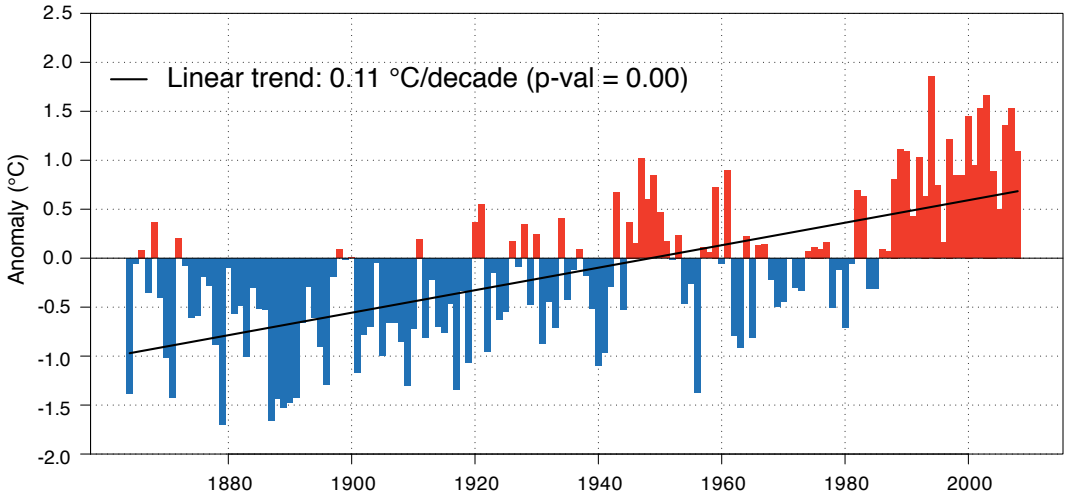

Figure 1.1: Time series of yearly temperature anomalies 1864-2008 (°C) with respect to the 1961-1990 reference period, averaged over 12 MeteoSwiss stations and based on homogenised data. Red and blue colors indicate positive and negative anomalies, respectively. The black line denotes the estimated linear trend.

mountain regions (e.g., the Alps, Himalayas) might induce a stronger atmospheric warming at elevations where the occurrence of a closed snow cover has diminished (Giorgi et al., 1997; Pepin and Lundquist, 2008).

In Switzerland, significant temperature trends have been observed over the last decades (Fig. 1.1), and the warming has occurred faster than on global average[1]. While the linear trend analysis reveals a mean warming rate (averaged over 12 Swiss stations) of 0.11 °C/decade since 1864, warming rates have not been constant in space and time. Indeed, an analysis of the seasonal trends at individual stations over the last 50 years reveals that the warming has been fastest in summer and slowest in autumn (Fig. 1.2), and regional differences in trend magnitude can also be observed[2]. This raises the question whether such spatial variations reflect an altitude dependence of the temperature trends.

Because the impact of an increase in mean temperatures is expected to be particularly strong in mountainous regions (see e.g. Frei et al., 2007; Houghton et al., 2001; Haeberli and Beniston, 1998), knowledge of the magnitude and elevation dependence of warming effects is vital for an Alpine country like Switzerland. Furthermore, a detailed understanding of the mechanisms controlling temperature trends is essential for the accuracy of future warming projections. This illustrates the importance of understanding the physical mechanisms that control warming rates on a regional scale.

1.2 Goals and structure of this thesis

The main goals of this thesis can be described as follows:

- quantify Swiss temperature trends on yearly and seasonal time scales over the last 50 years in high spatial resolution;

[1] See also `http://www.meteoschweiz.admin.ch/web/en/climate/climate_today/temperature_trends.html`.
[2] A detailed representation of temperature trends at MeteoSwiss stations can be found on `http://www.meteoschweiz.admin.ch/web/en/climate/climate_today/trends_from_stations.html`.

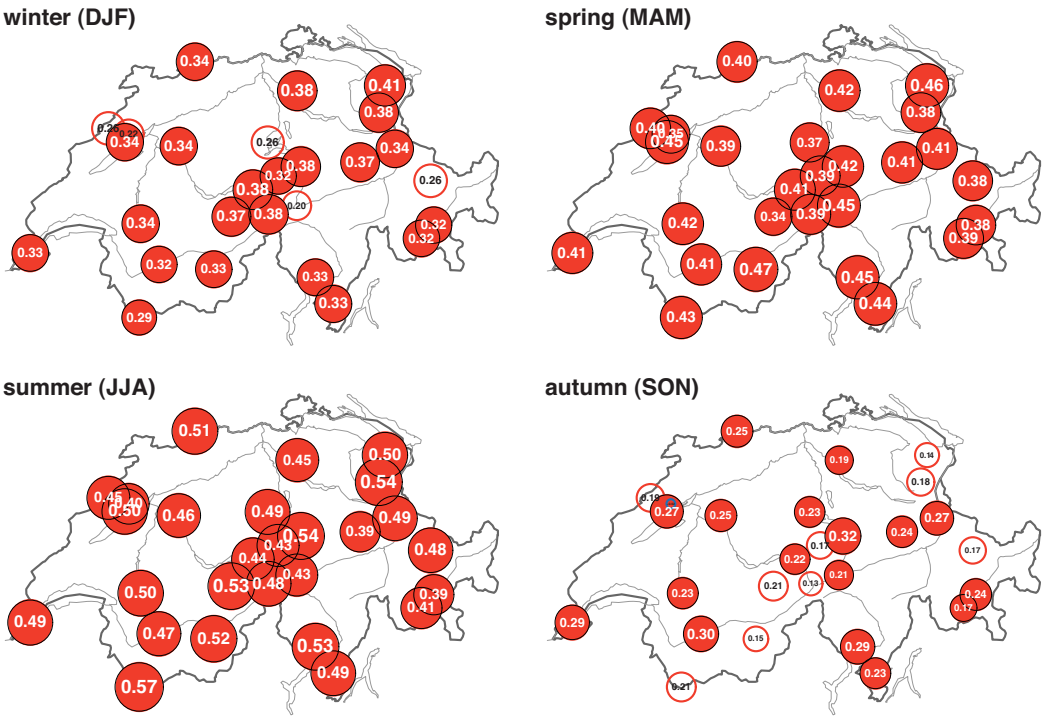

Figure 1.2: Temperature trends (°C/decade) at Swiss stations in winter, spring, summer and autumn, based on seasonally-averaged homogenised temperatures. The stations are represented by red circles, with circle areas being proportional to the trend magnitude. Open circles denote insignificant trends at the 5% significance level.

- identify possible physical large-scale and local mechanisms that control the trends, and attempt to quantify their impact;
- determine and explain the altitude dependence of the trends.

The core of our analysis consists in performing an estimation of Swiss temperature trends by using gridded data based on measurements from the MeteoSwiss observing network. This provides a data set of seasonal and yearly trends in high spatial resolution, which we use for the remaining analyses. To reach our second goal, we design a model which enables us to discriminate between large-scale and local influences on temperature trends. Finally, based on the previous results, we investigate the altitude dependence of our estimated trends, and attempt to identify relevant physical processes to explain the vertical structure of the trends.

The thesis is structured as follows: the data and the analysis methods are introduced in Chapters 2 and 3, respectively. The remainder of the thesis is divided into two parts. The following chapters contain the results of our work. In Chapter 4, we present the trend analysis in yearly and seasonal resolution. Since one of our goals is to understand what processes may have an influence on the trends, we first study the impact of large-scale weather patterns (Chapter 5). For this purpose, we perform a principal component analysis of 500 hPa geopotential height fields to identify the main circulation patterns over the North Atlantic and Europe. We then analyse the relationship between the circulation patterns and the gridded seasonal temperature anomalies by means of regression analysis. Based on these results, we investigate the altitude dependence of the trends in Chapter 6. In Chapter 7, our results are discussed, before concluding in Chapter 8 with a summary of our key results and some recommendations for further research.

Chapter 2

Data

The data for Switzerland (temperature and snow depth values) were obtained from the MeteoSwiss measurement network. Unless otherwise stated, the time period considered is always 1959-2008 and the data are in monthly resolution.

2.1 Swiss temperature data

We used a new gridded data set of monthly temperature anomalies over Switzerland. Gridding was performed using homogenised monthly data from 91 stations evenly distributed across Switzerland and situated at heights ranging from 203 to 3580 masl (Fig. 2.1). At each station, the anomalies were calculated with respect to the 1961-1990 reference period. These data have been carefully homogenised (Begert et al., 2005) and are thus adequate for statistical analysis. Note that 37 of the 91 temperature series used for gridding are not complete, i.e. the number of stations effectively used in the computation of monthly gridded temperature anomalies fluctuates and is always smaller than 91. Details on the stations used in the gridding procedure are given in Appendix A, Table A.1. The calculation method and characteristics of the gridded temperature data set are described in the Methods section below.

Furthermore, homogenised station-based temperature series from the MeteoSwiss measurement network were also used to calculate mean yearly anomalies and to estimate mean seasonal vertical temperature profiles (Section 3.5). The yearly temperature anomalies were calculated from a set of 12 representative MeteoSwiss stations with complete time series from 1959 to 2008, and were compared with the spatially-averaged gridded temperatures (Section 4.1). The 12 stations, which were also used in the gridding procedure, are represented in red bold typeface in Table A.1.

In the left panel of Fig. 2.1 we also compare the altitudinal distributions of gridpoints and stations. Since a large number of stations are situated in densely populated low-altitude regions such as the Swiss Plateau, the mean altitude of stations is lower than the average gridpoint elevation. The implications of this on the results of the trend analysis will be further discussed in Section 7.1.3.

2.2 Northern hemispheric temperatures and geopotential height

To estimate the influence of large-scale dynamics on the spatial characteristics of temperature trends, we considered spatially-averaged northern hemispheric (NH) temperature anomalies. (Only extratropical regions [23°-90°N] were included in the spatial averages.) The data

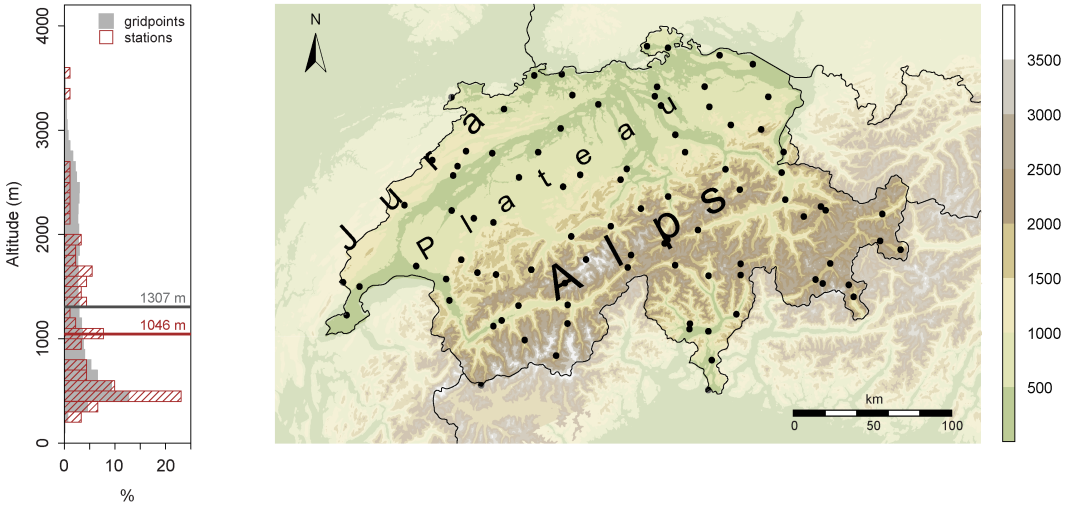

Figure 2.1: *Left*: Histogram of the altitudinal distribution of gridpoints (grey) and stations (brown). The dark grey and brown horizontal bars denote the mean altitudes of gridpoints and stations, respectively. *Right*: Swiss topography and main geographical areas: Jura (about 10% of land area), Plateau (30%) and Alps (60%). Altitudes are given in meters above sea level. Open black circles denote temperature measurement stations which were used for gridding. The topography data was derived from a high-resolution (1/120°) global digital elevation map by nearest neighbour interpolation.

were calculated from the HadCRUT3v[1] data set of combined land-sea monthly temperature anomalies on a $5 \times 5°$ grid, developed by the Climate Research Unit (CRU) of the University of East Anglia together with the Hadley Center of the UK Met Office (Brohan et al., 2006; Rayner et al., 2003, 2006).

We investigated the impact of atmospheric circulation patterns on Swiss temperatures by using principal components of seasonally-averaged 500 hPa geopotential height fields over the North Atlantic and Europe (80°W-60°E, 30°-80°N). The geopotential height data in monthly resolution were obtained from NCEP/NCAR reanalyses[2] (Kalnay et al., 1996).

2.3 Snow depth data

The snow depth data set included daily measurements from 420 stations from the observational networks of MeteoSwiss and of the Institute for Snow and Avalanche Research (SLF). Such series have been checked for quality and used for statistical analyses by Laternser (2002), Scherrer et al. (2004) and Scherrer and Appenzeller (2006). We only used series which were at least 10 years long. The snow depth observations were utilised to estimate vertical snow depth profiles (Section 3.5).

[1]URL: `http://www.cru.uea.ac.uk/cru/data/temperature/`, data downloaded on 18 August 2009
[2]URL: `ftp://ftp.cdc.noaa.gov/Datasets/ncep.reanalysis.derived/pressure/hgt.mon.mean.nc`, downloaded on 27 October 2009

Chapter 3

Methods

All calculations described in this section were performed using R, an open-source system for statistical computation and graphics (R Development Core Team, 2009).

3.1 Gridding

An innovative temperature gridding method has been developed at MeteoSwiss recently (C. Frei, unpublished material). The procedure takes into account the properties of the spatial distribution of temperature anomalies. As an example, temperature anomalies are typically highly dependent on altitude during winter months, because of cold air pools which may be present even in the interior of Alpine valleys. Such phenomena may lead to complicated spatial patterns, which often reflect the complex Swiss topography (cf. Fig. 2.1, right panel). The gridding technique applied here is able to reproduce such small-scale patterns.

Thanks to the relatively high spatial density of the MeteoSwiss measurement network, enough data are available to obtain accurate representations of the spatial distribution of temperatures. In particular, altitude-dependent anomalies can be rendered realistically, which is crucial for our study since we intend to analyse the height dependence of temperature trends. The gridding procedure yields a data set in a spatial resolution of $1/48^\circ$, which corresponds to a gridbox size of 2×2 km approximately, with 241 gridpoints in W-E direction and 103 gridpoints in N-S direction.

Two examples of gridded monthly temperature data are provided in Fig. 3.1. These illustrate how the gridding method is able to reproduce topography-related patterns in the temperature distribution; differences between the northern and the southern side of the Alps are also rendered realistically.

The computation of gridded monthly temperature anomalies involves several steps. First, a mean vertical temperature profile is fitted using all stations available in the data set. The residuals, corresponding to the differences between the station values and the fitted profile, are spatially interpolated onto a grid using a special weighting technique (see below), which yields a residual field. Finally, the gridpoint temperature anomalies are obtained from adding the temperature field estimated from the vertical profile to the residual field.

The weighting method used to calculate the residual field consists in estimating a distance parameter which we call *climatological distance*. The climatological distance measures how "climatologically close" two points are from each other, weighting the euclidean distance between that pair of points with a penalty that depends on the nature of the topography. The higher the topographical obstacle between two points or the longer the way to circumvent it, the larger the climatological distance will be. Thus, two points located in neighbouring valleys may be climatologically distant from each other, because a high mountain range needs to be passed over or circumvented to go from one point to the other.

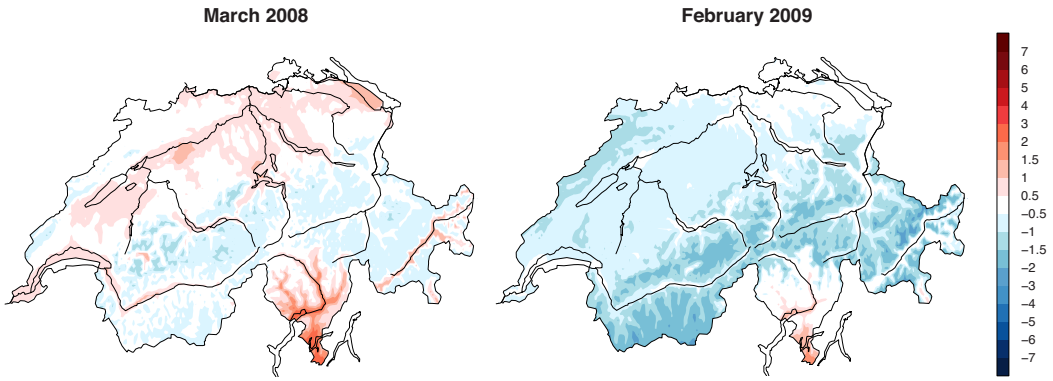

Figure 3.1: Gridded monthly temperature anomalies (°C) in March 2008 (left) and February 2009 (right).

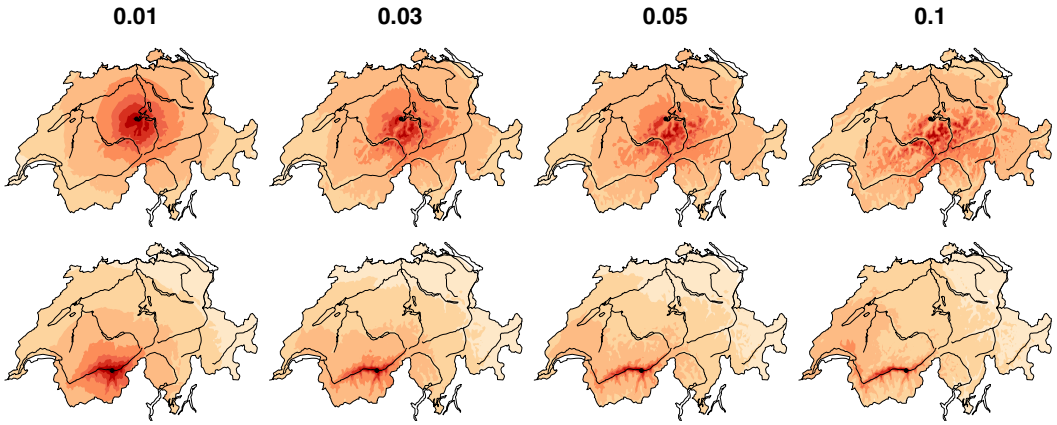

Figure 3.2: Visualisation of the influence region of a fictitious, localised anomaly (arbitrary units) with four different values of the lambda parameter (see text). The anomaly is centered on a mountain peak (upper row) or in a valley (lower row). From Frei et al. (unpublished material).

The impact of topography on the climatological distance can be regulated with a parameter called lambda. The effect of different values of the lambda parameter on the spatial interpolation is shown in Fig. 3.2. Two different topographical settings are represented, illustrating how the anomalies are gridded depending on topography. It can be seen that higher values of the lambda parameter induce patterns induce increasingly altitude-dependent climatological distances.

Note that the values of the lambda parameter are determined for each month separately (i.e. every month has another lambda value) using a cross-validation procedure to account for seasonal differences in the altitudinal temperature distribution.

3.2 Linear regression

Linear regression is a statistical analysis method that consists in modeling the relationship between one dependent and several independent (explanatory) variables. In this work, linear regression is used in two ways: first, to determine the magnitude of temperature trends by applying trend analysis methods; and second, to investigate to what extent temperature

trends can be explained by trends in other physical parameters coupled with temperature. Such parameters may include e.g. large-scale circulation patterns, or local processes such as relative sunshine duration or snow pack.

The theoretical foundations of linear regression are extensively covered in most statistical analysis handbooks (see e.g. Wilks, 2005; von Storch and Zwiers, 1999). Here we will restrict ourselves to a general description of the concepts and assumptions relevant to this study.

A linear regression model describes a linear relationship between a dependent and one or more independent variables. This can be expressed as

$$y_i = \beta_0 + \beta_1 x_{i1} + ... + \beta_p x_{ip} + \epsilon_i, \qquad i = 1, ..., n \tag{3.1}$$

where y_i is a dependent variable and $[x_{i1}, ..., x_{ip}]$ a vector of p independent variables. The indices n and p denote the number of observations and the number of independent variables, respectively. A model with several independent variables ($p > 1$) is called a *multiple* regression model; otherwise it is said to be *simple*. The $\beta = [\beta_0, ..., \beta_p]$ vector contains the regression coefficients, while ϵ_i describes the random error. In matrix notation, 3.1 can be written as

$$y = \mathbf{X}\beta + \epsilon$$

with $\mathbf{X}$ being a $n \times p$ matrix. The purpose of linear regression is to estimate the β coefficients, which measure the strength of the linear relationship between the independent and the dependent variables. The most common method for estimating the regression coefficients is called *ordinary least squares* and consists in minimising the sum of squared errors (SS_{err}):

$$SS_{err} = \epsilon^T \epsilon = (y - \mathbf{X}\beta)^T (y - \mathbf{X}\beta)$$

The value of β for which SS_{err} is smallest is the least squares estimator of the regression coefficient vector. It can be shown that in case of normally distributed error terms ϵ_i, ordinary least squares yields the maximum likelihood estimator of the regression coefficients.

The so-called *coefficient of determination*, R^2, measures the fraction of variance in the dependent variable y that can be explained by variations in the independent variables. It is defined as

$$R^2 = \frac{SS_{reg}}{SS_{tot}}$$

where $SS_{tot} = \frac{1}{n} y^T y$ represents the total sum of squares, and $SS_{reg} = 1 - SS_{err}$ is the regression sum of squares.

In multiple regression models, the value of R^2 can only grow if additional variables are taken into the model. For this reason, a corrected version of the coefficient of determination is often used to account for the number of explanatory variables in the model. The *adjusted R-squared* parameter

$$\bar{R}^2 = 1 - (1 - R^2)\frac{n - 1}{n - p - 1}$$

increases only if the new term improves the model more than would be expected by chance.

When setting up a multiple regression model, it is often important to know which variables are relevant to the relationship described by the model. A common way to select an appropriate set of variables is *stepwise regression*. This procedure involves applying a selection algorithm to a pre-defined set of variables, where the variables are tested for relevance using a goodness-of-fit criterion; a common choice (which we adopt here) is the *Akaike Information Criterion*, or AIC. The variables are chosen so that the value of the goodness-of-fit criterion is optimised.

Linear regression models are based on a series of assumptions. First, the relationship between dependent and independent variables should be linear. Second, the error terms should

be independent (uncorrelated), have constant variance and be normally distributed. Therefore, regression analysis always involves testing these assumptions and, if necessary, making changes to the model so that the assumptions are no longer violated (e.g. by performing data transformations before usage in the model).

3.3 Trend analysis

The analysis of trends in time series involves two steps: the calculation of the trend magnitude and the estimation of the trend significance.

The magnitude of the trend can be calculated following several methods. In this thesis we assume all trends to be linear and use simple linear regression (see Section 3.2 above) to estimate the rate of change of temperature with time. A model of the form

$$T(x, y, t) = T_0(x, y) + \beta(x, y)t + \epsilon(x, y, t), \qquad \epsilon(x, y, t) \sim N(0, \sigma^2)$$

describes the temporal change in temperature at a point $[x, y]$. The trend estimator is the regression coefficient β, which can be approximated with ordinary least squares.

Estimation of trend significance requires performing a statistical test. Here we use the Mann-Kendall trend test (Mann, 1945; Kendall, 1975), which tests the existence of a monotonic (not necessarily linear) trend. The null hypothesis H_0: "the time series values are independent, identically distributed" is tested against the alternative hypothesis H_A: "there is a monotonic trend". We consider trends to be statistically significant if the p-value of the null hypothesis H_0 is smaller than 0.05.

A common problem in trend analysis is serial correlation, which affects the results of the analysis in two ways: by decreasing the accuracy of the trend estimate, and by artificially increasing the significance (and thus the detection rate) of trends (Yue et al., 2002; Kulkarni and von Storch, 1995). One method to overcome this problem has been proposed by Wang and Swail (2001). It consists in correcting the time series for serial correlation (so-called "pre-whitening" procedure) as given by

$$x'_i = \frac{(x_i - r_1 x_{i-1})}{1 - r_1}$$

where x_i (x'_i) represents the ith data point in the (pre-whitened) time series and r_1 denotes the lag-1 autocorrelation. Since time series with trends are intrinsically autocorrelated, pre-whitening must be applied iteratively in order to discriminate between the contributions of the trend and of trend residuals to the autocorrelation. Details on the procedure are given in Wang and Swail (2001). Trend analysis can be applied to the pre-whitened (uncorrelated) time series, which yields a more accurate estimation of the trend than that based on the original series. Trend significance, however, is reduced, because the pre-whitened series has a larger residual variance than the original one.

To estimate the temperature trends, we performed trend analyses of both raw and pre-whitened temperature series. We found the results to be similar in magnitude, with significance being, as expected, slightly lower for the pre-whitened series. Since the magnitude of the trends did not seem to be affected by serial correlation, we will present and analyse in the following chapters only the results based on the original temperature series.

3.4 Principal component analysis

Principal component analysis (PCA) is a statistical method used in the analysis of large multivariate data sets. In simple words, PCA aims at extracting relevant information from large data sets and at revealing the main variation patterns of the data. This is done by

operating a coordinate system transformation, so that the first dimension describes as much variability as possible in the data, and each succeeding dimension accounts for as much of the remaining variability as possible. PCA was first applied in the context of climate research by Lorenz (1956).

Mathematically, the procedure consists in performing an eigenvalue decomposition of the variance matrix of the data. Here we present a calculation procedure based on von Storch and Zwiers (1999) and Wilks (2005). A more detailed description of the mathematical foundations of PCA and of its use in the context of climate science can also be obtained from Preisendorfer (1988).

We consider a data matrix $\mathbf{X_0}$, containing n variable vectors $x_1, ..., x_n$ as columns. This data matrix can be centred by subtracting the multivariate mean $\mathbf{M}$ from it, yielding a centred data matrix $\mathbf{X} = \mathbf{X_0} - \mathbf{M}$. Let $\mathbf{S} = var(\mathbf{X})$ represent the symmetric, positive semi-definite variance matrix, with $\dim(\mathbf{S}) = (n \times n)$. Then there must be n positive real numbers $\{\lambda_1, \lambda_2, ..., \lambda_n\}$ and n orthogonal vectors $\{e_1, e_2, ..., e_n\}$ of dimensions $(n \times 1)$ and of unit length, such that

$$\mathbf{S}e_k = \lambda_k e_k$$

The vectors $\{e_1, ..., e_n\}$ are the eigenvectors and the scalars $\{\lambda_1, ..., \lambda_n\}$ represent the eigenvalues of the matrix $\mathbf{S}$. The eigenvectors can be considered as an alternative orthonormal coordinate system with which the data can be described. The variance of the data along each of the eigenvectors is represented by the corresponding eigenvalues. The eigenvectors and eigenvalues are sorted in order of decreasing eigenvalue, ensuring that the first dimensions explain most of the variability of the data. Arranging the eigenvectors column-wise, we obtain a $(n \times n)$ eigenvector matrix $\mathbf{E}$, with which the coordinates of the data points can be transformed from one coordinate system to another. The projection of the data matrix $\mathbf{X}$ onto the new coordinate system is given by

$$\mathbf{Y} = \mathbf{E} \cdot \mathbf{X}$$

where the $(n \times n)$ matrix $\mathbf{Y}$, called the *score matrix*, represents the transformation of the data matrix $\mathbf{X}$ in the new coordinate system. The scores are the individual columns of the matrix $\mathbf{Y}$. The columns of the eigenvector matrix $\mathbf{E}$, which describe the new coordinate system, are also called *loadings*. (Note, however, that different nomenclatures are used in the literature; in climate research, PC loadings are often called empirical orthogonal functions [EOFs], while scores can be referred to as EOF coefficients.)

The coordinate transformation operated by PCA makes it possible to reduce the dimensionality of the data set. Indeed, the new coordinates are chosen so that most of the variability of the data can be explained by the first few dimensions. Thus, higher dimensions can be dropped with minimal loss of information. Since the eigenvalues describe the variance explained by each corresponding eigenvector, the total variance explained by the first l dimensions (the *cumulative explained variance fraction*) can be expressed as

$$CEVF_l = \frac{\sum_i^l \lambda_i}{\sigma_{tot}^2}$$

PCA is often used to reveal the dominant modes of variability of the data. From this viewpoint, the loadings can be interpreted as the patterns of these modes, whereas the scores describe the amplitude of the modes for each sample. One interesting property of PCA is that the modes are orthogonal and mutually uncorrelated. This makes the results of PCA particularly appropriate for further statistical analysis, for example by using the time series of the scores as explanatory variables in a linear regression model (cf. Section 3.2).

Principal components of 500 hPa geopotential height fields

In order to identify the main atmospheric circulation patterns relevant to the North Atlantic and European regions, we performed a PCA of 500 hPa geopotential height fields (cf. Section 2.2). The circulation patterns found by PCA are represented by the loadings of the geopotential height fields, while the scores indicate the magnitude (or amplitude) of the geopotential height perturbations described by the loadings. Since the scores can be negative, the patterns of the loadings can also be inverted. Thus, the loadings only describe *modes of variability* of geopotential height fields.

Figure 3.3 shows the loadings of the first 10 PCs of 500 hPa geopotential height in four seasons representative of the yearly cycle (MAM, JJA, SON, DJF). The cumulative explained variance fraction is also represented. The results for the eight other seasons are shown in Fig. 5.3 and Appendix B.

The seasonal variations in the amplitude of geopotential height perturbations are clearly visible from Fig. 3.3. The anomalies are strongest in winter and weakest in summer, reflecting the fact that the atmospheric flow is stronger in winter, whereas in summer flows tend to be weaker because of small pressure gradients over northern hemispheric regions (Hartmann, 1994). Also, the fraction of explained variance features a yearly cycle: while in DJF the first 10 (4) PCs explain 96% (81%) of the total variance, in JJA this value sinks to 89% (64%). This means that the natural variability of atmospheric circulation patterns can be better represented in winter than in other seasons.

Analysing the characteristics of the circulation patterns, we note that the first three to five PCs correspond to common, well-understood circulation patterns, while the remaining ones describe less typical perturbations of the mean state. The first PC always characterises a north-south geopotential height dipole similar to the North Atlantic Oscillation pattern (Hurrell, 1995; Scherrer et al., 2006), quantifying the intensity of the westerly flow over the North Atlantic and Europe. In winter, the PCs two to four describe other patterns known from the literature as European Blocking, East Atlantic pattern and Scandinavian patterns, respectively (Scherrer et al., 2006). In spring and autumn, similar patterns can also be recognised, albeit in a weaker form and in different order. As for summer, the patterns are so weak that it is difficult to classify them into any known categories.

In general, we believe that the geopotential height anomaly patterns found by PCA provide a realistic description of circulation patterns occurring in the atmosphere. One of our purposes in this thesis will be to estimate the influence of the individual flow patterns on Swiss temperatures by regression analysis (Chapter 5).

3.5 Data fitting

LOESS (locally weighted scatterplot smoothing)

LOESS is a method of fitting a smooth curve through a set of data points. This procedure, described extensively in Cleveland et al. (1992), is based on polynomial regression of degree two, with the least-squares fit being calculated locally. This means that at each point x of the data set, a quadratic fit is made using points in the neighbourhood of x, weighted by their distance from x. Since no function needs to be specified to fit a LOESS curve to the data, the method is particularly appropriate for modelling complex data sets where no theoretical models are known.

In this thesis, we use LOESS fits to model the vertical structure of temperature trends (see Chapter 6). For an example of an application in the context of climatology, see Scherrer and Appenzeller (2010).

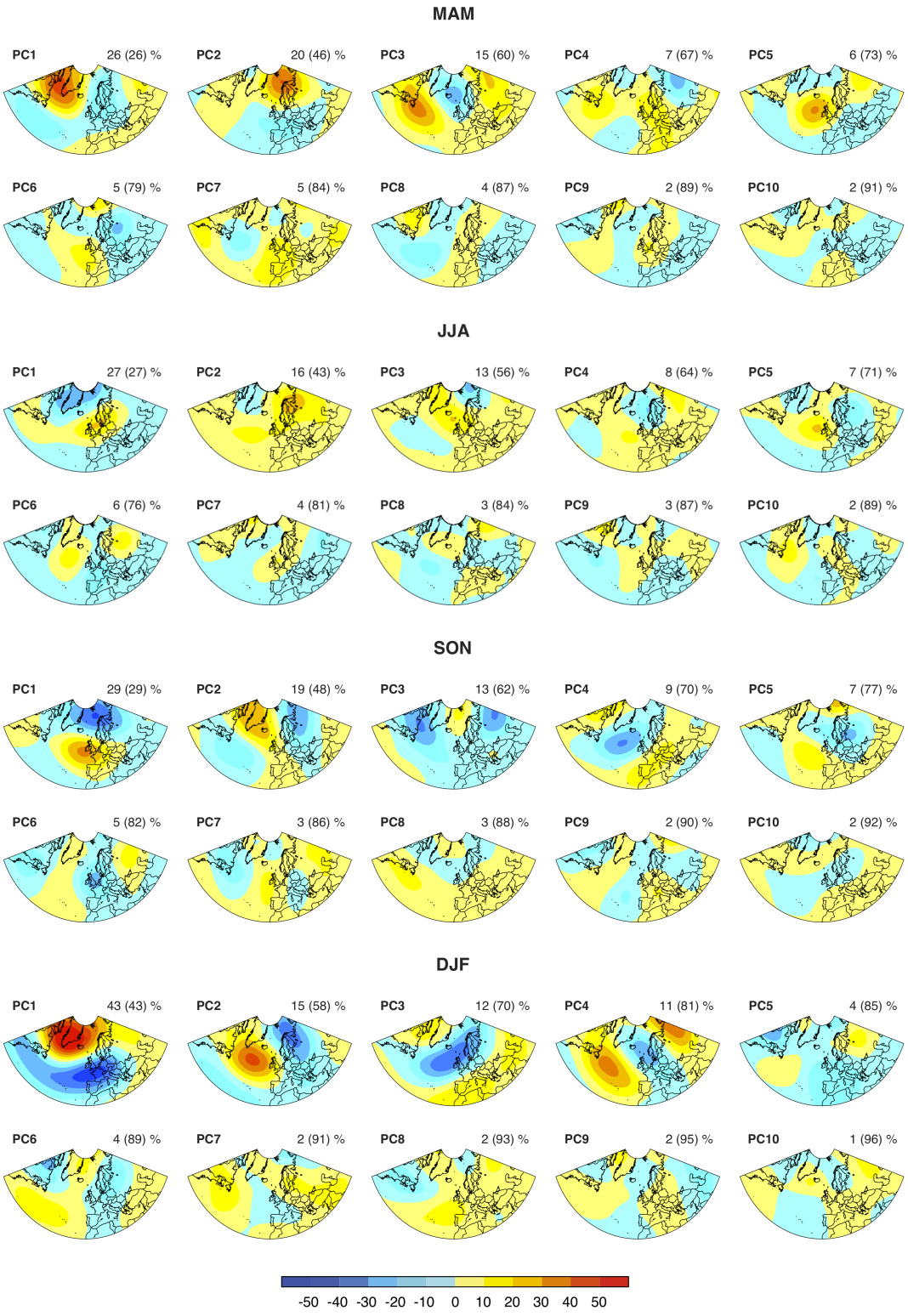

Figure 3.3: PC loading patterns of seasonally-averaged 500 hPa geopotential height fields, multiplied by one standard deviation (m). The cumulative explained variance fraction is shown in the top right corner of each figure. From top to bottom: MAM, JJA, SON, DJF.

Vertical profiles of temperature and snowpack

We estimated altitudinal profiles of mean seasonal temperature and snow cover, which we used in the analysis of the altitude dependence of the temperature trends. Since snow cover typically does not increase linearly with height, the snowpack profiles were calculated by fitting square root functions to the station-based snow depth measurements (see Section 2.3). This analysis was performed for the months October to May. In summer months, stations from the SLF network provide no data, and the number of MeteoSwiss stations reporting median snow values different from zero was too little to calculate representative snow profiles. As for mean seasonal temperatures, we approximated their altitude dependence by linear functions.

To assess the quality of the fits and the accuracy of the estimated vertical profiles, we checked the fits visually by comparing them to the data clouds. We found the vertical profiles to reproduce well the altitude dependence of mean temperatures and snowpack (not shown). Temperature and snow depth contour lines (see e.g. Fig. 6.3) were calculated from these profiles.

Chapter 4

Temperature trends in Switzerland

4.1 Yearly trends

We performed trend analyses at every gridpoint in different temporal resolutions: monthly, seasonal and yearly. The yearly trends are represented in Fig. 4.1. The extreme values are 0.23 and 0.44 °C/decade, while 90% of the values are comprised between 0.3 and 0.39 °C/decade (cf. discussion in Section 7.1 and Fig. 7.1).

Thus, on a yearly scale, temperatures have been rising quite similarly over all of Switzerland; the spatial variability is relatively small. In particular, no notable differences can be seen between the northern and southern side of the Alps, despite the different weather regimes induced by the mountain range.

Furthermore, the trends seem to be slightly weaker in the mountains than in other regions, especially over the Jura mountains and in pre-Alpine regions. The altitude dependence of the trends will be analysed in more detail in Chapter 6.

All trends are very highly significant, the p-values of the test being smaller than $5 \cdot 10^{-4}$ at every gridpoint.

Averaging the values spatially, we obtain a mean Swiss trend of 0.35 °C/decade. This means that mean yearly Swiss temperatures have increased by 1.75 °C over the study period (1959-2008). The spatially-averaged time series of Swiss yearly temperature anomalies is represented in Fig. 4.2, along with mean yearly temperature anomalies from 12 representative MeteoSwiss stations (cf. Section 2.1). Both time series are very similar and highly correlated (0.99), and show the same positive trend of 0.35 °C/decade. This indicates that on a yearly scale, the spatially-averaged gridded temperature anomalies are highly representative of mean Swiss temperatures.

4.2 Seasonal trends

The estimation of seasonal trends involved calculating seasonally-averaged gridpoint temperature anomalies. For this purpose, 12 overlapping three-month seasons were defined (JFM, FMA, MAM, AMJ, MJJ, JJA, JAS, ASO, SON, OND, NDJ, DJF). Note that the seasons NDJ and DJF cover the years x and $x+1$; we thus obtain seasonal time series of length 50, except for the two seasons NDJ and DJF which only have 49 elements.

Several comments can be made from the graphical representation of the seasonal trends (Fig. 4.3). First, the trends are positive in all seasons and at nearly every gridpoint. Nevertheless, there are considerable seasonal variations in trend magnitude, with trends being clearly weakest in autumn (SON: 0.02 to 0.38 °C/decade, mean value: 0.17 °C/decade) and strongest in late spring to early summer (JJA: 0.34 to 0.62 °C/decade, mean: 0.46

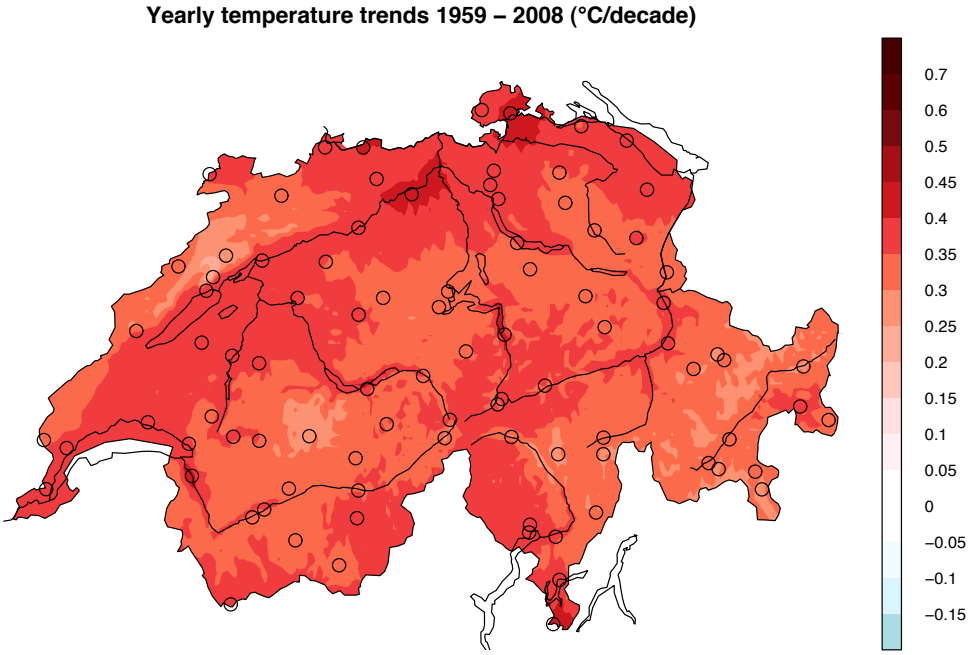

Figure 4.1: Swiss yearly temperature trends 1959-2008 (°C/decade). The open black circles represent the 91 measurement stations used for calculation of gridded temperature maps. All trends are highly significant.

°C/decade). Non-significant trends (hatched regions in Fig. 4.3) are found mainly in autumn and in winter. Note that because of the large interannual temperature variability, statistical significance is more difficult to reach in winter than in other seasons.

Second, contrary to the yearly trends, in seasonal resolution many spatial trend patterns can be observed. In particular, some of the seasons feature altitude-dependent trends, especially from late summer to early winter (roughly ASO to NDJ), where the trends seem to decrease with altitude. Other seasons also feature some patterns in the spatial distribution of trends, but it is difficult to relate such patterns to altitude effects, at least with this kind of representation.

Our results are in good agreement with findings from previous studies on Swiss temperature trends (Begert et al., 2005). Rebetez and Reinhard (2007), who analysed the trends at 12 Swiss stations over the 30-year period 1975-2004, also observed stronger trends in spring and summer than in autumn and winter. A slight tendency toward faster warming at low altitudes was present in the results of Rebetez and Reinhard (2007) and Appenzeller et al. (2008) for autumn.

The representation of the seasonal trends in Fig. 4.3 demonstrates how accurately our gridding method is able to reproduce temperature anomalies related to small-scale topographic features. In autumn seasons (ASO, SON, OND), the altitude dependence of the trends is rendered very realistically in regions of complex topography such as Alpine valleys. This will enable us to perform a detailed study of the altitude dependence of Swiss temperature trends in the remainder of this thesis.

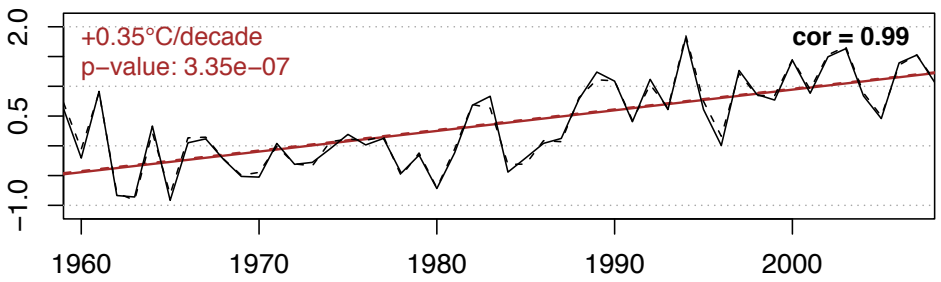

Figure 4.2: Spatially-averaged yearly temperature anomalies from gridpoints (solid lines) and 12 representative MeteoSwiss stations (dashed lines). The values are yearly anomalies 1959-2008 (°C). The straight lines denote the trends estimated by linear regression.

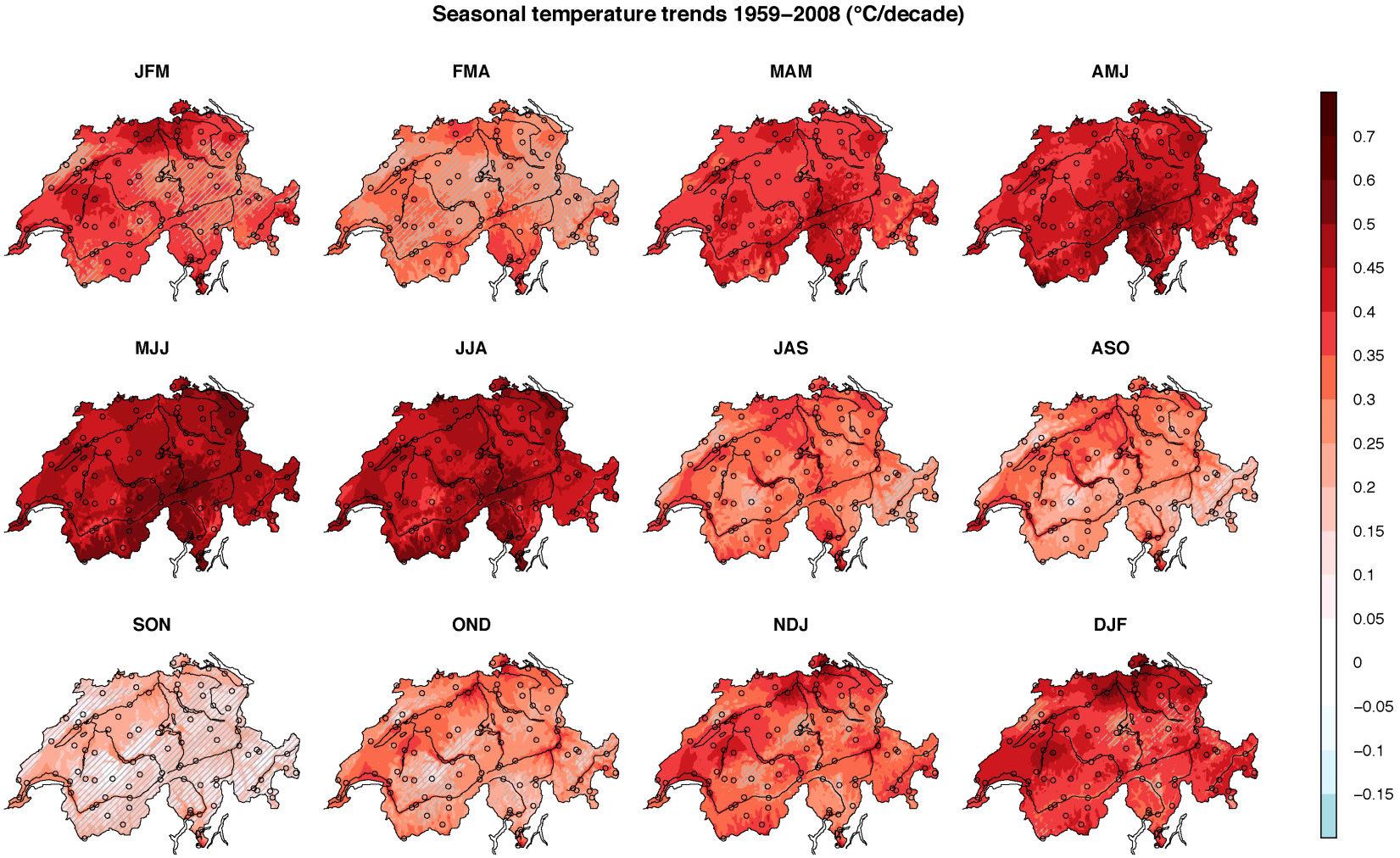

Figure 4.3: Swiss seasonal temperature trends 1959-2008 (°C/decade). Hatched areas represent non-significant trends at the 5% level.

Chapter 5

Regression analysis of Swiss gridded temperatures

5.1 Northern hemispheric warming corrected trends

Summarising the results of our trend analysis of Swiss temperatures, we can make two important remarks. First, we found that Swiss temperature trends are subject to considerable seasonal variability (see Section 4.2). Second, we observed spatial patterns which are partly due to altitudinal differences in the temperature trends.

These observations raise the question of which physical processes might explain the seasonal changes and/or the altitude effects. Many factors are known to have an influence on temperatures; examples include changes in the frequency of particular circulation patterns (Vautard and Yiou, 2009; van Oldenborgh and van Ulden, 2003), trends in incoming radiation (due to changes in cloudiness or visibility; see e.g. Philipona et al., 2009; Vautard et al., 2009), or any kind of climate feedback effect. An example of a process that might be important on a limited temporal and spatial scale is the snow-albedo feedback (Giorgi et al., 1997; Pepin and Lundquist, 2008), which could play a role in mountain regions in spring and autumn, i.e. in the time window where snow cover is most likely to disappear in case of higher temperatures.

In the remainder of this study, we attempt to identify the processes that may have an impact on the magnitude and altitude dependence of the trends. This implies that the direct effects of global warming and of local processes must be considered separately. For this purpose, we decompose the observed gridpoint temperature trends into an "external" warming forcing, modelled by the NH temperature trend, and a local warming component. By doing this, we assume the two trend components to be purely additive. Since we are only interested in understanding the local contribution, we eliminate the external forcing on local temperatures by removing the mean NH warming trend from the monthly gridpoint temperature series. The obtained trend term

$$\frac{dT}{dt}_{corr} = \frac{dT}{dt}_{obs} - \frac{dT}{dt}_{NH\ mean}$$

can be described as a NH warming corrected temperature trend. In the following and for the sake of simplicity, the observed, warming-corrected trends will be always referred to as *corrected trends*, and the corresponding temperature time series will be described as *corrected temperature anomalies*.

In Fig. 5.1 we represent the corrected seasonal temperature trends. One can see that in spite of the correction, the seasonal trends are generally positive, confirming that the temperature trends observed in Switzerland are stronger than the NH mean trends. In

autumn, the corrected trends are almost inexistent in mountain regions and slightly positive in the lowlands. Generally, the corrected trends are statistically insignificant, except in summer. Note that the spatial patterns of the corrected trends are exactly the same as in Fig. 4.3, since the same NH mean trend was removed at each gridpoint. In other words, only the magnitude of the trends has been modified, not their spatial distribution.

5.2 Regression model

Assuming that the corrected seasonal trends result from physical processes such as those described above, we attempt to identify the important processes and to quantify their impact on the temperature trends. For this purpose, we perform a regression analysis of the corrected temperature anomalies (for details on the gridded temperature anomaly data, see Section 2.1).

We design a regression model to explain the corrected temperature anomalies with principal components (PCs) of geopotential height at 500 hPa and with anomalies of warming-corrected NH temperatures. The model takes the form

$$T_{corr}(x,y,t) = \beta_0(x,y)\, T_{NH,\ corr}(t) + \sum_{i=1}^{10} \beta_i(x,y)\, PC_i(t) + \epsilon(x,y,t) \tag{5.1}$$

Similar approaches of quantifying the dependence of temperatures on other variables by regression analysis can be found in the literature (e.g. van den Besselaar et al., 2009; Junge and Stephenson, 2003; Linderson, 2001).

In order to ensure that only those flow patterns which have an influence on temperatures in Switzerland are represented in the model, we select the relevant PCs by stepwise regression (see Section 3.2). The stepwise algorithm may include any combination of the 10 first PCs. We limit the maximum number of PCs to 10 because this is a good compromise between two requirements. On the one hand, enough PCs should be included so that all circulation patterns that have an influence on temperatures are considered; on the other hand, however, high-order PCs often describe complex patterns which are difficult to interpret and are not representative of common, physically sensible circulation patterns. In addition, limiting the maximum number of PCs is necessary to prevent the model from being overfit (see discussion in Section 7.2).

The analysis was conducted for each season separately, with seasonally-averaged values. The time series of the gridpoint and NH temperature anomalies were corrected in such a way that $T_{NH,\ corr}$ has no trend. This step is important, as the non-corrected NH temperature series is strongly correlated with Swiss temperatures because of the positive trends. By considering *corrected* NH temperatures, we take into account the effect of large-scale temperature anomalies on Swiss temperatures *relative to the mean NH trend* only.

In our model, the corrected NH temperatures represent a large-scale, external forcing on the gridpoint temperatures, summarising a series of factors that can hardly be assessed individually (SSTs, changes in solar activity, impact of volcanic eruptions, and other unknown processes). The remaining explanatory variables are the time series of the first 10 PC scores of 500 hPa geopotential height fields over the North Atlantic and Europe (see Section 2.2 for more details). They are a representation of the atmospheric circulation, and quantify the frequency of occurrence and the intensity of particular weather patterns. Note that the time series of the PCs of geopotential height were not corrected for trends, i.e. any possible trends in the large-scale circulation patterns remain in the model.

Our approach consists in determining how much of the Swiss temperature variability and trends can be explained by the variables in our model (i.e., essentially by atmospheric flow changes). NH temperatures are also part of our model because they may explain part of the

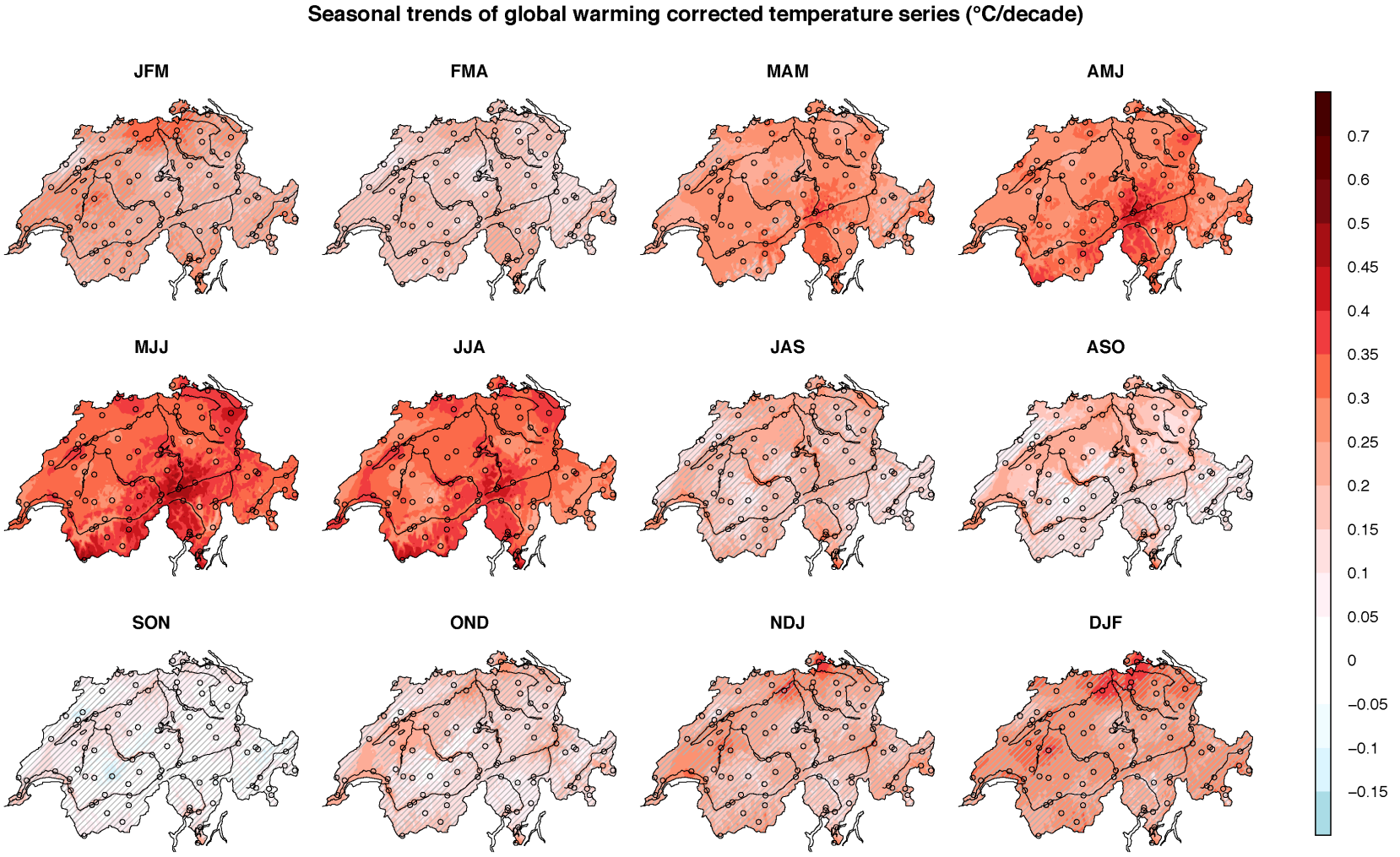

Figure 5.1: As in Fig. 4.3, but corrected for NH mean warming. See text for details.

seasonal variability of Swiss temperatures, but since they have been detrended, we do not expect them to make a significant contribution to Swiss temperature trends in this model.

Other factors than the large-scale dynamics may also affect temperature trends in Switzerland. Ideally, we would include in our regression model all potentially important processes, since our purpose is to estimate the impact of all factors relevant to temperature trends. However, many phenomena are very difficult to quantify with index variables, either because of a lack of measurements, or because the effect of a particular process is difficult to isolate. Moreover, the processes are often correlated with each other; incoming radiation, for example, is directly influenced by the occurrence of given circulation patterns which affect cloudiness. Therefore, we first assess the influence of the large-scale processes, and try then to estimate the local effects from the unexplained part.

We thus include in our regression model only variables quantifying large-scale influences, without considering any local factors; our aim is then to determine to what extent the magnitude and the altitude dependence of the trends can be explained by changes in the occurrence frequency of particular circulation patterns. By a process of exclusion, we consider the part of the corrected trends that remains unexplained by our model as being induced by local processes other than the atmospheric circulation patterns.

In the following, we describe the results of the regression analysis by describing the estimated influences of the NH temperatures and of the circulation patterns on the gridpoint temperatures.

5.3 Influence of northern hemispheric temperatures

The anomalies of the corrected gridpoint temperatures corresponding to a positive anomaly of corrected NH temperatures by one standard deviation are shown in Fig. 5.2. The values are derived from the calculated regression coefficients of corrected NH temperatures (Eq. 5.1). Note that since we are considering a multiple regression model, Fig. 5.2 represents the impact of NH mean temperatures on gridpoint temperatures given all other variables included in the model.

We deduce from the results that the warming-corrected NH temperatures have indeed an influence on gridpoint-scale temperatures in Switzerland, since all anomalies are positive or close to zero. However, while there are variations from one season to another, it is difficult to distinguish a clear seasonal cycle in the results. We also observe complex spatial patterns which cannot be easily interpreted from a physical standpoint. In particular, the patterns do not seem to be related to altitude.

The accurate estimation of the influence of corrected NH temperatures by the regression model is likely to be hindered by the low signal-to-noise ratio in the relationship with corrected gridpoint temperatures. Nevertheless, the results still give qualitative evidence that Swiss seasonal temperatures are influenced by external forcings (represented by the corrected NH temperatures).

5.4 Influence of large-scale circulation patterns

Understanding the temperature anomalies induced by specific circulation patterns requires visualising the corresponding geopotential height distributions. In Fig. 5.3, the loadings of the first 10 PCs of 500 hPa geopotential height fields are represented together with the corresponding temperature anomalies over Switzerland. Here we only show the results for JFM as an example; however, the analysis was performed similarly for the 11 other seasons and the results are shown in Appendix B.

The characteristics of the circulation patterns found by PCA were described in detail in Section 3.4. Here we merely analyse the temperature anomalies and their relationship to

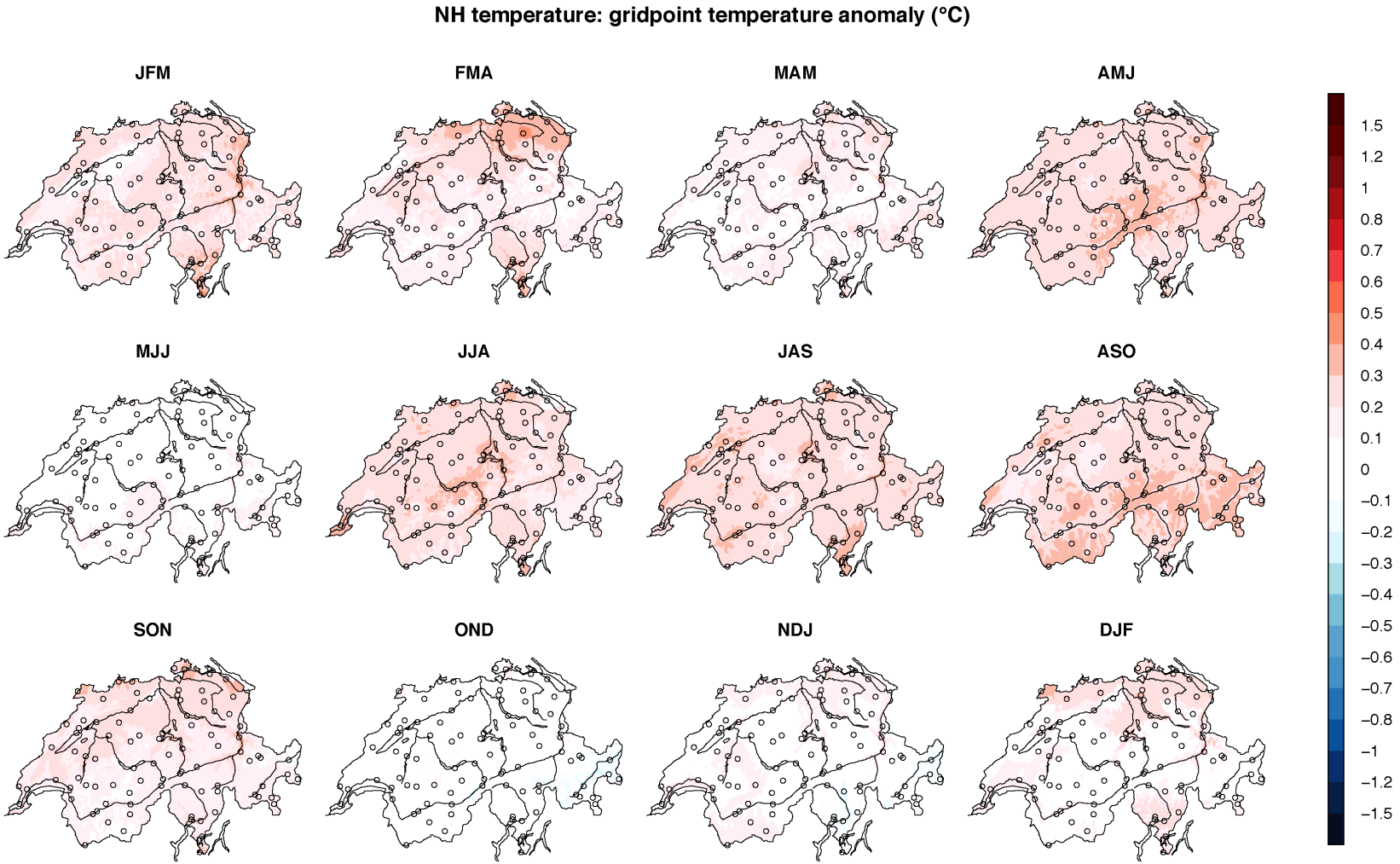

Figure 5.2: Anomalies of corrected gridpoint temperatures (in °C) corresponding to a positive anomaly of corrected NH temperatures by one standard deviation (0.52 °C).

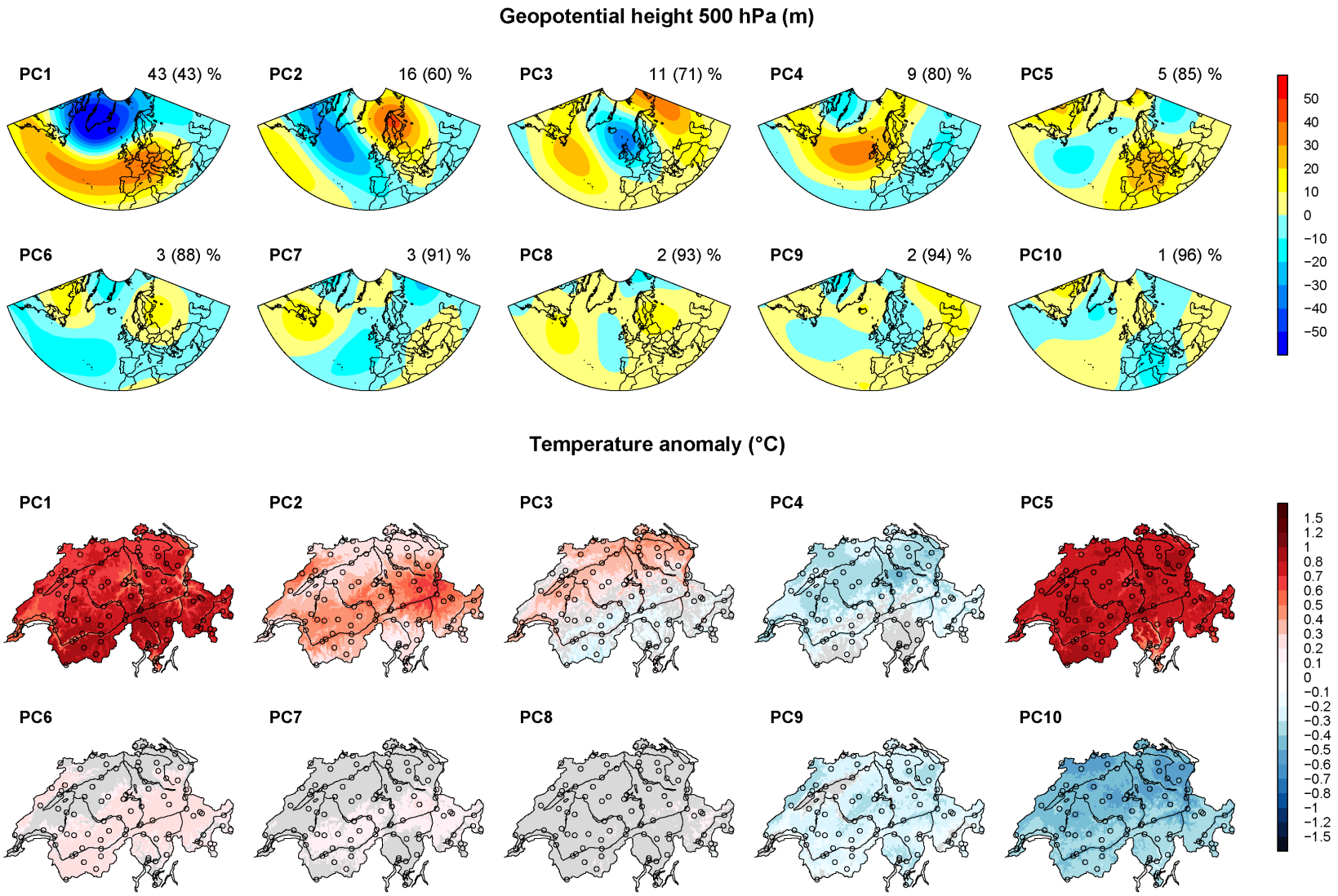

Figure 5.3: *Top*: PC loadings of 500 hPa seasonally-averaged geopotential height fields, multiplied by one standard deviation (m). The cumulative explained variance fraction (cf. Section 3.4) is given in the top right corner of each figure. *Bottom*: associated temperature anomalies for January-February-March (°C). Gridpoints where a particular PC was not kept in the model are represented in grey.

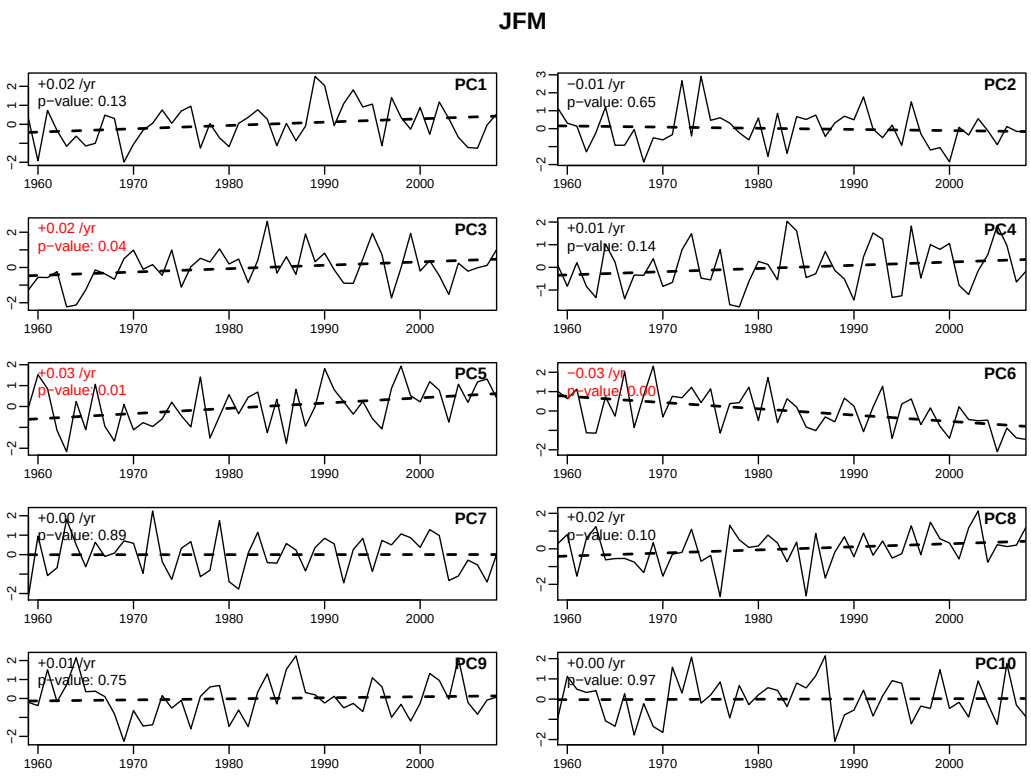

Figure 5.4: Time series of the first 10 PCs of 500 hPa geopotential height fields over the North Atlantic and Europe. The dashed lines denote the estimated trends. Significant trends at the 5% level are marked in red. For other seasons, see Appendix C.

the circulation patterns.

Considering the flow patterns, the corresponding estimated temperature anomalies make sense from a physical perspective in all cases. For instance, the first PC, which describes a mild southwesterly flow over Central Europe (NAO-like pattern), is associated with strong positive temperature anomalies (Hurrell, 1995). Given the season, this is exactly what one would expect from such a flow pattern. Often, circulation patterns which one would not expect to have a clear effect on temperatures (from a visual estimation) are excluded from the model by the stepwise selection process. In general, at each gridpoint, about five to eight PCs are kept in the model (Fig. 5.3 and Appendix B).

A careful examination of the spatial distribution of the temperature anomalies reveals that some circulation patterns induce altitude-dependent effects. In some cases, the anomalies have opposite signs at low and high altitudes (see e.g. PC3 in Fig. 5.3). This implies that temporal changes in the frequency of occurrence of particular weather patterns could lead to altitudinal differences in temperature trends. To assess the importance of trends in circulation patterns, we represent in Fig. 5.4 the time series of the first 10 geopotential height PC scores from Fig. 5.3 (for other seasons, see Appendix C).

One can see that several PCs feature trends, some of which are significant. In particular, the first PC, which describes an NAO-like pattern and explains over 40% of the winter-time interannual temperature variability, shows a trend toward a stronger North-South geopotential height dipole (i.e., increasing NAO indices) in NDJ, DJF and JFM. However, the trend is significant in DJF only. Previous studies on North Atlantic and European circulation

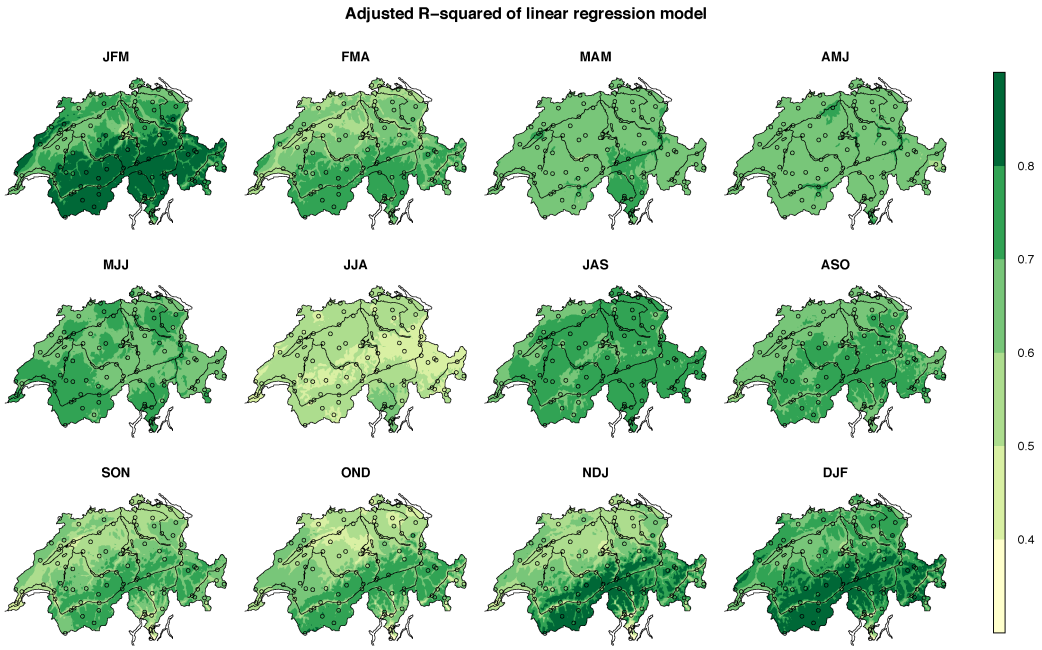

Figure 5.5: Adjusted R-squared of the multiple linear regression model.

patterns have also shown a tendency toward higher NAO indices during the last decades, even though lower indices have been observed in recent years (Hurrell et al., 2003; Raible et al., 2005). In agreement with those studies, our analysis indicates that stronger westerlies over the European region lead to higher winter-time temperatures, especially in mountain regions (Figs. 5.3 and B.1). Nevertheless, other PCs also show trends, some of which have opposite effects on Swiss temperatures. Because of this, an assessment of the net impact of trends in circulation patterns on Swiss temperatures is particularly difficult, and would go beyond the scope of this thesis.

It is interesting to note that some temperature anomaly patterns are clearly altitude-dependent in autumn and winter seasons. The altitudinal effects that can be explained by our model are discussed in detail in Chapter 6.

5.5 Adjusted coefficient of determination

An indication of the fraction of variance that the model is able to explain is given by the adjusted coefficient of determination $\overline{R}^2$ (Section 3.2). The values displayed in Fig. 5.5 are relatively high, generally ranging between 0.45 and 0.8. The highest values are found in high-altitude Alpine regions in winter seasons. The distribution of the $\overline{R}^2$ values features an altitude dependence in winter, indicating that temperature anomalies are more difficult to predict in the lowlands with the large-scale dynamics variables we use in our model, as found in earlier studies (Beniston and Rebetez, 1996). This aspect will be discussed in Section 7.2.

5.6 Constructed temperature series

From the results of the regression analysis, it is possible to generate a modelled time series of temperature anomalies at each gridpoint. Such time series, which we call *constructed*

temperature anomalies, are calculated for each season using the relationship

$$T_{constr}(x,y,t) = \hat{\beta}_0(x,y)\, T_{NH,\ corr}(t) + \sum_{i=1}^{10} \hat{\beta}_i(x,y)\, PC_i(t) \tag{5.2}$$

which is very similar to (5.1), except that the unknown error term is not considered here. The $\hat{\beta}_i$ terms denote the estimated regression coefficients. The variables which were not kept in the model by the stepwise selection process (Section 5.2) have a coefficient of zero. Applying this formula, we obtain 12 seasonal time series at every gridpoint, which are an approximation of the observed, corrected temperature anomalies.

The constructed time series can be subjected to a trend analysis, following the procedure described in Section 3.3. The spatial distribution of these constructed trends (Fig. 5.6) should be compared to that of the observed, corrected trends (Fig. 5.1), since we are interested in determining what part of the trends can be reproduced by our regression model including only large-scale dynamical influences. To facilitate the comparison, a plot of the differences in the trends (calculated as NH warming corrected minus constructed trends, i.e. $\frac{dT}{dt}_{diff} = \frac{dT}{dt}_{corr} - \frac{dT}{dt}_{constr}$) is shown in Fig. 5.7.

In general, the magnitude of the constructed trends is fairly accurate, and the seasonal variations in trend magnitude are very similar to those found in the observations. The time series of the spatially-averaged constructed trends, shown in Fig. 5.8, reveals that the corrected temperature anomalies are well reproduced on a yearly scale. The correlation between spatially-averaged corrected and constructed trends is high (0.90) and the trends are identical (0.21 °C/decade). Considering the spatial distribution of the trends, however, we see somewhat less variability in the constructed trends than in the observed ones (Figs. 5.1 and 5.6). This means that our regression model is not always able to render the spatial distribution of the trends in its full complexity.

Considering the trend differences (Fig. 5.7), we find three main patterns of differences. In summer (mainly MJJ, JJA), the differences are positive all over Switzerland, which means that the trends are underestimated by the model. In autumn (SON, OND, NDJ), the model also underestimates the trends, but mainly in the Swiss Plateau. Here the difference patterns are clearly altitude-dependent. Finally, in late winter to early spring (JFM, FMA), the anomaly has the opposite sign: the constructed trends are stronger than the corrected ones at low elevations, and the effect is restricted to the Swiss Plateau.

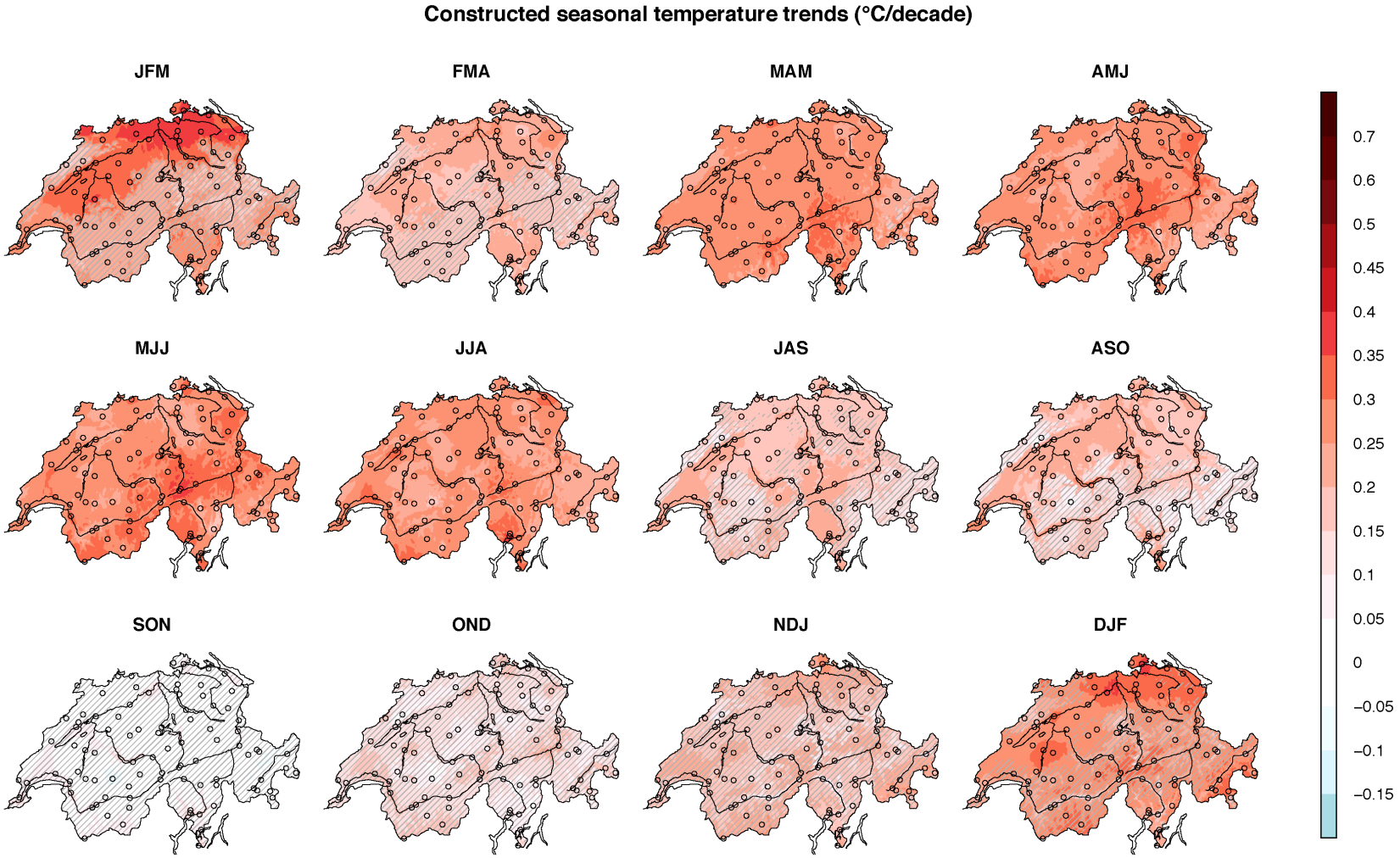

Figure 5.6: Constructed temperature trends (°C/decade). Hatched areas represent non-significant trends at the 5% level.

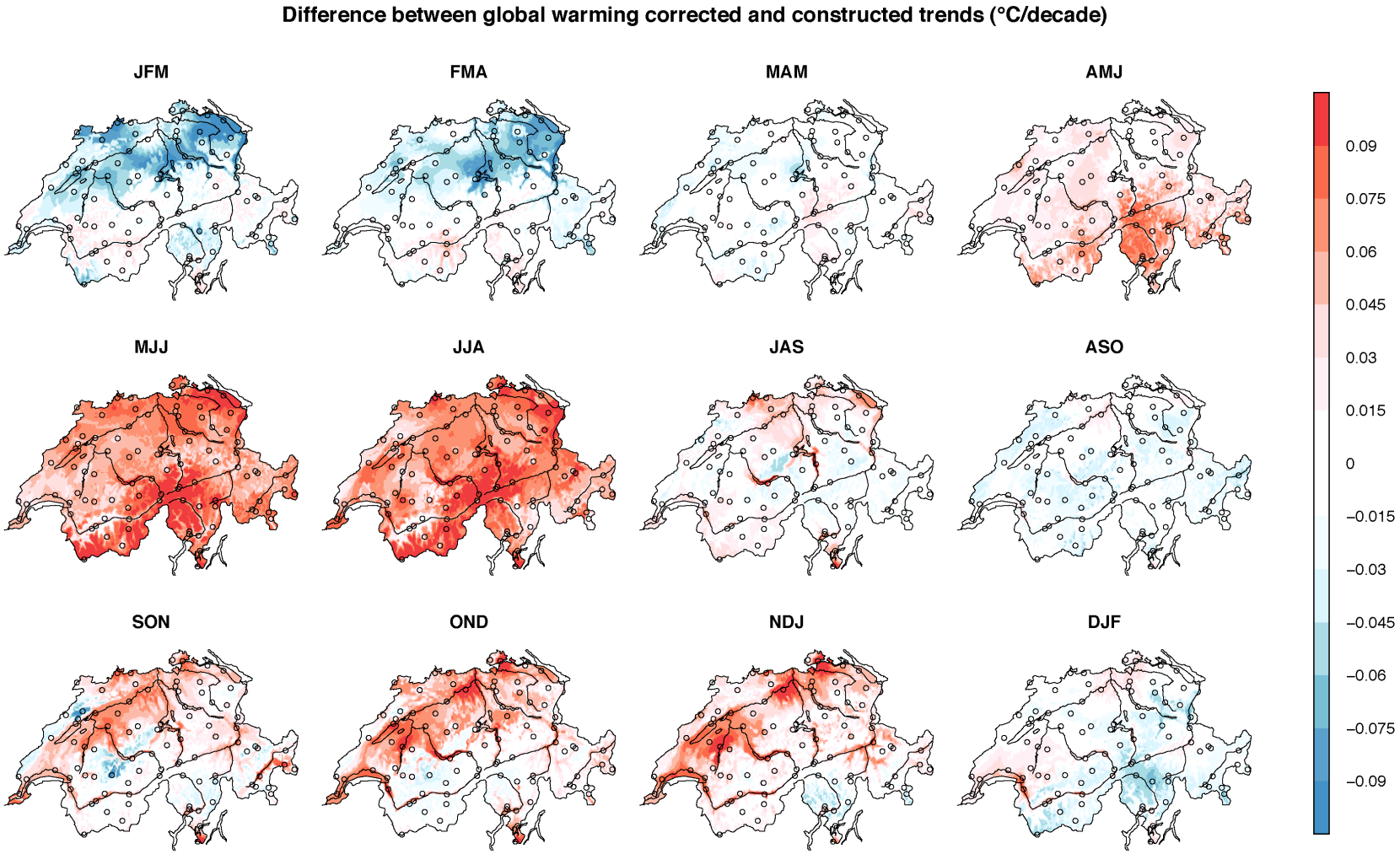

Figure 5.7: Difference between NH warming corrected and constructed trends (°C/decade). Note that the colour scale is different than in Fig. 5.6.

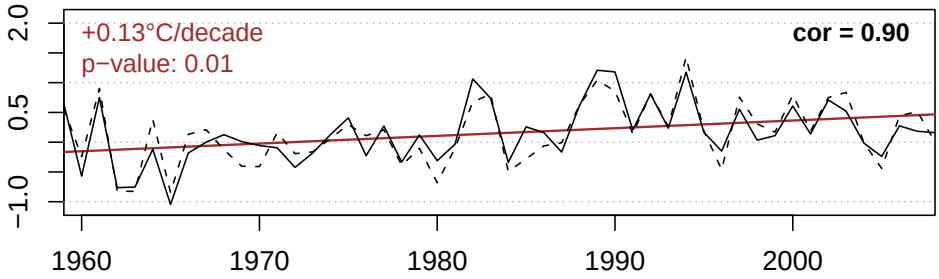

Figure 5.8: Time series of spatially-averaged constructed temperature anomalies (°C). The NH warming corrected time series is represented by a dashed line. The brown line denotes the estimated linear trend function. Note that both corrected and constructed temperatures have the same linear trend.

Chapter 6

Altitude dependence of temperature trends

6.1 Vertical trend profiles

One of the main purposes of this thesis is to better understand what physical phenomena may have an influence on Swiss temperature trends. From the graphical representation of the seasonal trends (Fig. 4.3), we have seen that there are spatial differences in trend magnitude. Assuming that global warming were the only process responsible for the positive trends in Switzerland, we would expect the trends to be of approximately equal magnitude at all gridpoints. However, since we observe spatial variability and altitude effects, we deduce that the magnitude of the trends must be influenced by other phenomena on a regional and/or local scale.

In order to further investigate the impact of physical processes on the altitude dependence of temperature trends, we now consider the vertical structure of the trends in more detail. Trend profiles, which describe the trend magnitude as a function of altitude, represent a convenient way to visualise the altitude dependence of the trends. Figure 6.1 shows the vertical profiles of both corrected and constructed trends. The calculated LOESS fits (see Section 3.5 for details on the methodology) symbolise the general relationship between trend magnitude and altitude.

The vertical trend profiles reproduce the altitude effects observed in Figs. 4.3 and 5.6. In particular, the positive anomaly in autumn at low altitudes is clearly distinguishable (ASO, SON, OND). In general, the constructed trends reproduce the corrected trends well, but feature slightly different vertical structures than the observations, with somewhat less altitude dependence (see e.g. AMJ). Also, in early summer the constructed trends clearly underestimate the corrected ones (MJJ, JJA), indicating that the atmospheric circulation does not suffice to explain the trends.

Generally, it can be said that the gridpoint trends form coherent, structured vertical patterns, which justifies the representation of the data with LOESS fits. Note, however, that the reliability of the fits is low above 3000 m because the amount of gridpoints decreases with height. At such heights, some distinct "branches" can be seen in the gridpoint data in several seasons (e.g. ASO), which reflects the fact that the portions of the Swiss territory situated above 3000 m form obvious clusters of gridpoints with similar trends.

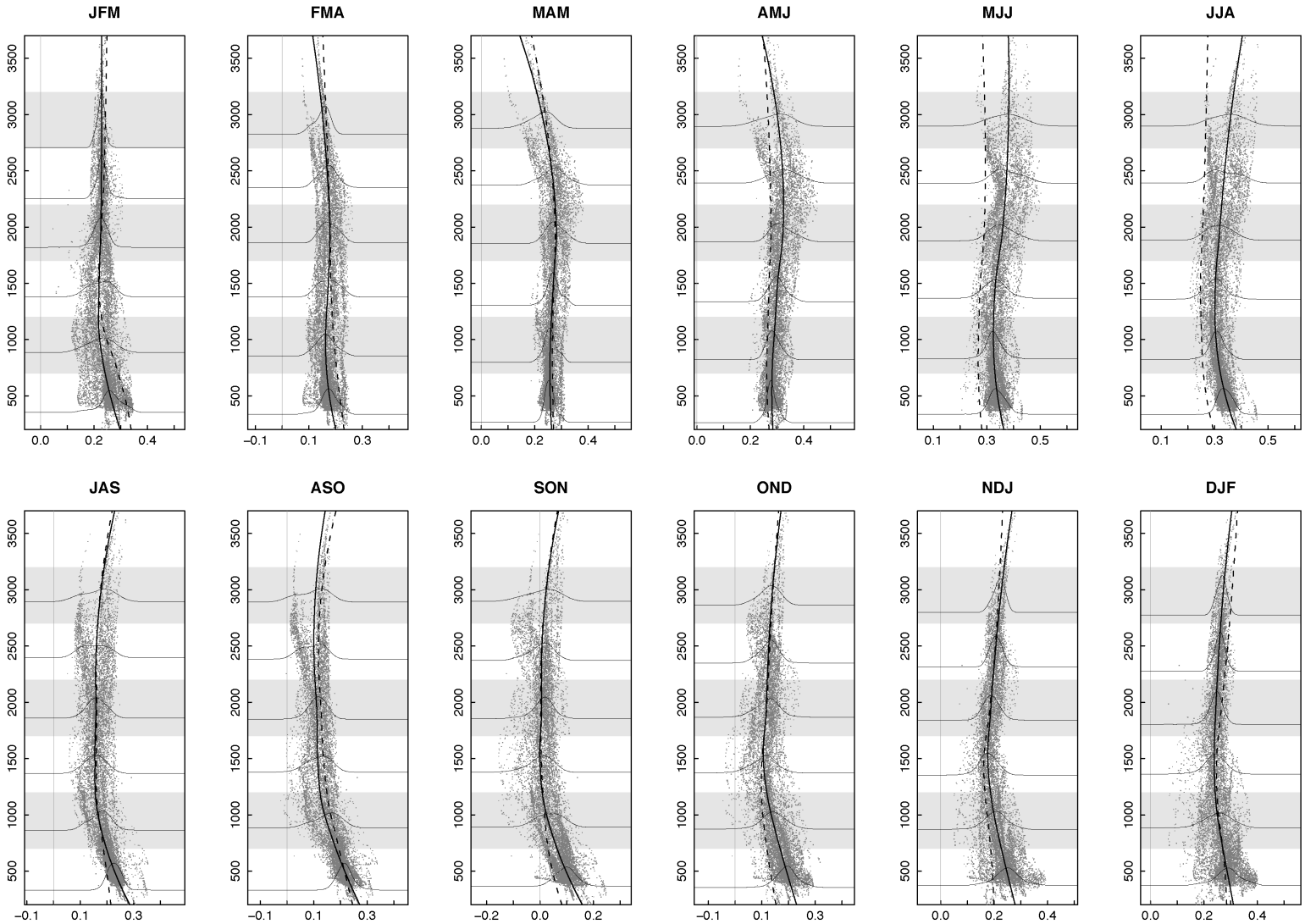

Figure 6.1: Vertical profiles of seasonal temperature trends. The grey dots denote the magnitude of observed, corrected temperature trends at individual gridpoints, while the vertical black curves represent LOESS fits of the corrected (solid) and constructed (dashed) trends. The thin horizontal black curves are estimated density distributions of the trends for 6 height classes of 500 m each (alternating grey and white bands). The zero-trend line is represented by a thin vertical grey line.

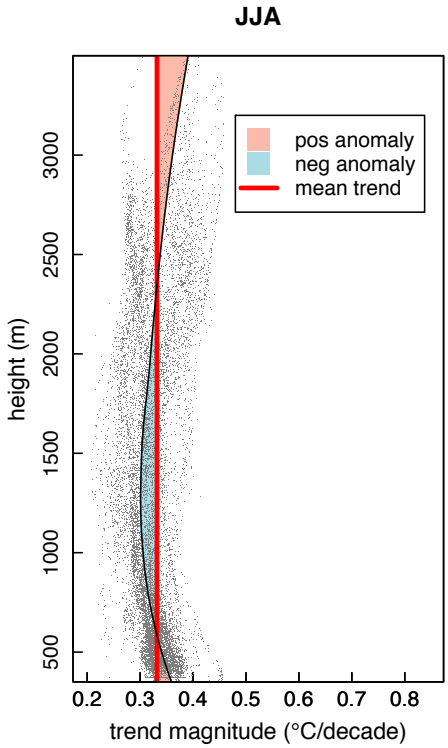

Figure 6.2: Representation of the vertical trend anomalies in JJA. See text for more details.

6.2 Vertical trend anomalies

From the trend profiles shown in Fig. 6.1, we sought a way to represent the temporal changes in the vertical structure of the seasonal trends in one single plot. For this purpose, we calculated the deviations of the vertical profiles from the respective mean seasonal trends. This procedure, which was applied to each of the 12 seasons in a manner illustrated in Fig. 6.2, consisted in calculating the mean seasonal trend (red line in Fig. 6.2), and subtracting this value from the trend values at each point of the curve. We thus obtained vertical deviations from the mean seasonal trend (red and blue surfaces in Fig. 6.2). We then plotted these deviations (which we will refer to as *trend anomalies* in the following) as a function of the season using contour lines.

The vertical anomalies of the observed and constructed trends are shown in Figs. 6.3 and 6.4, along with estimated isolines of temperature and snow depth (see Sections 2.1 and 2.3 for the data, and 3.5 for details on the methodology).

Considering first the observed vertical trend anomalies (Fig. 6.3), we note that the anomalies seem to form coherent patterns rather than random variations. We distinguish two main patterns of positive trend anomalies. The first pattern, which is relatively weak in amplitude, occurs in spring (FMA to MJJ) at mid to high altitudes (from 1500 masl upward); it can be described as a band of positive anomalies closely following the zero-degree isotherm and the snow depth isolines. Another much more pronounced pattern is found in late summer to middle winter (JAS to JFM) at the lowest altitudes (below 800 masl).

The constructed trends, in contrast, feature generally weaker vertical anomalies (Fig. 6.4). In particular, the two patterns found in the observed trends are much less visible. The positive anomaly found in autumn at low altitudes is weaker and more limited in time than in the observations. Moreover, the anomaly patterns appear to be less coherent; this is

probably due to the fact that the goodness of the regression fit varies from one season to another, so that the vertical structure of the temperature trends can be more or less well reproduced.

The differences between the observed and constructed trends can be better understood with a difference plot of the vertical anomalies (Fig. 6.5). Since the differences are small, the colour scale has been slightly modified with respect to Fig. 6.3 for better visualisation. The differences were calculated as "corrected minus constructed trends", so that positive values (in red) indicate domains where the constructed anomalies are smaller than those of the NH warming corrected observations.

The difference plot reproduces the two patterns found in the observations (upper panel of Fig. 6.3) to a large extent. This means that the regression model is not able to fully reproduce these anomalies, as already observed in the lower panel of Fig. 6.3. The implications of these results are discussed in the following chapter.

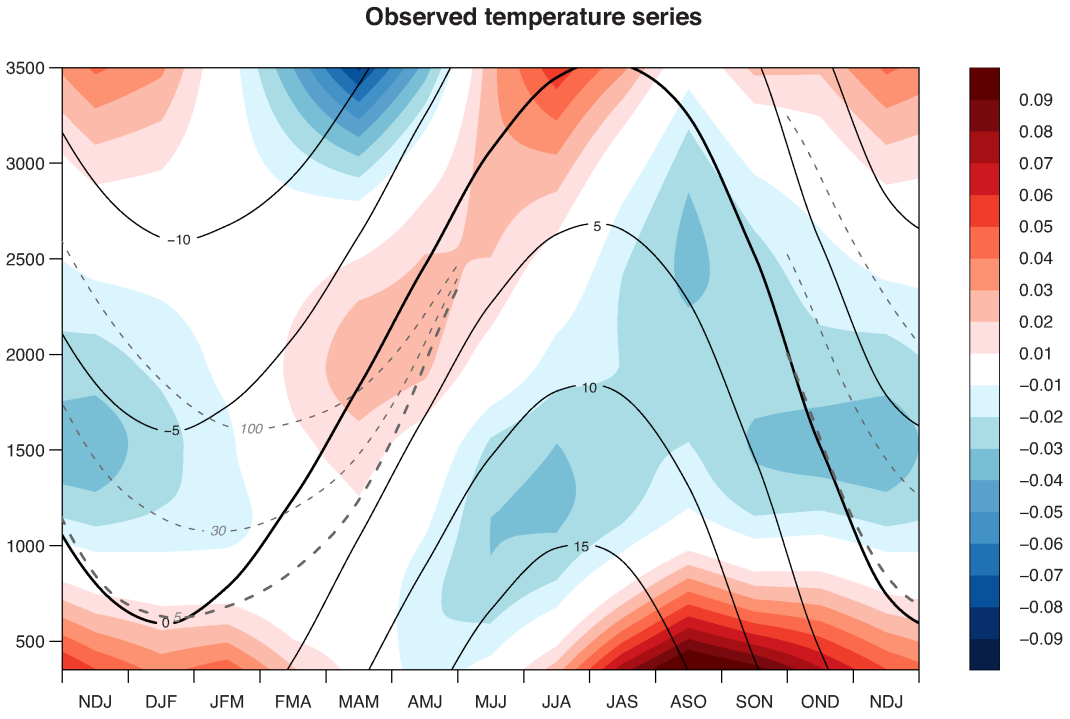

Figure 6.3: Vertical trend anomalies of observed trends in °C/decade. The solid black lines denote estimated temperature isotherms, while the dashed grey lines represent isolines of 5, 30 and 100 cm snow depth.

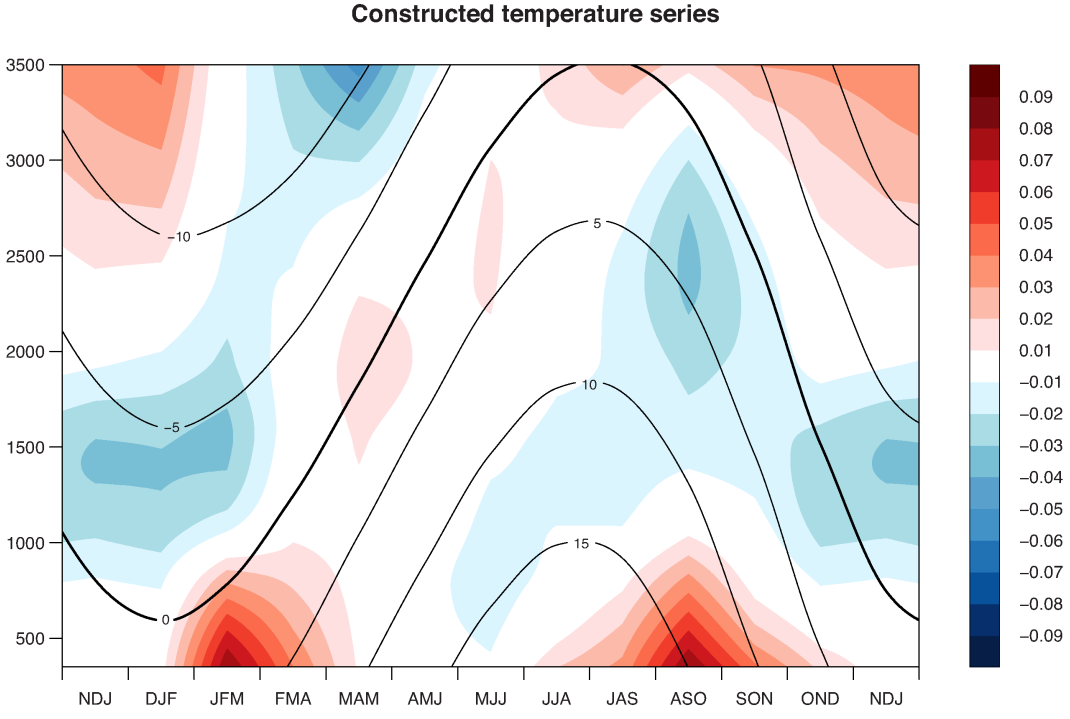

Figure 6.4: Vertical trend anomalies of constructed trends in °C/decade. See Fig. 6.3 for details.

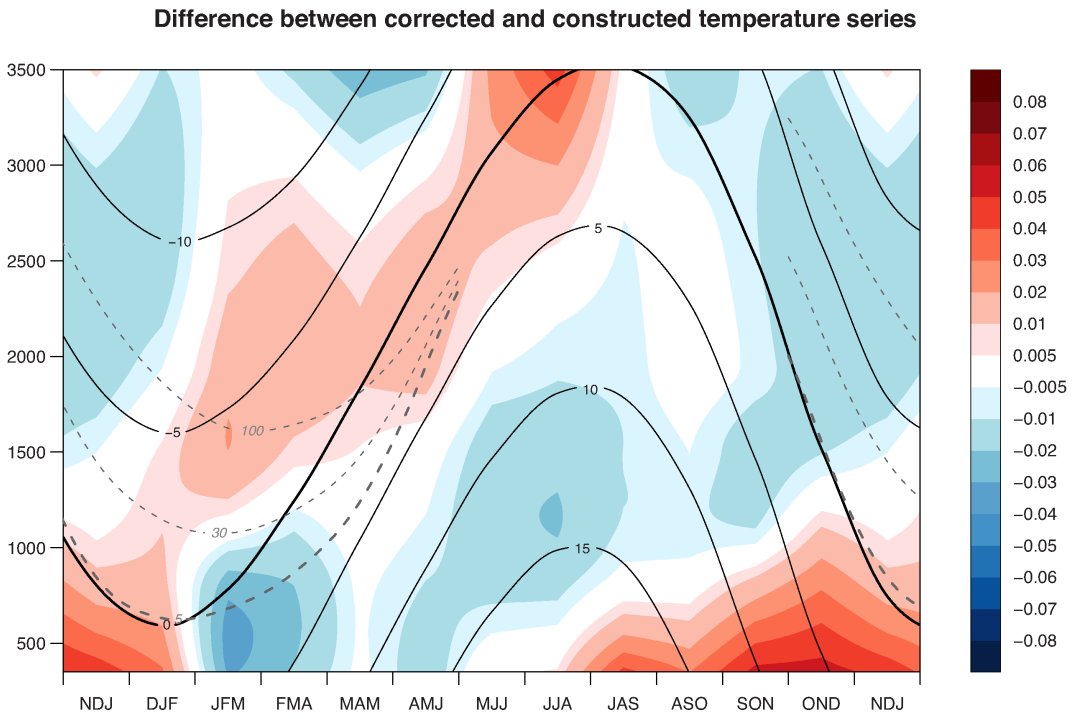

Figure 6.5: Vertical anomalies of trend differences (corrected minus constructed trends) in °C/decade. Note the slightly modified colour scale compared to Fig. 6.3.

Chapter 7

Discussion

7.1 Yearly and seasonal temperature trends

7.1.1 Magnitude of the trends

As shown in Figs. 4.1 and 4.2, our results reveal that both yearly and seasonal trends are positive. The very high statistical significance of the yearly trends (smaller than 0.05% at all gridpoints) provides strong evidence to support the hypothesis that Swiss temperatures have risen in recent decades. This result is consistent with previous trend analyses on Swiss (Begert et al., 2005; Rebetez and Reinhard, 2007), European (Klein Tank et al., 2005; Luterbacher et al., 2004) or global scales (IPCC, 2007b; Rahmstorf et al., 2007; Jones and Moberg, 2003). It is very likely that most of the warming observed over the past five decades has been induced by an increase in greenhouse gas concentrations due to anthropogenic emissions (IPCC, 2007b).

The warming rates found in our study (spatial average of 0.35 °C/decade for yearly trends, peaking at 0.48 °C/decade in MJJ) are stronger than NH or global warming rates. This is known from previous studies, which have also found faster-than-average warming over Switzerland and Europe (Rebetez and Reinhard, 2007; IPCC, 2007c). Over the last 50 years, Swiss temperatures have increased about 1.6 times faster than in NH extratropical regions (0.22 °C/decade).

7.1.2 Spatial and temporal variability

Our results reveal that temperature trends are subject to variations in space (e.g. altitude dependence) and time (seasonal variability) in Switzerland. This indicates that the trends must be driven (at least in part) by physical mechanisms which act on more local scales. Such mechanisms could also contribute to a local increase in warming rates, which might explain the larger trend magnitudes in Switzerland compared with NH extratropical regions. Possible physical processes have been mentioned in the Introduction of this thesis, and include e.g. changes in incoming shortwave radiation or in fog frequency, snow-albedo feedback effects, or upper-air dynamical flow changes. We will analyse and discuss the impact of such processes in the following sections.

7.1.3 Limitations of our analysis

A few limitations of our analysis method need to be taken into account in the discussion of our results. As mentioned in the Methods section (2.1), the number of stations used for calculating the gridded temperature anomalies changes over time, because 37 of the 91

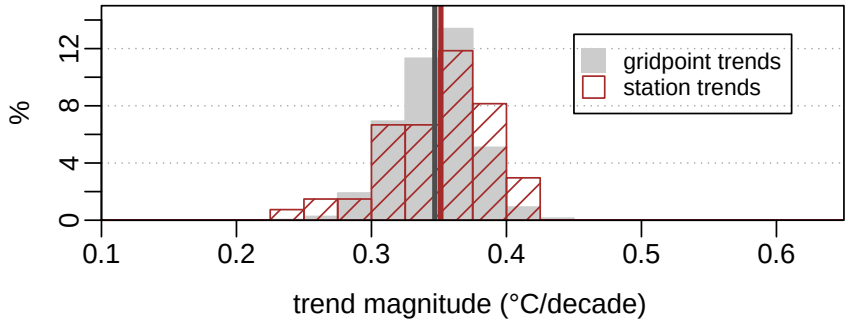

Figure 7.1: Histograms of the distribution of yearly trend magnitudes at gridpoints (grey bars) and 54 stations with full time series (brown shaded bars). The vertical bars denote the mean trend magnitudes for gridpoints and stations (dark grey and brown, respectively).

stations do not have complete measurement series. This may induce some heterogeneities in the gridpoint temperature time series, because the gridded values at particular gridpoints are influenced by a variable number of stations. To verify whether this has an impact on the interpretation of our results, we calculated the gridded temperatures with a constant number of stations (i.e. with the 54 stations having full time series) and performed the trend analysis on that data set (not shown). The results remained qualitatively unchanged. The trends were similar in magnitude to those obtained from the full set of stations, and showed similar variations in space and time. The spatial patterns, however, were somewhat less detailed because of the smaller number of stations used in the computation.

Another source of inaccuracy arises from the fact that the spatial coverage of high-altitude regions is low. As can be seen in Fig. 2.1, only eight stations are situated above 2000 masl, and there are no stations between 2700 and 3300 masl. This means that the temperature anomalies at high-altitude gridpoints are based on a small number of stations, and are interpolated from stations which may be located at different altitudes (see Section 3.1 for details on the gridding procedure).

It must also be mentioned that the gridding procedure tends to "smoothen" the trends spatially. In Fig. 7.1, we compare the distribution of yearly trends from gridpoints with those obtained from station measurements (only the 54 stations with full time series are considered). Compared with the station-based trends, the gridpoint trends feature somewhat less variability. It is thus possible that the spatial variability of the temperature trends presented in this thesis is slightly underestimated. However, since the mean trend magnitudes are very similar (0.35 °C/decade for both stations and gridpoints; see also Fig. 4.2), we consider that the gridded temperature series provide a good representation of the overall magnitude of Swiss temperature trends.

7.2 Regression analysis

7.2.1 Explanatory power of the regression model

Modelling the gridpoint temperature anomalies in a stepwise regression analysis with NH temperature anomalies and PCs of 500 hPa geopotential height as explanatory variables, we found that a substantial fraction of the variability of temperature anomalies could be reproduced.

The $\overline{R}^2$ values (Fig. 5.5) indicated that 45 to 80% of the temperature variance was explained by the model. This means that most of the temperature variability is controlled by the large-scale forcings described in the model. Such forcings include atmospheric circulation patterns (modelled by PCs of 500 hPa geopotential height) and other external influences represented by NH extratropical temperature anomalies, such as SSTs and continental-scale temperature anomalies.

As described in Section 5.5, the highest $\overline{R}^2$ values are found in winter at high altitudes, while the fraction of the temperature variability explained by the model is smaller in summer (minimum in JJA with about 45-55% explained variance; Fig. 5.5). This means that our circulation patterns have a seasonally variable impact on temperatures in Switzerland. This effect can be understood by considering the characteristics of the atmospheric circulation patterns (Section 3.4 and Fig. 3.3). In winter, geopotential height anomalies tend to be strong and pressure gradients are large, so that changes in geopotential height patterns have a large influence on the characteristics of the air masses affecting Switzerland. This influence is strongest at mid to high altitudes, probably because the frequent cold air pools in lowland regions induce a more complex relationship between weather patterns and temperature anomalies in those regions. In summer, atmospheric flows are generally weaker and their effects (regarding the type of air masses advected to Switzerland) are less clear, so that local effects (e.g. induced by soil-atmosphere interactions and convection) are more important.

7.2.2 Implications of the results

From the results of the regression analysis, we were able to analyse the influence of individual atmospheric flow patterns on temperatures in Switzerland. In all cases, we obtained physically coherent estimates of temperature anomalies (Fig. 5.3 and Appendix B). The anomaly patterns often featured altitude dependence, and differences between the north and the south side of the Alps could sometimes be observed. This confirms the hypothesis that circulation patterns have spatially variable effects on temperatures. Thus, changes in the frequency of atmospheric flow patterns might explain part of the magnitude and spatial variability of the trends. We will discuss this point in more detail in Section 7.4 below.

7.2.3 Overfitting

Considering the relatively large number of explanatory variables in our model and the high $\overline{R}^2$ values (Fig. 5.5), it is possible that the model is slightly overfit. Overfitting is a common problem in multiple regression models with many variables. Because of random effects, some variables (which in reality are not relevant to the relationship described by the model) may be included because they contribute to explain more variance. Even though the model fits the data more closely, there is a loss in predictive power, as some of the effects characterised by the model are irrelevant. In our particular case, it is likely that the chosen explanatory variables actually determine a smaller fraction of the temperature variance than what the $\overline{R}^2$ values indicate.

Stepwise regression models, as applied in this study (Section 5.2), are known to have a tendency to overfit the data, because the choice of relevant variables is based on goodness-of-fit criteria only (Section 3.2), regardless of the physical relationship between the variables (Foster and Stine, 2006). In this study, a manual selection of the variables would have been impossible because of the large number gridpoints in our dataset; therefore, stepwise regression was used despite the risk of overfitting.

To test whether overfitting might be a problem, we performed two other regression analyses: one with only the first half of the time series (1959-1983), and another with every second year of the time series (results not shown). The regression coefficients (and thus the calculated temperature anomalies) were found to be very robust and fairly insensitive to the

chosen time period. The only exception were the gridpoint regression coefficients β_0 of the NH corrected temperature (see Eq. 5.1), which showed high spatial variability, so that the estimated values did not seem very reliable.

Overfitting implies that variations in gridpoint temperatures may be described "too well" by the model. Our approach here consists in determining what part of the temperature trends can be explained by the variables in our model, which represent large-scale influences on Swiss temperatures. Proceeding by elimination, we consider the part of the corrected trends not explained by the model to be due to other processes, taking place on a local scale. If our model is overfit, we are probably overestimating the influence of large-scale processes on Swiss temperature trends; this allows us to make a conservative estimate of the impact of local-scale physical mechanisms on the trends. In other words, analysing a model that is possibly overfit enables to determine the *minimum* influence of local processes on temperature trends.

7.3 Interpretation of the differences between NH warming corrected and constructed temperatures

With the estimated regression coefficients, we were able to generate model-based temperature series at each gridpoint, which we call *constructed* temperatures. We performed a trend analysis of the constructed series (Fig. 5.6), and compared the results to those based on the observations with a plot of the trend differences (Fig. 5.7). As mentioned earlier, in our approach the trend differences represent the fraction of the trends which remains unexplained by our regression model, i.e. cannot be explained by large-scale influences. We thus interpret the patterns found in the difference plot as being caused by other factors, acting on a regional or local scale.

Overall, we found the trend differences to be relatively small, with maximum differences amounting to approx. 20% of the observed trends. This means that our model was able to reproduce the corrected trends to a large extent. However, in some seasons clear difference patterns were found, which we discuss in this section.

In autumn and early winter (SON, OND, NDJ), the model underestimates the trends in the Swiss Plateau by 10 to 20%. In Switzerland, a common phenomenon at low altitudes in autumn is the formation of fog at the top of a temperature inversion layer. Fog occurrence is often related to wind-calm weather conditions, where cold air pools can form over low-altitude valleys and plains. Because of its special topographical setting between the Alps and the Jura mountains, the Swiss Plateau is subject to frequent fog events in autumn and winter (von Dach, 2006; Troxler and Wanner, 1991). While fog formation depends on temperature and on the atmospheric lapse rate, fog also feeds back on temperature by intercepting a large part of the downward solar radiation, thereby contributing to preserve the cold air pool (Beniston and Rebetez, 1996). However, fog occurrence is also controlled by other factors, such as relative humidity as well as aerosol composition and number concentration (Vautard et al., 2009).

In recent decades, a clear decrease in fog frequency has been observed in Europe, and Switzerland was no exception (von Dach, 2006; Vautard et al., 2009). This negative trend is believed to be related to changes in air quality and aerosol concentrations in the first place (Vautard et al., 2009), but land-use changes and urbanisation might also have played a role (Sachweh and Koepke, 1995). Since fog layers have a net cooling effect at low altitudes by blocking part of the incoming solar radiation, a regional decrease in fog frequency may induce a localised warming in those regions. Thus, our hypothesis is that the warming over the Swiss Plateau has been accelerated by a decrease in fog frequency over the time period considered in this study, as suggested by Vautard et al. (2009) for European temperatures.

In late winter (JFM, FMA), the sign of the anomaly in the Swiss Plateau reverses and

the model overestimates the trends by up to 20%. This means that based on atmospheric circulation patterns, the low-altitude trends should be stronger than observed. In fact, the observations show altitude-dependent trends with the strongest values at low elevations (Fig. 6.1), and the model reproduces this well but with even stronger altitude dependence in late winter. This is in contrast to other seasons, mostly in autumn (SON, OND, NDJ), where the model failed to reproduce the stronger low-altitude trends. The fact that the observed trends feature stronger trends at low altitudes is in agreement with the hypothesis that fog could be a key factor in explaining autumn- and winter-time lowland trends.

It is unclear, however, why the regression model overestimates low-altitude warming rates in late winter. Perhaps another process than fog-related radiation changes and large-scale atmospheric circulation has had a cooling effect on temperatures, which would explain the negative trend difference at low altitudes. Another possibility is that our model simply fails to accurately simulate the effect of circulation patterns on low-altitude temperatures in those seasons, leading to an overestimation of the warming induced by changes in flow pattern frequency. A more detailed analysis of the temporal evolution of the circulation patterns (i.e., of the time series of the PC scores) would be required to clarify this question, but goes beyond the scope of this thesis.

Finally, positive trend differences are also present in late spring to early summer (mainly MJJ and JJA), indicating that the trends are being underestimated by the model. The differences account for up to 20% of the observed values. Here the effect is not limited to a particular region, and shows no clear altitude dependence. In recent studies on European summer temperatures, soil moisture has been identified as a key parameter in explaining the recent increase in mean summer temperatures (Seneviratne et al., 2006; Fischer et al., 2007; Della-Marta et al., 2007). Such a process, which is not described by our model, might be a reason for the observed discrepancy.

In theory, changes in soil moisture could have an impact on all regions which are not covered by water bodies or glaciers. However, since Swiss mountain regions receive more precipitation than the lowlands, one would expect the effect of reduced soil moisture content to be strongest in lowland regions. This is not the case in our results, so the question remains open whether another process could also play a role in mountain regions. It should be noted that the two seasons MJJ and JJA also reported the strongest seasonal trends in the observations (Fig. 4.2).

7.4 Altitude dependence of temperature trends

As discussed in Section 7.3, our hypothesis is that the spatial variability (and thus the altitude dependence) of the trends can only be explained by the fact that certain physical processes have an impact on warming rates on a local scale. In this section we discuss mechanisms that act specifically on the altitude dependence of temperature trends.

The observed trends were found to be altitude-dependent on a seasonal scale. By representing the vertical anomalies of the observed trends (Fig. 6.3), we found two patterns of positive anomalies. The first occurs in spring (FMA to MJJ) and appears as a band propagating toward higher altitudes with time, parallel to the temperature and snow depth isolines. The second pattern, which is stronger in amplitude, may be observed in late summer to late winter (JAS to JFM) at low altitudes (below 800 masl).

The positive trend anomaly at low altitudes in autumn and winter was discussed in Section 7.3. We attributed this effect to the observed recent decrease in fog frequency. From Fig. 6.3, we note that this anomaly is strongest in late summer and autumn (ASO, SON) in the observations, while the difference between the constructed and the NH warming corrected trends is largest in SON and OND.

In the case of the positive anomaly in spring at mid altitudes, there seems to be a clear

coupling with temperature, as the pattern follows the isotherms. An important process in spring at mid altitudes is snowmelt. The presence of a snow layer is known to have an impact on air temperatures through the snow-albedo feedback, even though this effect is difficult to quantify (Pepin and Lundquist, 2008). Because of the warming, snowmelt is likely to have occurred earlier in recent decades. Moreover, higher temperatures may also have induced smaller snow accumulations during winter, leading to even faster melting in spring. We would therefore expect to find anomalously strong warming in spring at altitudes where such phenomena occur, i.e. where mean temperatures are close to zero or slightly positive. This corresponds exactly to our results, which seems to confirm the hypothesis that snow-related processes may have an impact on Swiss Alpine temperature trends. Pepin and Lundquist (2008) also found stronger trends close to the zero-degree isotherm and attributed this effect to the snow-albedo feedback. Their analysis, however, was performed on a much larger spatial scale.

Since the presence of a snow cover affects temperatures only indirectly, one would expect the effect of the snow-albedo feedback on temperature trends to be weak. In our observations, the positive anomaly in spring can be quantified to account for up to 10% of the observed warming.

Chapter 8

Conclusions and recommendations for further research

8.1 Conclusions

We performed a trend analysis of gridded Swiss temperatures with homogenised data from 91 MeteoSwiss stations. The time period considered was 1959 to 2008. Yearly trends are all positive and highly significant, with an average warming rate of 0.35 °C/decade. The values show fairly little spatial variability, with 90% of all gridpoint trends between 0.30 and 0.39 °C/decade (extreme values: 0.23 and 0.44 °C/decade). This reveals that the warming in Switzerland has been 1.6 times the NH extratropical mean trend over the last five decades.

On a seasonal scale, the analysis also reveals overall positive trends, but seasonal and spatial variability are pronounced. The weakest trends (mostly insignificant at the 5% level) are observed in SON (0.17 °C/decade on average). In contrast, early summer features the strongest warming rates, peaking at 0.48 °C/decade in MJJ.

Contrary to the yearly trends, clear spatial differences are found on a seasonal scale, and in some seasons the patterns of variability are related to elevation. The altitude dependence is strongest in late summer to winter seasons, with large positive anomalies in lowland regions. Further, anomalously strong trends are also found in spring at mid to high elevations, close to the zero-degree isotherm and to the seasonal altitude limit of snow cover. In other seasons, no clear relationship between trend magnitude and altitude is found.

We assume that we can separate the processes responsible for the observed trends into a large-scale and a local-scale contribution. Our hypothesis is that the spatial and seasonal variability of the trends must be driven by specific physical processes whose impacts are limited in space and time. Possible mechanisms include changes in large-scale atmospheric circulation patterns, positive trends in incoming radiation possibly related to a decrease in fog frequency, snow-albedo feedback effects, or any other process affecting temperatures on a local scale.

To better understand the nature of the processes driving the warming rates, we analysed Swiss seasonal gridpoint temperatures using a multiple regression model with atmospheric circulation patterns (represented by principal components of 500 hPa geopotential height fields) and NH temperature anomalies as explanatory variables. It is found that most of interannual temperature variability (from approx. 45% in summer to 80% in winter) can be explained by large-scale circulation patterns and NH extratropical temperatures. The estimated temperature anomalies induced by the large-scale flow patterns appear reasonable from a physical perspective.

The magnitude as well as the spatial distribution of the trends are reproduced realistically

by the model. In some seasons, however, coherent patterns of differences are found between observed and modelled trends. In early summer (MJJ, JJA), the model underestimates the trends all over Switzerland by up to 20%. In autumn (SON to NDJ), the strong positive anomaly that is observed at low elevations is underestimated in the modelled temperature trends by about 20%. In spring (MAM to MJJ), the positive anomaly at mid to high elevations (accounting for about 10% of the mean seasonal trend) cannot be reproduced. Finally, in winter the model overestimates low-altitude warming rates by up to 20%.

These results indicate that other physical processes than large-scale influences alone must also contribute to the observed local warming. Given the spatial and temporal scales of the trend patterns, we suggest that, in summer, the difference between modelled and observed trends could be linked to changes in soil-atmosphere interactions. The positive trend anomaly at low elevations in autumn could be induced by a decreasing occurrence of fog days in recent decades. In the case of spring, the snow-albedo feedback may be the key process to explain the positive trend anomaly close to the zero-degree isotherm. The overestimation of winter temperature trends at low altitudes could be due either to a process which remains unidentified, or simply to an inaccurate representation of the influence of circulation patterns on temperatures. Our results likely tend to overestimate the impact of the large-scale flow, meaning that the effect of local processes could be even larger than estimated here.

8.2 Recommendations for further research

One of the main challenges of this thesis consisted in finding a way to determine the impact of particular physical processes on temperatures. To do this, we used multiple regression analysis, which has the advantage of being simple to implement and to interpret. It also has some disadvantages, particularly with regard to overfitting when analysing a large number of variables, as is the case here (see Section 7.2.3). To confirm the results of our study, the relationship between atmospheric circulation patterns and Swiss gridpoint temperatures could be investigated with other methods. Approaches that have been suggested in the literature include circulation analogues (Lorenz, 1956; Vautard and Yiou, 2009), and methods involving the use of circulation indices based on geostrophic wind and vorticity anomalies (van Ulden and van Oldenborgh, 2006; van Oldenborgh et al., 2009a) or weather type classes (van den Besselaar et al., 2009).

Furthermore, the effect of processes other than the large-scale dynamics could be further examined. A main difficulty in this task results from the fact that the impacts of physical processes such as snow-albedo interactions, soil moisture or fog cannot be easily quantified. It is thus often necessary to use variables that provide an indirect measure of a specific process. In the case of fog, for instance, sunshine duration measurements might provide information on fog-related processes. Gridded relative sunshine duration data in monthly resolution will soon become available at MeteoSwiss (Frei et al., in preparation), and could be used for this purpose. Unfortunately, since many processes are coupled with each other (e.g., fog occurrence is correlated with specific weather patterns; van Oldenborgh et al., 2009b), the use of regression analysis is made difficult by the correlations between the variables. Hence, further investigation of relevant physical mechanisms would involve finding accurate quantifications of the processes, and appropriate analysis methods of their effects on temperatures.

Finally, a possible extension of this study could involve an analysis of the altitude dependence of trends on a regional or continental scale. Because of the good spatial coverage, the large number of mid- to high-altitude stations and the quality of the time series, the Alps would be an ideal study region to corroborate our results.

Acknowledgements

I am very grateful to my supervisors, Christof Appenzeller and Simon Scherrer, for giving me the opportunity to write this thesis at MeteoSwiss. As my day-to-day supervisor, Simon dedicated much time and effort in tutoring me, and I greatly benefited from his advice and scientific expertise. I am also most thankful to Christof for reviewing this work and providing many pertinent remarks and ideas. Thanks to the dedication and support of both, I very much enjoyed writing my thesis and learnt a lot.

This study would not have been possible without the work of Christoph Frei, who developed the gridding method for temperature anomalies. I thank him for providing the gridded datasets and taking time to explain the principle of his gridding procedure.

One of the factors that contributed to making my stay at MeteoSwiss a pleasant one was the excellent working atmosphere. For this I wish to thank my colleages at MeteoSwiss for their kindness and the interest they showed for my work. My special thanks go to Mischa Croci-Maspoli, the leader of my work team, who was very committed in integrating me into the Climate Information team. I very much appreciated the stimulating discussions with him and the other team members.

Bibliography

Appenzeller, C., Begert, M., Zenklusen, E., Scherrer, S. C., 2008. Monitoring climate at Jungfraujoch in the high Swiss Alpine region. Science of the Total Environment 391 (2-3), 262–268.

Begert, M., Schlegel, T., Kirchhofer, W., 2005. Homogeneous temperature and precipitation series of Switzerland from 1864 to 2000. Int. J. Climatol. 25, 65–80.

Beniston, M., Rebetez, M., Dec. 1996. Regional behavior of minimum temperatures in Switzerland for the period 1979-1993. Theoretical and Applied Climatology 53 (4), 231–243.
URL http://dx.doi.org/10.1007/BF00871739

Bradley, R. S., Keimig, F. T., Diaz, H. F., 2004. Projected temperature changes along the American cordillera and the planned GCOS network. Geophysical Research Lett. 31 (16).

Brohan, P., Kennedy, J. J., Harris, I., Tett, S. F. B., Jones, P. D., Jun. 2006. Uncertainty estimates in regional and global observed temperature changes: A new data set from 1850. J. Geophys. Res. 111.
URL http://dx.doi.org/10.1029/2005JD006548

Clements, C. B., Whiteman, C. D., Horel, J. D., 2003. Cold-air-pool structure and evolution in a mountain basin: Peter Sinks, Utah. J. Appl. Meteor. 42, 752–768.

Cleveland, W. S., Grosse, E., Shyu, M. J., 1992. Local Regression Models. Statistical Models in S. Chapman and Hall, New York.

Corti, S., Molteni, F., Palmer, T. N., 1999. Signature of recent climate change in frequencies of natural atmospheric circulation regimes. Nature 398 (6730), 799–802.

Della-Marta, P., Luterbacher, J., von Weissenfluh, H., Xoplaki, E., Brunet, M., Wanner, H., Aug. 2007. Summer heat waves over western Europe 1880–2003, their relationship to large-scale forcings and predictability. Climate Dynamics 29 (2), 251–275.
URL http://dx.doi.org/10.1007/s00382-007-0233-1

Fischer, E. M., Seneviratne, S. I., Lüthi, D., Schär, C., Mar. 2007. Contribution of land-atmosphere coupling to recent European summer heat waves. Geophys. Res. Lett. 34.
URL http://dx.doi.org/10.1029/2006GL029068

Foster, D. P., Stine, R. A., Jan. 2006. Honest confidence intervals for the error variance in stepwise regression. Journal of Economic and Social Measurement 31 (1), 89–102.
URL http://iospress.metapress.com/content/evn0p0w1q48gju9y

Frei, C., et al., 2007. Climate Change and Switzerland 2050. Expected Impacts on Environment, Society and Economy. OcCC/ProClim-, Berne, Switzerland.

Giorgi, F., Hurrell, J. W., Marinucci, M. R., Beniston, M., 1997. Elevation dependency of the surface climate change signal: A model study. J. Climate 10 (2), 288–296.

Grant, A. N., Broennimann, S., Haimberger, L., Sep. 2008. Recent Arctic warming vertical structure contested. Nature 455 (7210), E2–E3.
URL http://dx.doi.org/10.1038/nature07257

Haeberli, W., Beniston, M., 1998. Climate change and its impacts on glaciers and permafrost in the Alps. Ambio 27 (4), 258–265.

Hartmann, D. L., 1994. Global Physical Climatology. International Geophysics Series. Academic Press.

Hegerl, G. C., Wallace, J. M., 2002. Influence of patterns of climate variability on the difference between satellite and surface temperature trends. J. Climate 15 (17), 2412–2428.

Houghton, J. T., Ding, Y., Griggs, D. J., Noguer, M., van der Linden, P. J., Dai, X., Maskell, K., Johnson, C. A. (Eds.), 2001. Climate Change 2001: The Scientific Basis. Contribution of Working Group I to the Third Assessment Report of the Intergovernmental Panel on Climate Change. Cambridge University Press, Cambridge, UK.

Hurrell, J. W., 1995. Decadal Trends in the North Atlantic Oscillation: Regional Temperatures and Precipitation. Science 269, 676–679.

Hurrell, J. W., Kushnir, Y., Ottersen, G., Visbeck, M., 2003. The North Atlantic Oscillation: Climate Significance and Environmental Impact. Geophys. Monogr. Series, Vol. 134. Amer. Geophys. Union.

IPCC, February 2007a. Climate Change 2007: Impacts, Adaptation and Vulnerability. Working Group II contribution to the Fourth Assessment Report of the Intergovernmental Panel on Climate Change [M.L. Parry, O.F. Canziani, J.P. Palutikof, P.J. van der Linden and C.E. Hanson (eds.)], 1st Edition. Cambridge University Press, Cambridge, UK.

IPCC, 2007b. Climate Change 2007: Synthesis Report. Summary for Policymakers. Tech. rep.
URL http://www.ipcc.ch/ipccreports/ar4-syr.htm

IPCC, July 2007c. Climate Change 2007: The Physical Science Basis. Contribution of Working Group I to the Fourth Assessment Report of the Intergovernmental Panel on Climate Change [Solomon, S., D. Qin, M. Manning, Z. Chen, M. Marquis, K.B. Averyt, M. Tignor and H.L. Miller (eds.)]. Cambridge University Press.

Jones, P. D., Moberg, A., 2003. Hemispheric and large-scale surface air temperature variations: An extensive revision and an update to 2001. J. Climate 16 (2), 206–223.

Junge, M. M., Stephenson, D. B., 2003. Mediated and direct effects of the North Atlantic Ocean on winter temperatures in northwest Europe. International Journal of Climatology 23 (3), 245–261.
URL http://dx.doi.org/10.1002/joc.867

Kalnay, E., Kanamitsu, M., Kistler, R., Collins, W., et al., March 1996. The NCEP/NCAR 40-Year Reanalysis Project. Bulletin of the American Meteorological Society 77, 437–472.

Kendall, M. G., 1975. Rank Correlation Methods. Charles Griffin.

Klein Tank, A. M. G., Können, G. P., Selten, F. M., 2005. Signals of anthropogenic influence on European warming as seen in the trend patterns of daily temperature variance. International Journal of Climatology 25 (1), 1–16.
URL http://dx.doi.org/10.1002/joc.1087

Kulkarni, A., von Storch, H., 1995. Monte Carlo experiments on the effect of serial correlation on the Mann-Kendall test of trend. Meteorologische Zeitschrift 4, 82–85.

Laternser, M. C., 2002. Snow and Avalanche Climatology of Switzerland. Ph.D. thesis, Swiss Federal Institute of Technology, Zurich.

Linderson, M.-L., 2001. Objective classification of atmospheric circulation over southern Scandinavia. International Journal of Climatology 21 (2), 155–169.
URL http://dx.doi.org/10.1002/joc.604

Lorenz, E. N., 1956. Empirical orthogonal functions and statistical weather prediction. Science Report No. 1, Statistical Forecasting Project, MIT Cambridge, USA.

Luterbacher, J., Dietrich, D., Xoplaki, E., Grosjean, M., Wanner, H., 2004. European Seasonal and Annual Temperature Variability, Trends, and Extremes Since 1500. Science 303 (5663), 1499–1503.
URL http://www.sciencemag.org/cgi/content/abstract/303/5663/1499

Mann, H. B., 1945. Nonparametric tests against trend. Econometrica 13, 245–259.

Pepin, N. C., Lundquist, J. D., 2008. Temperature trends at high elevations: Patterns across the globe. Geophysical Research Lett. 35 (14).

Pepin, N. C., Seidel, D. J., 2005. A global comparison of surface and free-air temperatures at high elevations. J. Geophysical Research-atmospheres 110 (D3), D03104.

Philipona, R., Behrens, K., Ruckstuhl, C., 2009. How declining aerosols and rising greenhouse gases forced rapid warming in Europe since the 1980s. Geophysical Research Lett. 36.

Preisendorfer, R. W., 1988. Principal Component Analysis in Meteorology and Oceanography. Elsevier.

R Development Core Team, 2009. R: A Language and Environment for Statistical Computing. R Foundation for Statistical Computing, Vienna, Austria, ISBN 3-900051-07-0.
URL http://www.R-project.org

Rahmstorf, S., Cazenave, A., Church, J. A., Hansen, J. E., Keeling, R. F., Parker, D. E., Somerville, R. C. J., 2007. Recent Climate Observations Compared to Projections. Science 316 (5825), 709–.
URL http://www.sciencemag.org/cgi/content/abstract/316/5825/709

Raible, C. C., Stocker, T. F., Yoshimori, M., Renold, M., Beyerle, U., Casty, C., Luterbacher, J., 2005. Northern Hemispheric Trends of Pressure Indices and Atmospheric Circulation Patterns in Observations, Reconstructions, and Coupled GCM Simulations. Journal of Climate 18 (19), 3968–3982.

Rayner, N. A., Brohan, P., Parker, D. E., Folland, C. K., Kennedy, J. J., Vanicek, M., Ansell, T. J., Tett, S. F. B., Feb. 2006. Improved analyses of changes and uncertainties in sea surface temperature measured in situ since the mid-nineteenth century: The HadSST2 dataset. Journal of Climate 19 (3), 446–469.

Rayner, N. A., Parker, D. E., Horton, E. B., Folland, C. K., Alexander, L. V., Rowell, D. P., Kent, E. C., Kaplan, A., Jul. 2003. Global analyses of sea surface temperature, sea ice, and night marine air temperature since the late nineteenth century. J. Geophys. Res. 108, –.

Rebetez, M., Reinhard, M., 2007. Monthly air temperature trends in Switzerland 1901-2000 and 1975-2004. Theoretical Appl. Climatology 91 (1-4), 27–34.

Sachweh, M., Koepke, P., 1995. Radiation fog and urban climate. Geophys. Res. Lett. 22. URL http://dx.doi.org/10.1029/95GL00907

Scherrer, S. C., Appenzeller, C., 2006. Swiss Alpine snow pack variability: major patterns and links to local climate and large-scale flow. Climate Research 32 (3), 187–199.

Scherrer, S. C., Appenzeller, C., 2010. A simple approach to estimate possible altitudinal changes in future Swiss Alpine snowfall amounts, submitted.

Scherrer, S. C., Appenzeller, C., Laternser, M., 2004. Trends in Swiss Alpine snow days: The role of local-and large-scale climate variability. Geophys. Res. Lett. 31, L13215.

Scherrer, S. C., Croci-Maspoli, M., Schwierz, C., Appenzeller, C., 2006. Two-dimensional indices of atmospheric blocking and their statistical relationship with winter climate patterns in the Euro-Atlantic region. Int. J. Climatology 26 (2), 233–249.

Seneviratne, S. I., Lüthi, D., Litschi, M., Schär, C., Sep. 2006. Land-atmosphere coupling and climate change in Europe. Nature 443 (7108), 205–209. URL http://dx.doi.org/10.1038/nature05095

Troxler, F.-X., Wanner, H., 1991. Nebelkarten der Schweiz. Geographica Helvetica 46, 21–31.

van den Besselaar, E., Klein Tank, A., van der Schrier, G., 2009. Influence of circulation types on temperature extremes in europe. Theoretical and Applied Climatology, –. URL http://dx.doi.org/10.1007/s00704-009-0153-6

van Oldenborgh, G., Drijfthout, S., van Ulden, A., Haarsma, R., Sterl, A., Severijns, C., Hazeleger, W., Dijkstra, H., 2009a. Western Europe is warming much faster than expected. Clim. Past 5, 1–12.

van Oldenborgh, G. J., van Ulden, A., 2003. On the relationship between global warming, local warming in the Netherlands and changes in circulation in the 20th century. Int. J. Climatology 23 (14), 1711–1724.

van Oldenborgh, G. J., Yiou, P., Vautard, R., Nov. 2009b. On the roles of circulation and aerosols in the decline of mist and dense fog in Europe over the last 30 years. URL http://www.atmos-chem-phys-discuss.net/9/23987/2009/

van Ulden, A. P., van Oldenborgh, G. J., 2006. Large-scale atmospheric circulation biases and changes in global climate model simulations and their importance for climate change in Central Europe. Atmospheric Chemistry and Physics 6 (4), 863–881. URL http://www.atmos-chem-phys.net/6/863/2006/

Vautard, R., Yiou, P., Nov. 2009. Control of recent European surface climate change by atmospheric flow. Geophys. Res. Lett. 36. URL http://dx.doi.org/10.1029/2009GL040480

Vautard, R., Yiou, P., Oldenborgh, G. J. v., Feb. 2009. Decline of fog, mist and haze in Europe over the past 30 years. Nature Geosci 2 (2), 115–119. URL http://dx.doi.org/10.1038/ngeo414

von Dach, L., 2006. Nebelhäufigkeit in der Schweiz: Entwicklung und Trends im Winterhalbjahr von 1864 bis 2006. Master's thesis, Geografisches Institut der Universität Bern.

von Storch, H., Zwiers, F. W., 1999. Statistical Analysis in Climate Research. Cambridge University Press.

Wang, X. L., Swail, V. R., May 2001. Changes of extreme wave heights in northern hemisphere oceans and related atmospheric circulation regimes. Journal of Climate 14 (10), 2204–2221.

Wild, M., Gilgen, H., Roesch, A., Ohmura, A., Long, C. N., Dutton, E. G., Forgan, B., Kallis, A., Russak, V., Tsvetkov, A., May 2005. From dimming to brightening: Decadal changes in solar radiation at Earth's surface. Science 308 (5723), 847–850.
URL http://www.sciencemag.org/cgi/content/abstract/308/5723/847

Wilks, D. S., 2005. Statistical Methods in the Atmospheric Sciences, 2nd Edition. Vol. 59 of International Geophysics Series. Academic Press.

Yue, S., Pilona, P., Cavadias, G., 2002. Power of the Mann-Kendall and Spearman's rho tests for detecting monotonic trends in hydrological series. Journal of Hydrology 264, 262–263.

Appendix A

Stations used in the gridding procedure

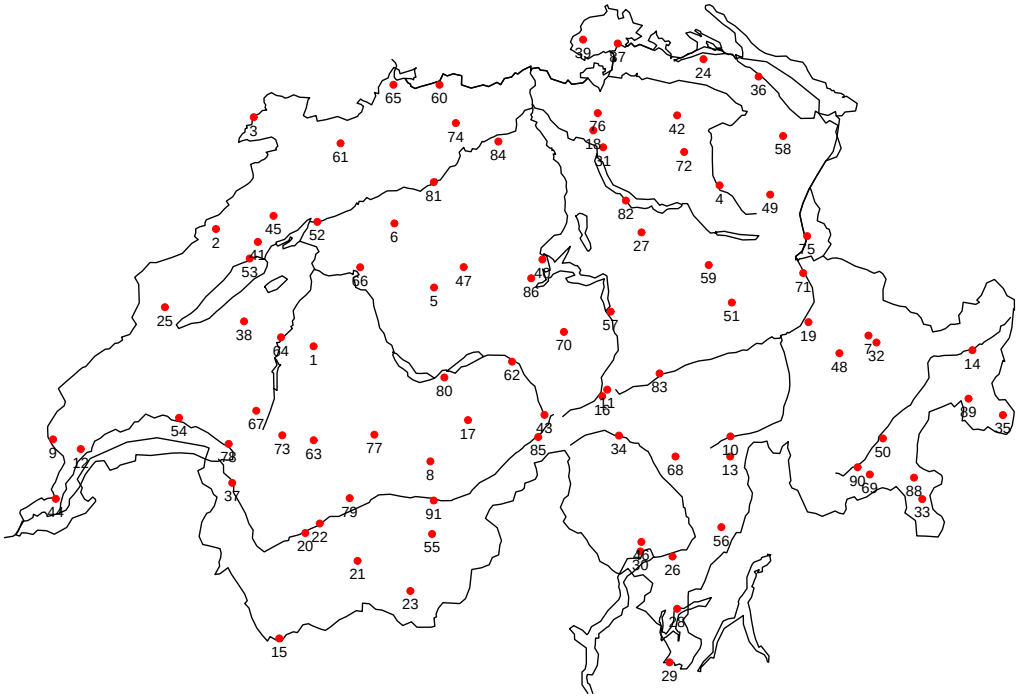

Figure A.1: Stations used in the gridding procedure. The numbers refer to Table A.1 below.

Table A.1: Stations used in the calculation of gridded temperatures. The 12 stations from which mean temperature anomalies were determined (cf. Section 4.1) are represented in red bold typeface. The numbers in the first column refer to the map in Fig. A.1 above. The beginning and end dates (format mm.yyyy) of the temperature time series are given in the two last columns.

	name	lon (°E)	lat (°N)	height (masl)	start date	end date
1	Aadorf / Tänikon	8.90	47.48	539	01.1971	12.2008
2	Acquarossa / Comprovasco	8.94	46.46	575	01.1959 02.1988	01.1977 12.2008
3	Adelboden	7.56	46.49	1320	01.1959	12.2008
4	Aigle	6.92	46.33	381	01.1981	12.2008
5	Altdorf	8.62	46.89	438	01.1959	12.2008
6	Andermatt	8.59	46.63	1442	01.1959	12.2008
7	Arosa	9.67	46.78	1840	01.1959	12.2008
8	Bad Ragaz	9.50	47.02	496	01.1959	12.2008
9	**Basel / Binningen**	7.58	47.54	316	01.1959	12.2008
10	**Bern / Zollikofen**	7.46	46.99	553	01.1959	12.2008
11	Biel/Bienne	7.26	47.12	433	01.1959	12.2008
12	Blatten, Lötschental	7.82	46.42	1535	01.1974 03.2001	02.1999 12.2008
13	Buchs / Aarau	8.08	47.38	387	01.1959	12.2008
14	Buffalora	10.27	46.65	1970	01.1959	12.2008
15	Bullet / La Frétaz	6.58	46.84	1205	01.1978	12.2008
16	Chasseral	7.05	47.13	1599	01.1981	12.2008
17	**Château-d'Oex**	7.14	46.48	985	01.1959	12.2008
18	**Chaumont**	6.99	47.05	1073	01.1959	12.2008
19	Chur	9.53	46.87	556	01.1959	12.2008
20	Cimetta	8.79	46.20	1672	01.1982	12.2008
21	Col du Grand St-Bernard	7.17	45.87	2472	01.1959	12.2008
22	**Davos**	9.84	46.81	1594	01.1959	12.2008
23	Delémont	7.35	47.36	415	01.1959	12.2008
24	Disentis / Sedrun	8.85	46.71	1197	01.1959	12.2008
25	Ebnat-Kappel	9.11	47.27	623	01.1959	12.2008
26	Einsiedeln	8.75	47.13	910	01.1959	12.2008
27	Elm	9.18	46.92	965	01.1959	12.2008
28	**Engelberg**	8.41	46.82	1036	01.1959	12.2008
29	Evolène / Villa	7.51	46.11	1825	10.1986	12.2008
30	Fahy	6.94	47.42	596	01.1981	12.2008
31	Fey	7.27	46.19	737	07.1959 08.1984	01.1981 11.2005
32	Fribourg / Posieux	7.12	46.77	634	01.1959	12.2008
33	**Genève-Cointrin**	6.13	46.25	420	01.1959	12.2008
34	Glarus	9.07	47.03	517	01.1959	12.2008
35	Grächen	7.84	46.20	1550	01.1959	12.2008
36	Grimsel Hospiz	8.33	46.57	1980	01.1959	12.2008
37	Grono	9.15	46.25	382	01.1959	12.2008
38	Gstaad	7.29	46.47	1045	03.1981	12.2008
39	Gütsch ob Andermatt	8.62	46.65	2287	01.1959	12.2008

Table A.1: Stations used in the calculation of gridded temperatures. The 12 stations from which mean temperature anomalies were determined (cf. Section 4.1) are represented in red bold typeface. The numbers in the first column refer to the map in Fig. A.1 above. The beginning and end dates (format mm.yyyy) of the temperature time series are given in the two last columns.

	name	lon (°E)	lat (°N)	height (masl)	start date	end date
40	Güttingen	9.28	47.60	440	06.1976	12.2008
41	Hallau	8.46	47.70	432	01.1959	12.2008
42	Hinterrhein	9.18	46.52	1611	01.1968	12.2008
43	Hörnli	8.94	47.37	1132	12.1991	12.2008
44	Interlaken	7.87	46.67	577	01.1959	12.2008
45	Jungfraujoch	7.99	46.55	3580	01.1959	12.2008
46	Koppigen	7.61	47.13	483	12.1960	12.2008
47	La Chaux-de-Fonds	6.79	47.08	1018	01.1959	12.2008
48	La Dôle	6.10	46.42	1670	01.1973	12.2008
49	Langnau i. E.	7.81	46.94	755	01.1959	12.2008
50	Le Moléson	7.02	46.55	1974	10.1982	12.2008
51	Locarno / Monti	8.79	46.17	367	01.1959	12.2008
52	**Lugano**	8.96	46.00	273	01.1959	12.2008
53	Luzern	8.30	47.04	454	01.1959	12.2008
54	Magadino / Cadenazzo	8.93	46.16	203	01.1959	12.2008
55	Meiringen	8.18	46.73	595	01.1959	12.2008
56	Montana	7.46	46.30	1427	01.1959	12.2008
57	Montreux-Clarens	6.90	46.44	405	01.1959	11.2005
58	Napf	7.94	47.00	1404	01.1978	12.2008
59	Neuchâtel	6.95	47.00	485	01.1959	12.2008
60	Nyon / Changins	6.23	46.40	455	01.1965	12.2008
61	Passo del Bernina	10.02	46.41	2307	01.1972	12.2008
62	Payerne	6.94	46.81	490	08.1964	12.2008
63	Pilatus	8.25	46.98	2106	01.1981	12.2008
64	Piotta	8.68	46.52	1007	02.1979	12.2008
65	Piz Corvatsch	9.82	46.42	3315	08.1979	12.2008
66	Plaffeien	7.27	46.75	1042	01.1972	12.2008
67	Poschiavo / Robbia	10.06	46.35	1078	01.1959	12.2008
68	Pully	6.67	46.51	456	01.1959	12.2008
69	Rheinfelden	7.80	47.55	300	01.1959	12.2005
70	Rünenberg	7.88	47.43	611	11.1982	12.2008
71	S. Bernardino	9.18	46.46	1639	01.1968	12.2008
72	Salen-Reutenen	9.02	47.65	702	01.1959	12.2008
73	Samedan	9.88	46.53	1709	01.1959	12.2008
74	**Säntis**	9.34	47.25	2502	01.1959	12.2008
75	Schaffhausen	8.62	47.69	438	01.1959	12.2008
76	Scuol	10.28	46.79	1304	01.1959	12.2008
77	**Segl-Maria**	9.77	46.44	1798	01.1959	12.2008
78	**Sion**	7.33	46.22	482	01.1959	12.2008
79	St. Gallen	9.40	47.43	776	01.1959	12.2008
80	Sta. Maria, Val Müstair	10.42	46.60	1390	01.1959	12.2008

Table A.1: Stations used in the calculation of gridded temperatures. The 12 stations from which mean temperature anomalies were determined (cf. Section 4.1) are represented in red bold typeface. The numbers in the first column refer to the map in Fig. A.1 above. The beginning and end dates (format mm.yyyy) of the temperature time series are given in the two last columns.

	name	lon (°E)	lat (°N)	height (masl)	start date	end date
81	Stabio	8.93	45.84	353	08.1981	12.2008
82	Ulrichen	8.31	46.50	1346	01.1981	12.2008
83	Vaduz	9.52	47.13	457	01.1971	12.2008
84	Visp	7.84	46.30	639	07.1959 01.1980	01.1971 12.2008
85	Wädenswil	8.68	47.22	485	01.1981	12.2008
86	Weissfluhjoch	9.81	46.83	2690	01.1959	12.2008
87	Wynau	7.79	47.26	422	01.1978	12.2008
88	Zermatt	7.75	46.03	1638	01.1959 12.1981	11.1971 12.2008
89	Zürich / Affoltern	8.52	47.43	444	08.1978	12.2008
90	**Zürich / Fluntern**	8.57	47.38	556	01.1959	12.2008
91	Zürich / Kloten	8.54	47.48	436	01.1959	12.2008

Appendix B

Atmospheric circulation patterns and estimated temperature anomalies

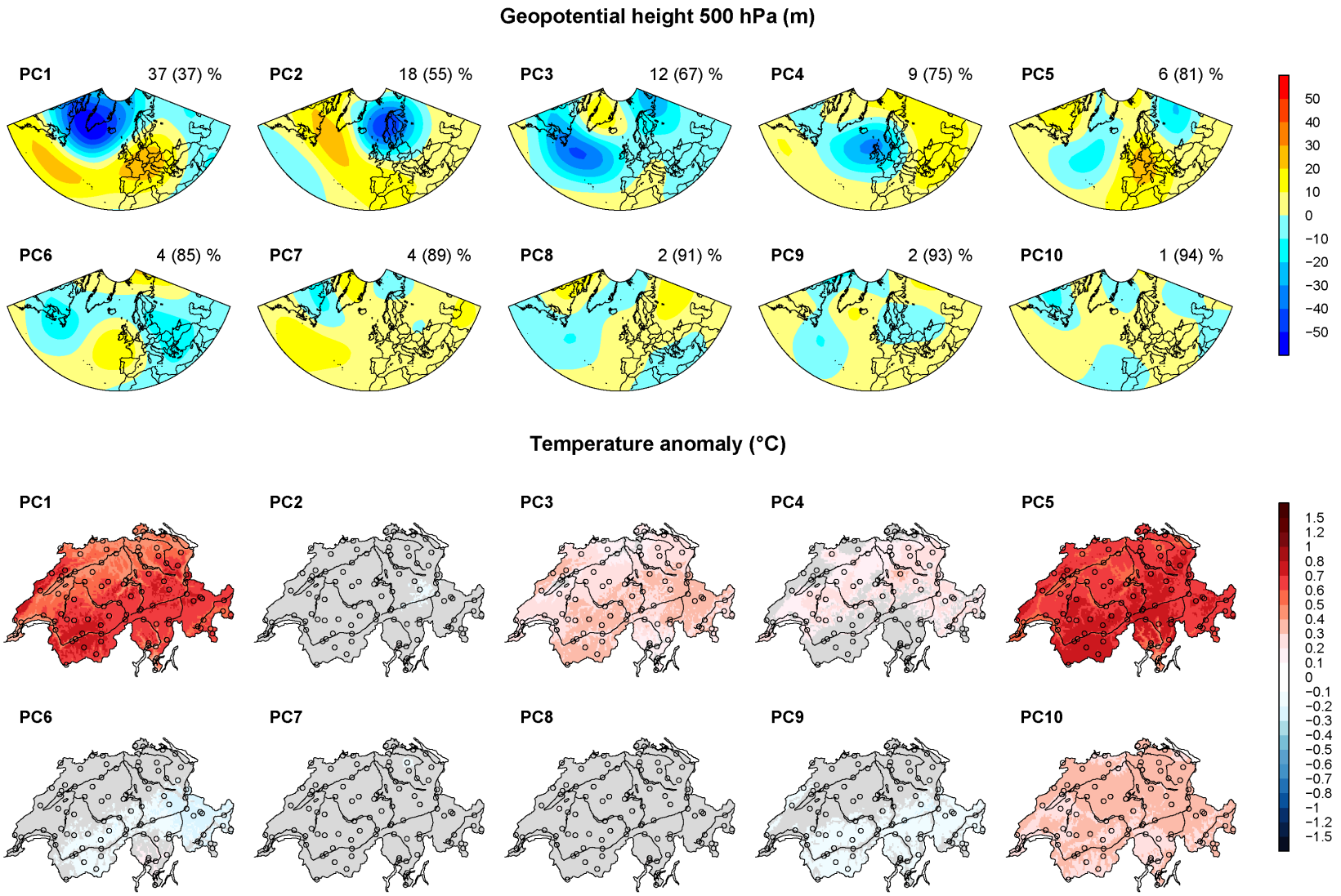

Figure B.1: *Top*: PC loadings of 500 hPa seasonally-averaged geopotential height fields, multiplied by one standard deviation (m). *Bottom*: associated temperature anomalies in February-March-April (°C). Gridpoints where a particular PC was not kept in the model are represented in grey. See also Fig. 5.3.

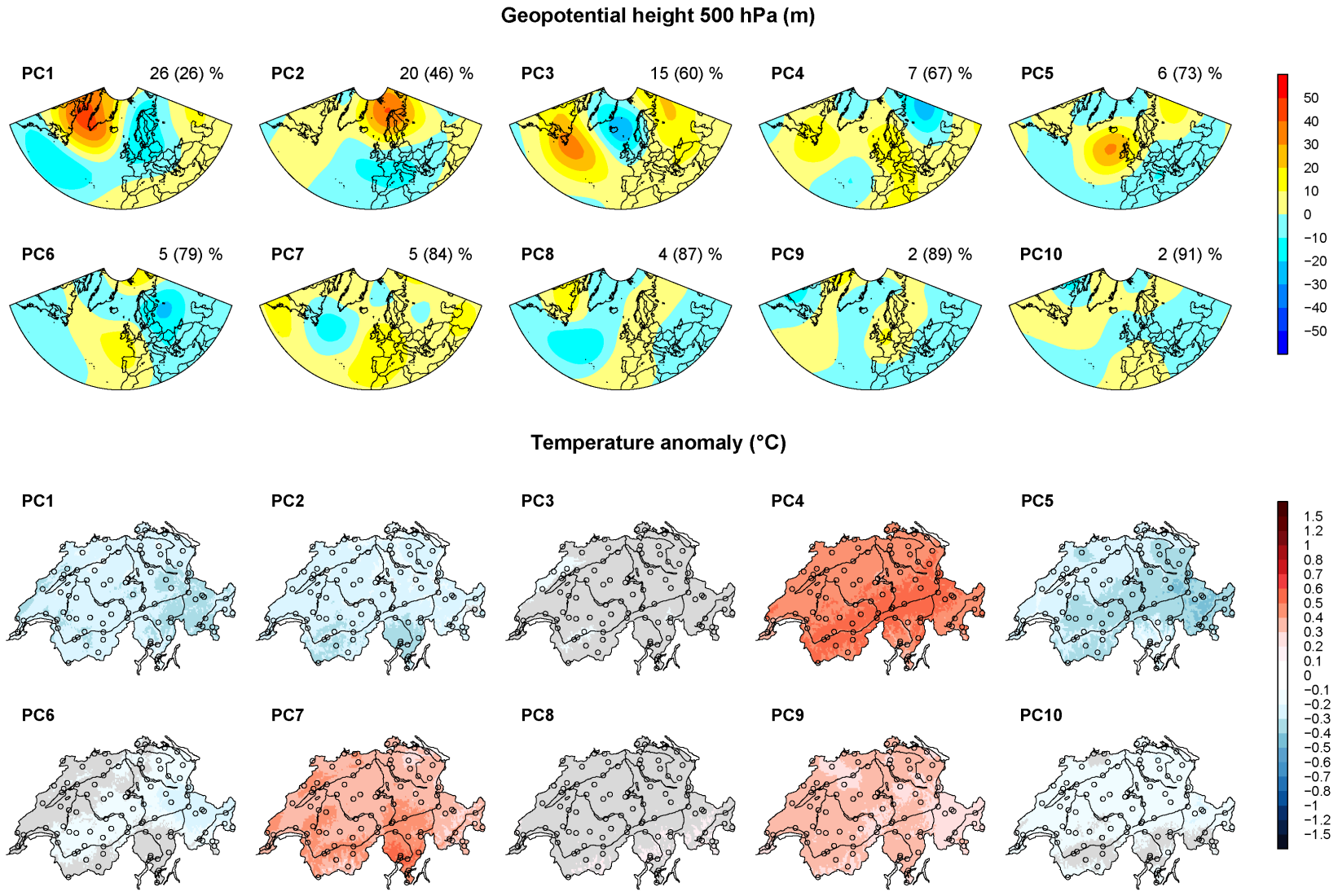

Figure B.2: As in Fig. B.1 for MAM.

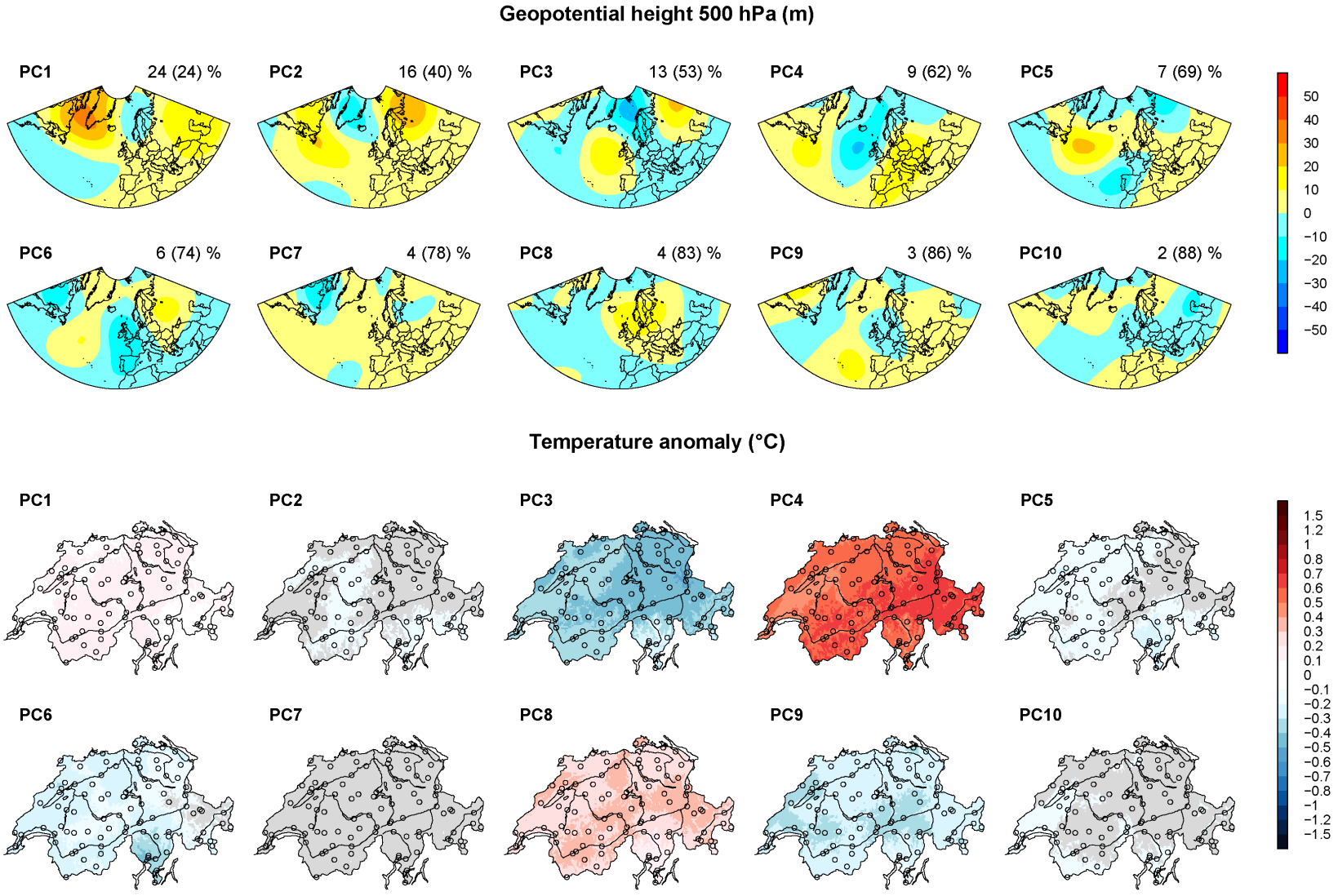

Figure B.3: As in Fig. B.1 for AMJ.

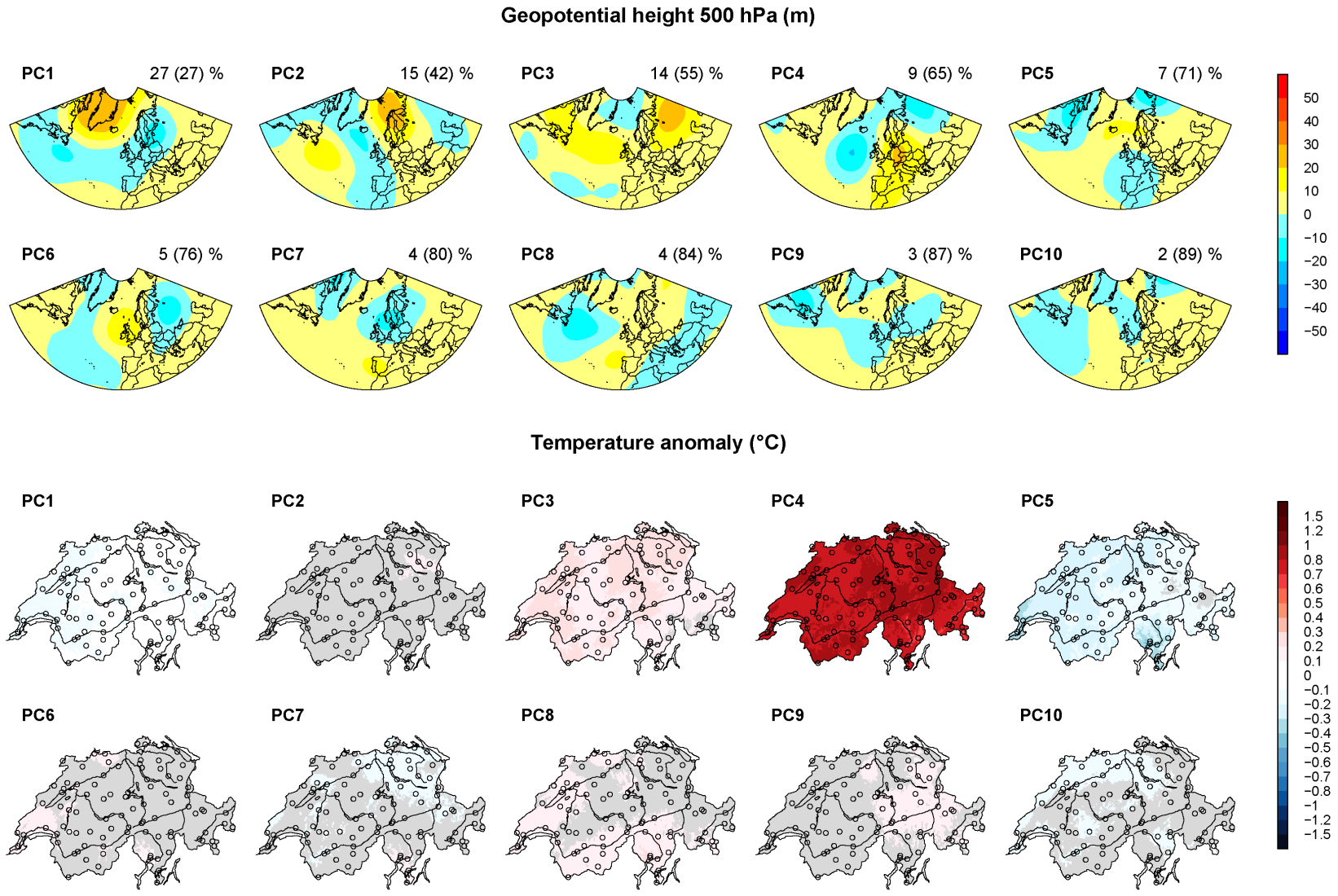

Figure B.4: As in Fig. B.1 for MJJ.

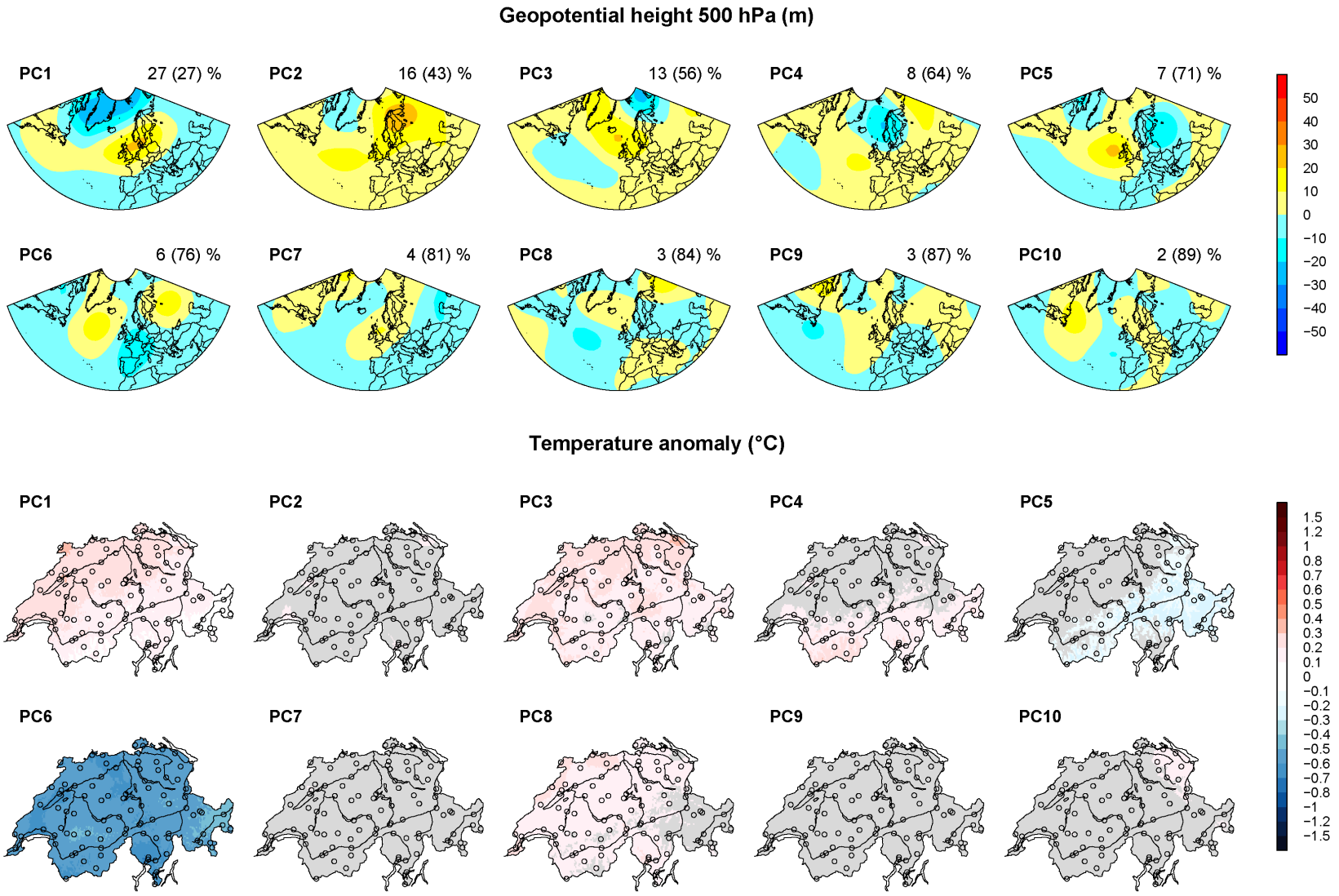

Figure B.5: As in Fig. B.1 for JJA.

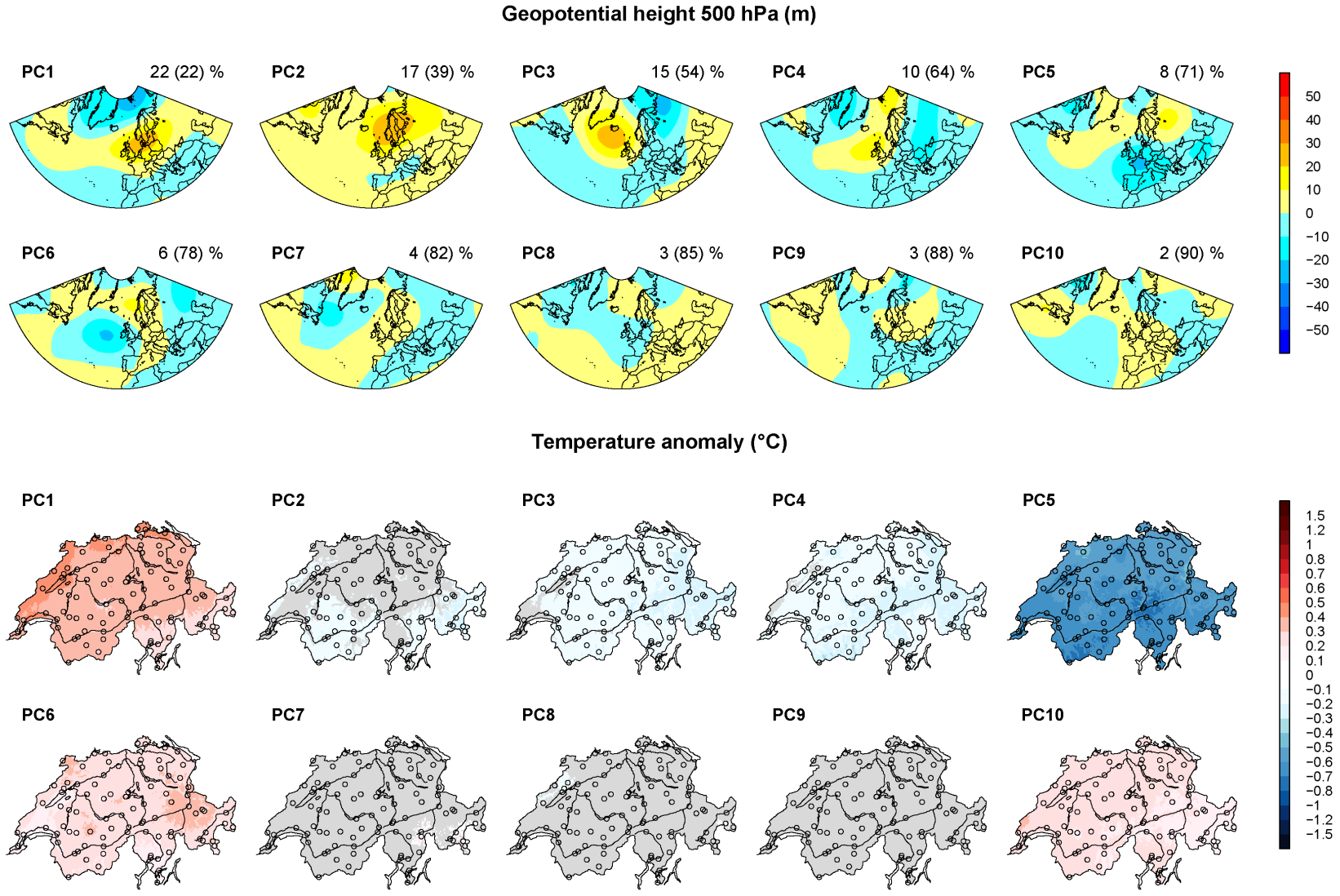

Figure B.6: As in Fig. B.1 for JAS.

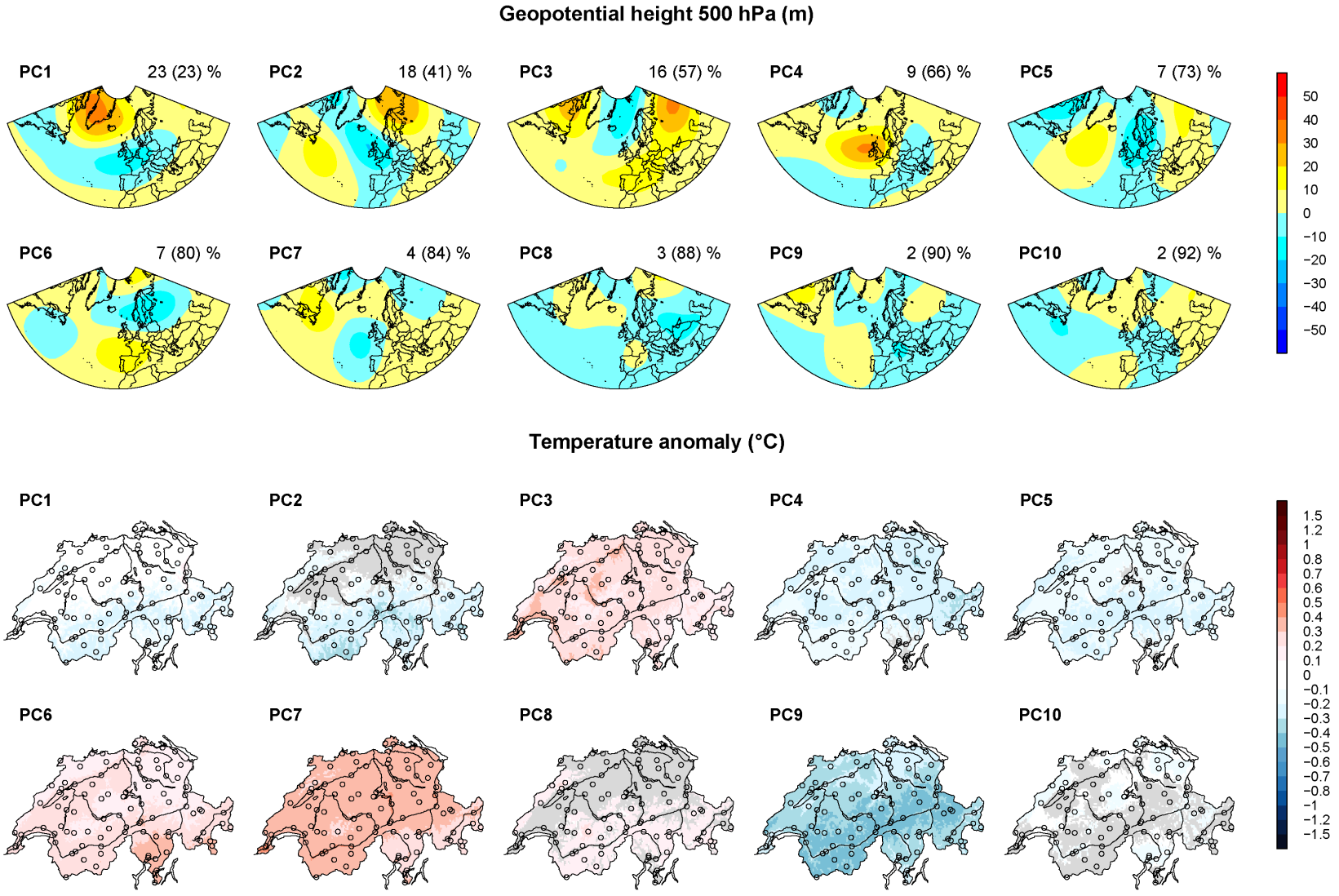

Figure B.7: As in Fig. B.1 for ASO.

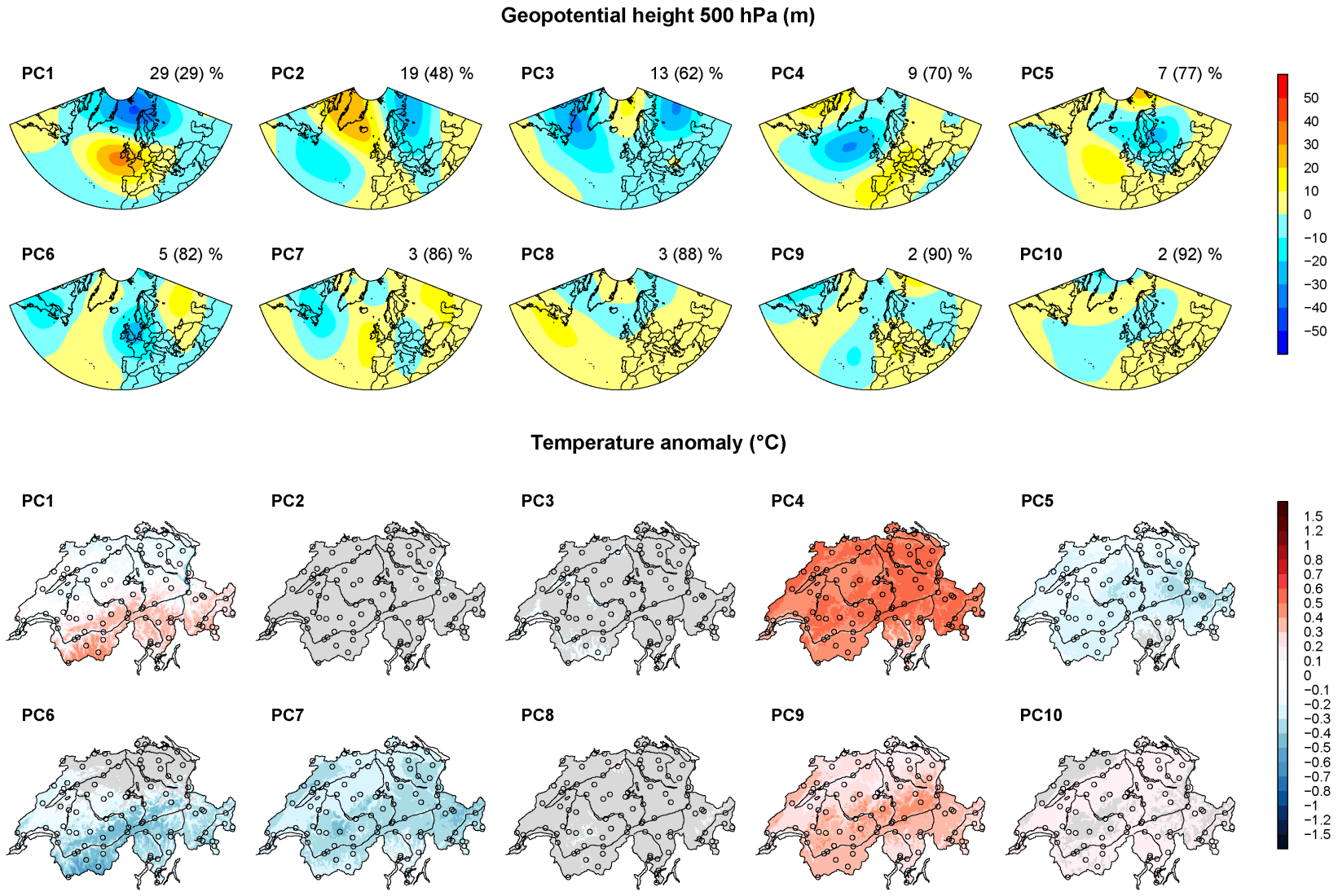

Figure B.8: As in Fig. B.1 for SON.

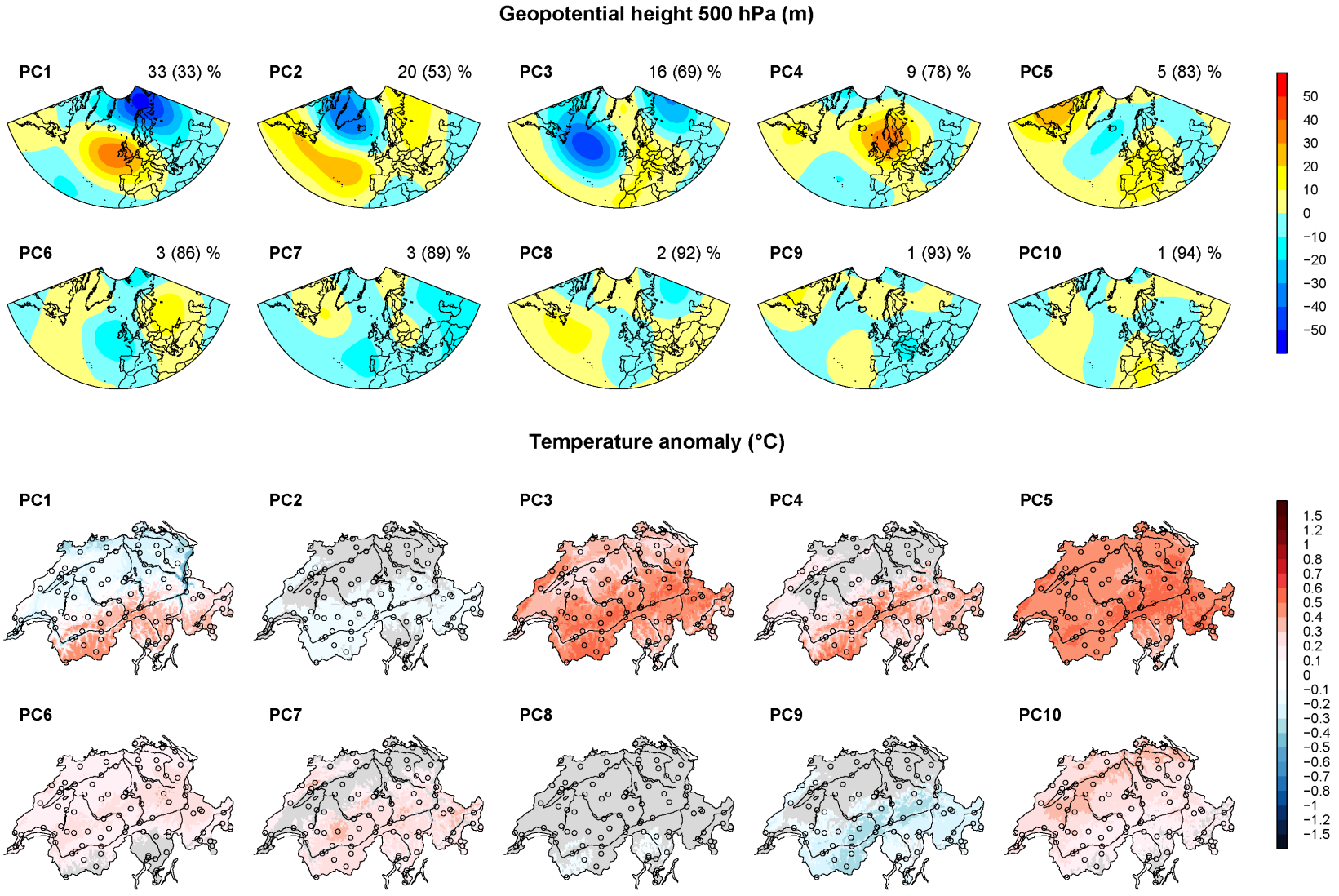

Figure B.9: As in Fig. B.1 for OND.

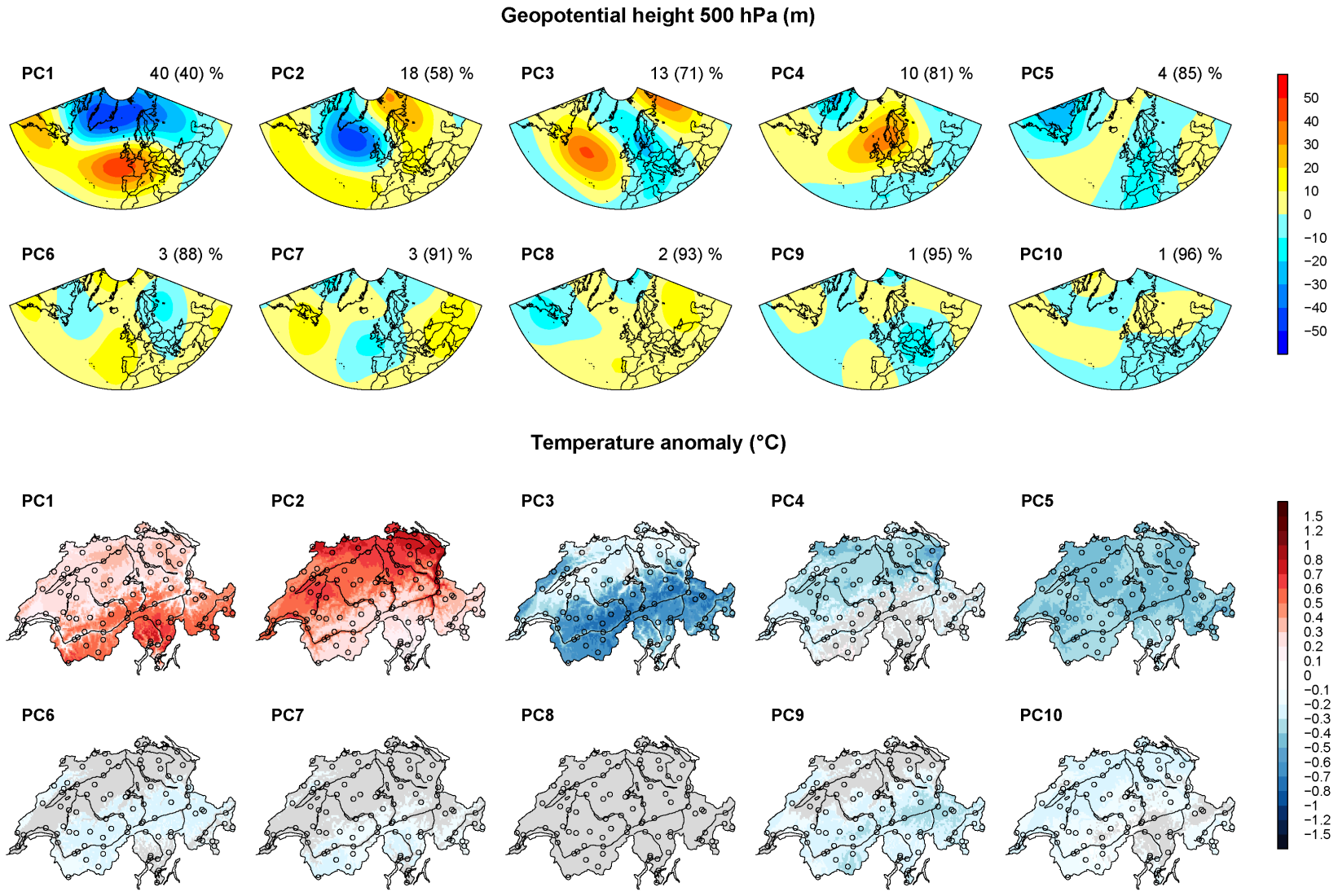

Figure B.10: As in Fig. B.1 for NDJ.

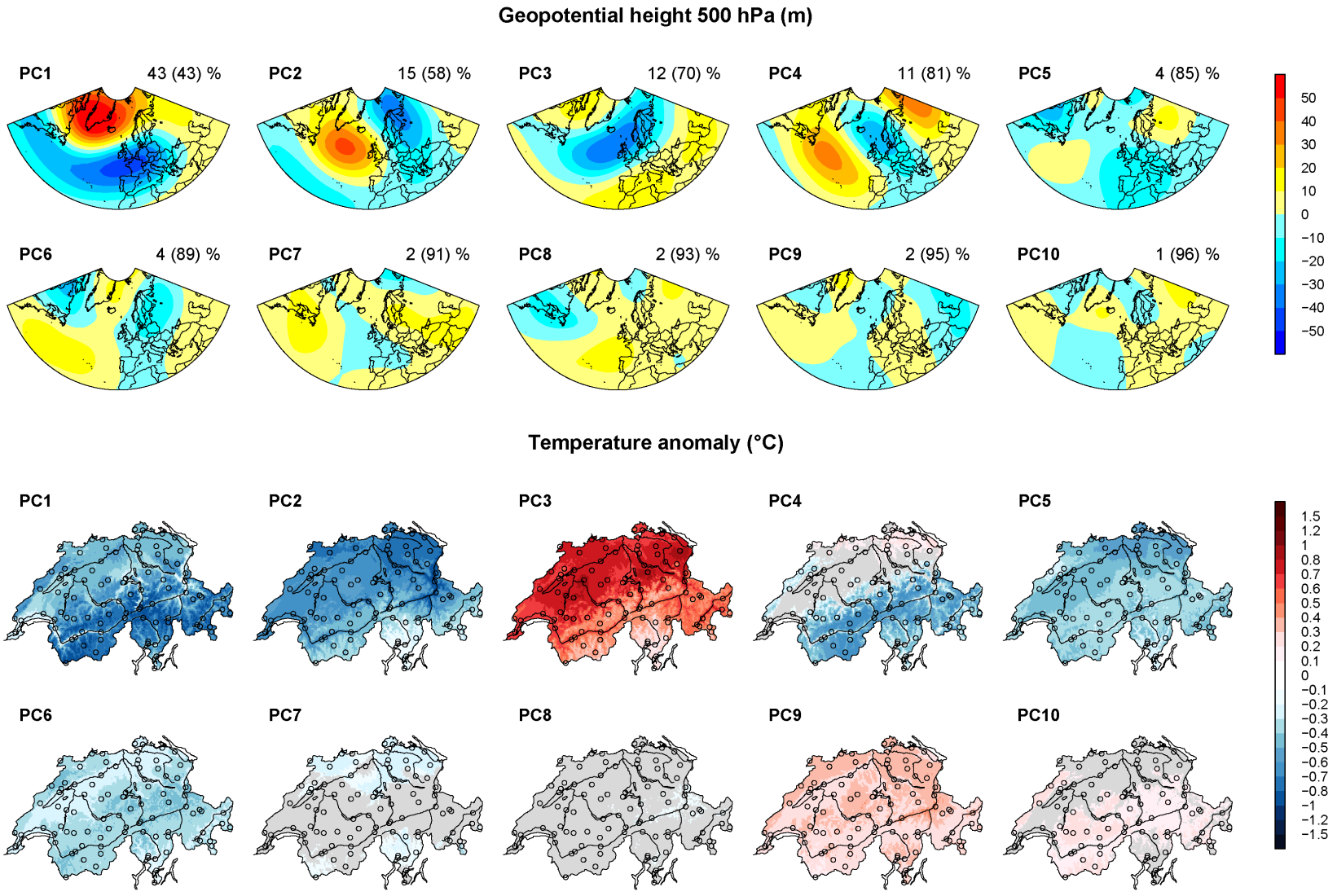

Figure B.11: As in Fig. B.1 for DJF.

Appendix C

Time series of 500 hPa geopotential height PC scores

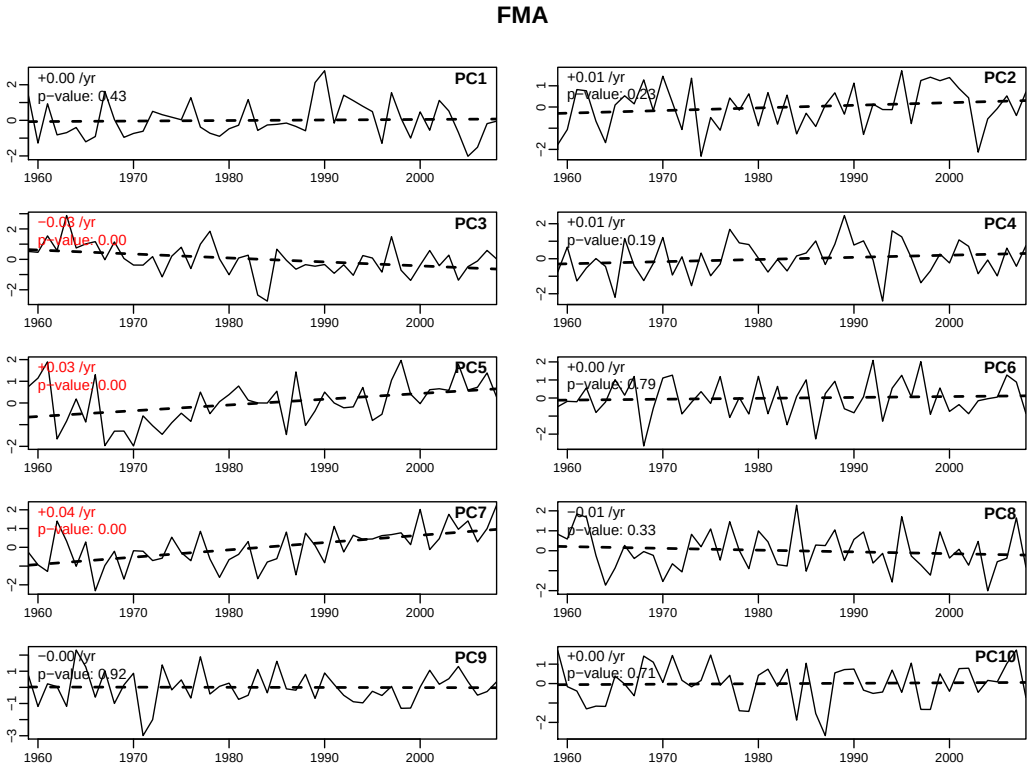

Figure C.1: Time series of the first 10 PCs of 500 hPa geopotential height fields over the North Atlantic and Europe. The dashed lines denote the estimated trends. Significant trends at the 5% level are marked in red. See also Fig. 5.4.

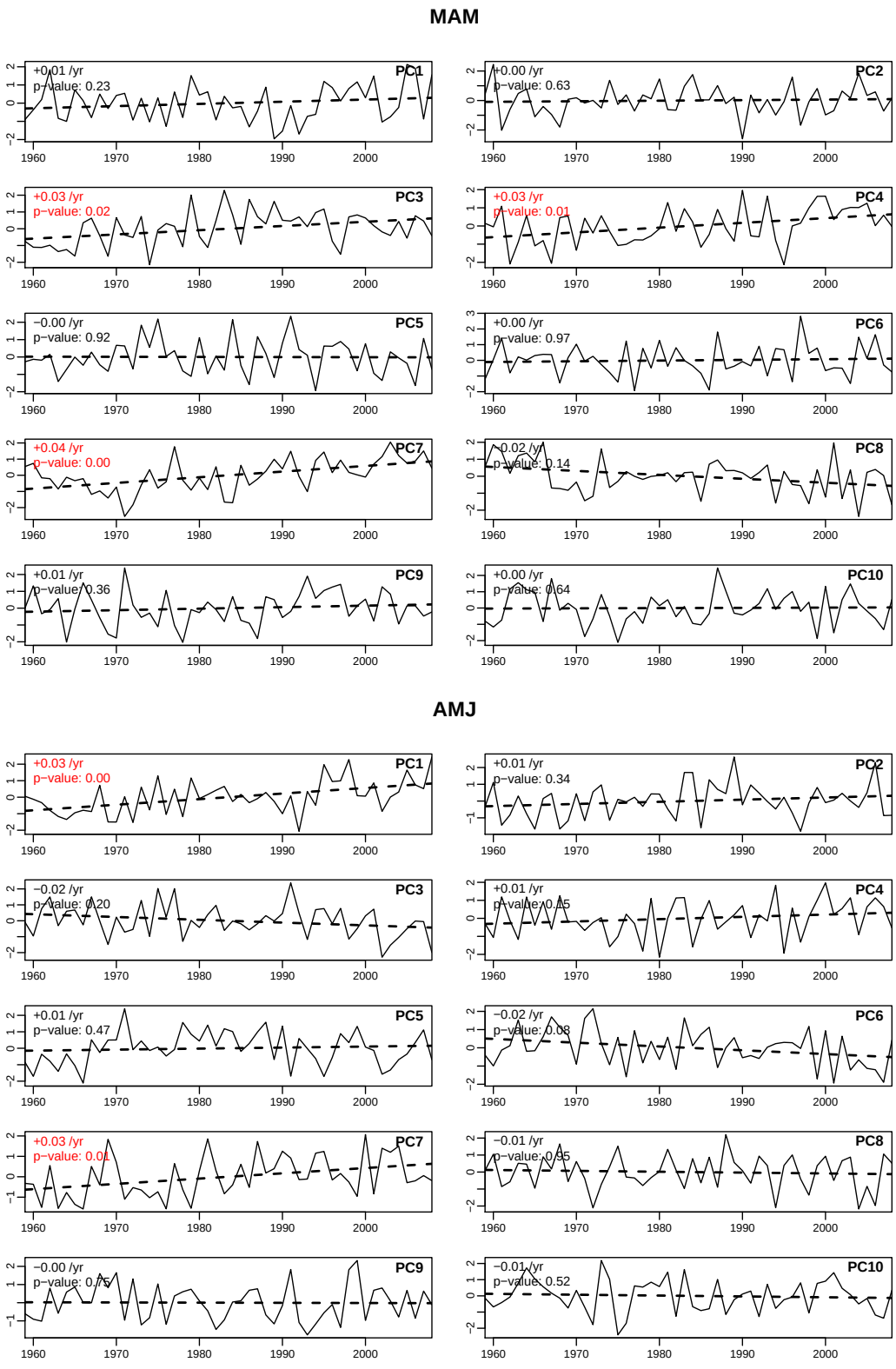

Figure C.2: As in Fig. C.1.

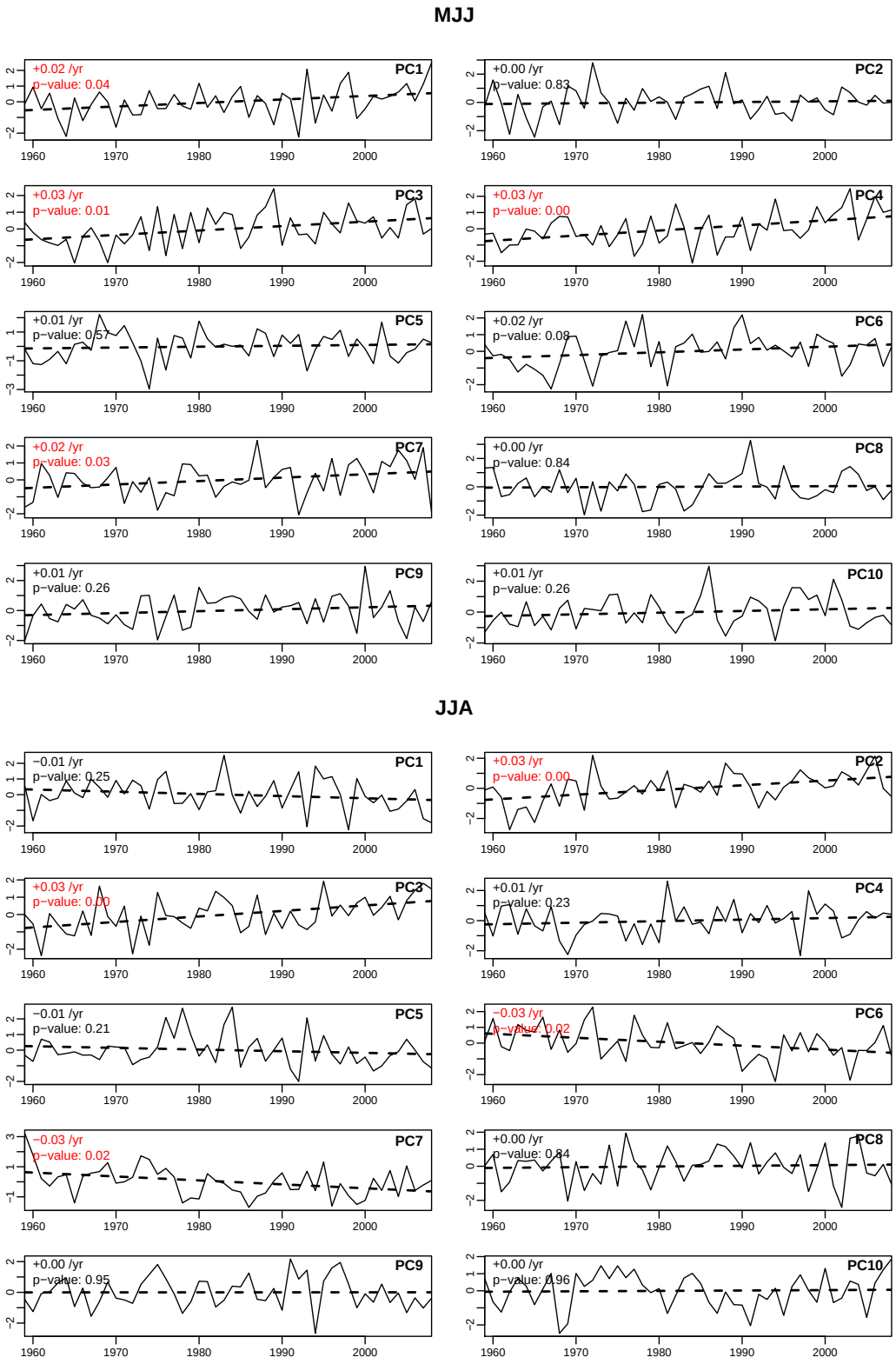

Figure C.3: As in Fig. C.1.

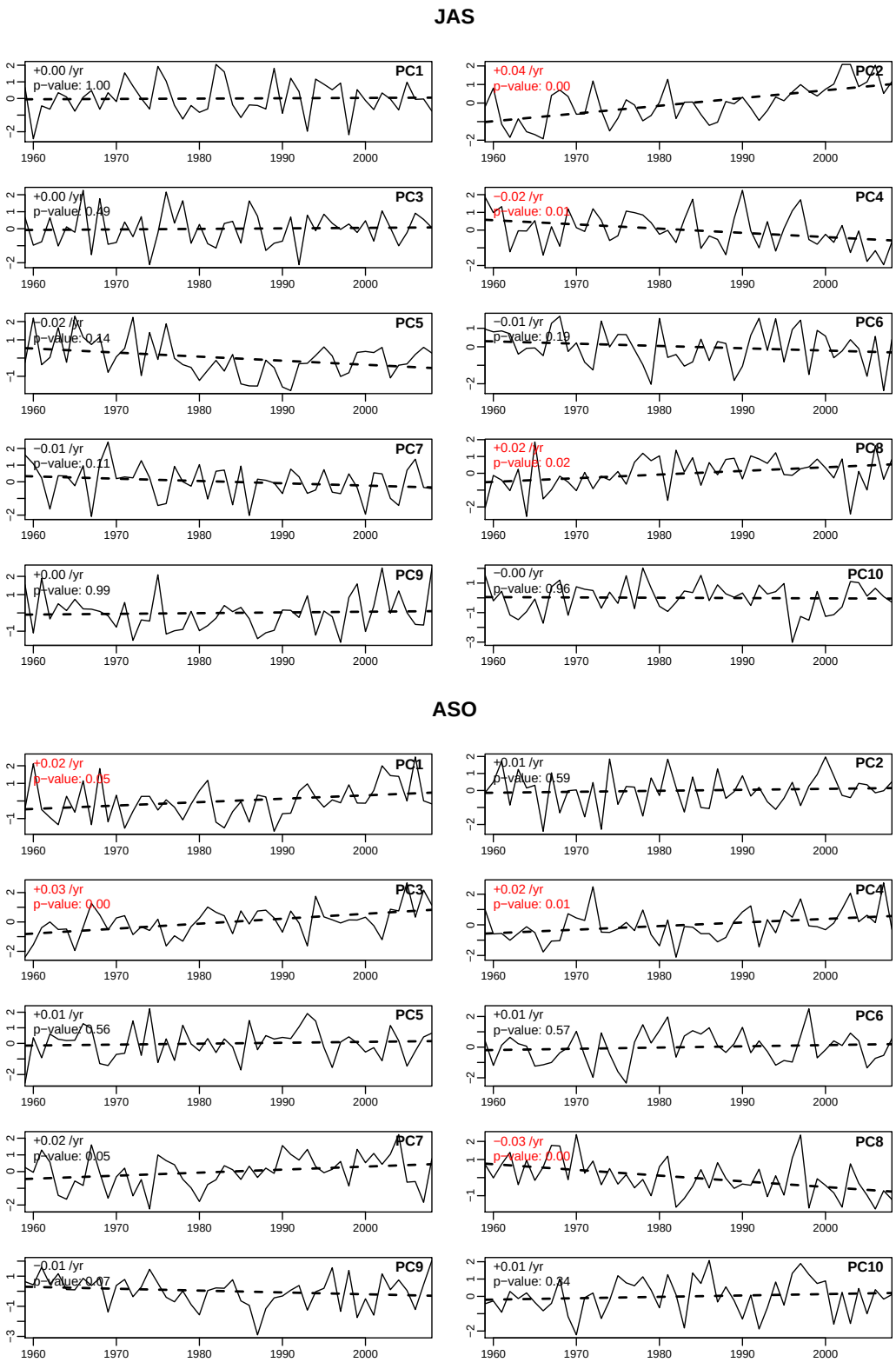

Figure C.4: As in Fig. C.1.

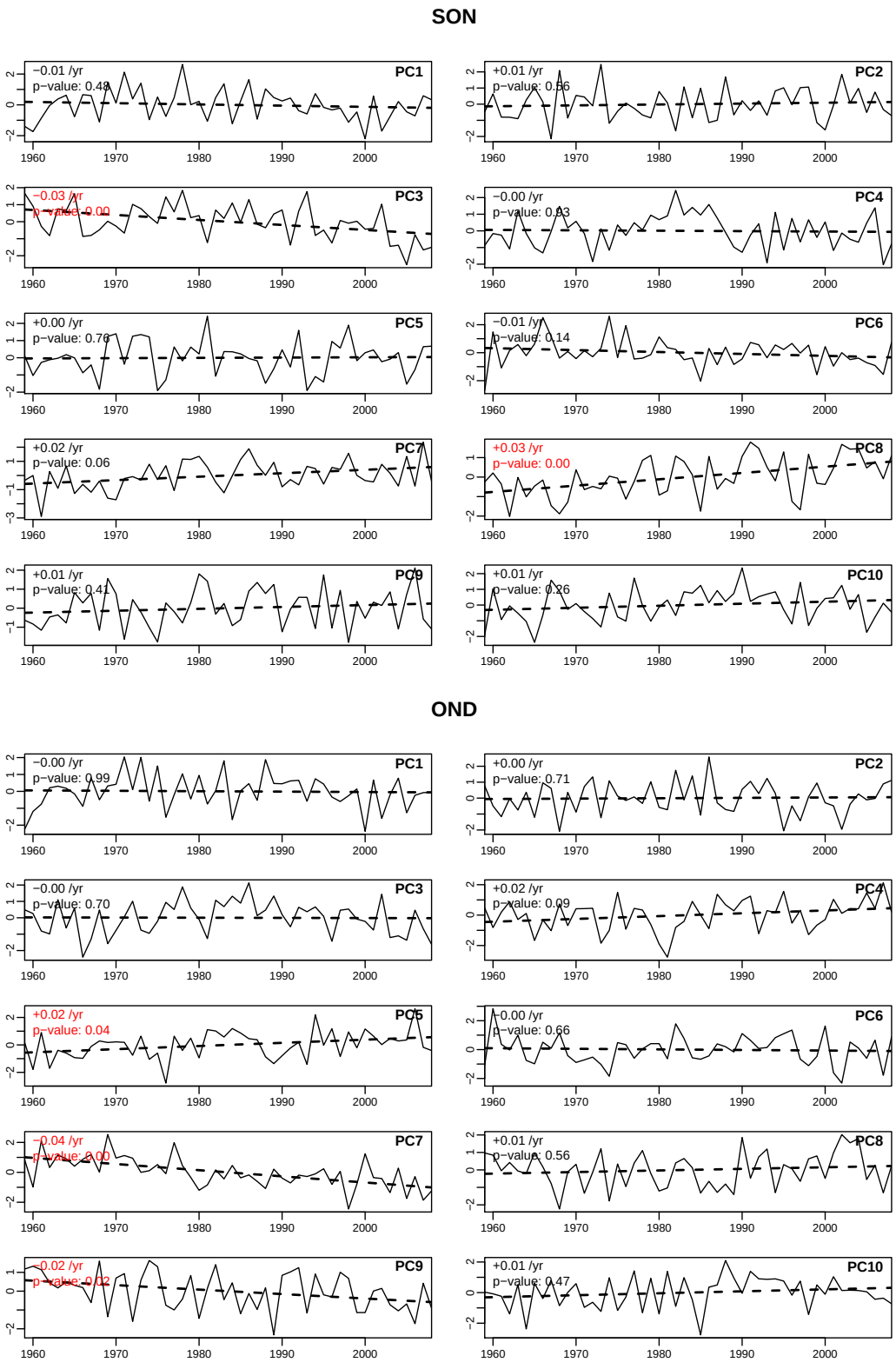

Figure C.5: As in Fig. C.1.

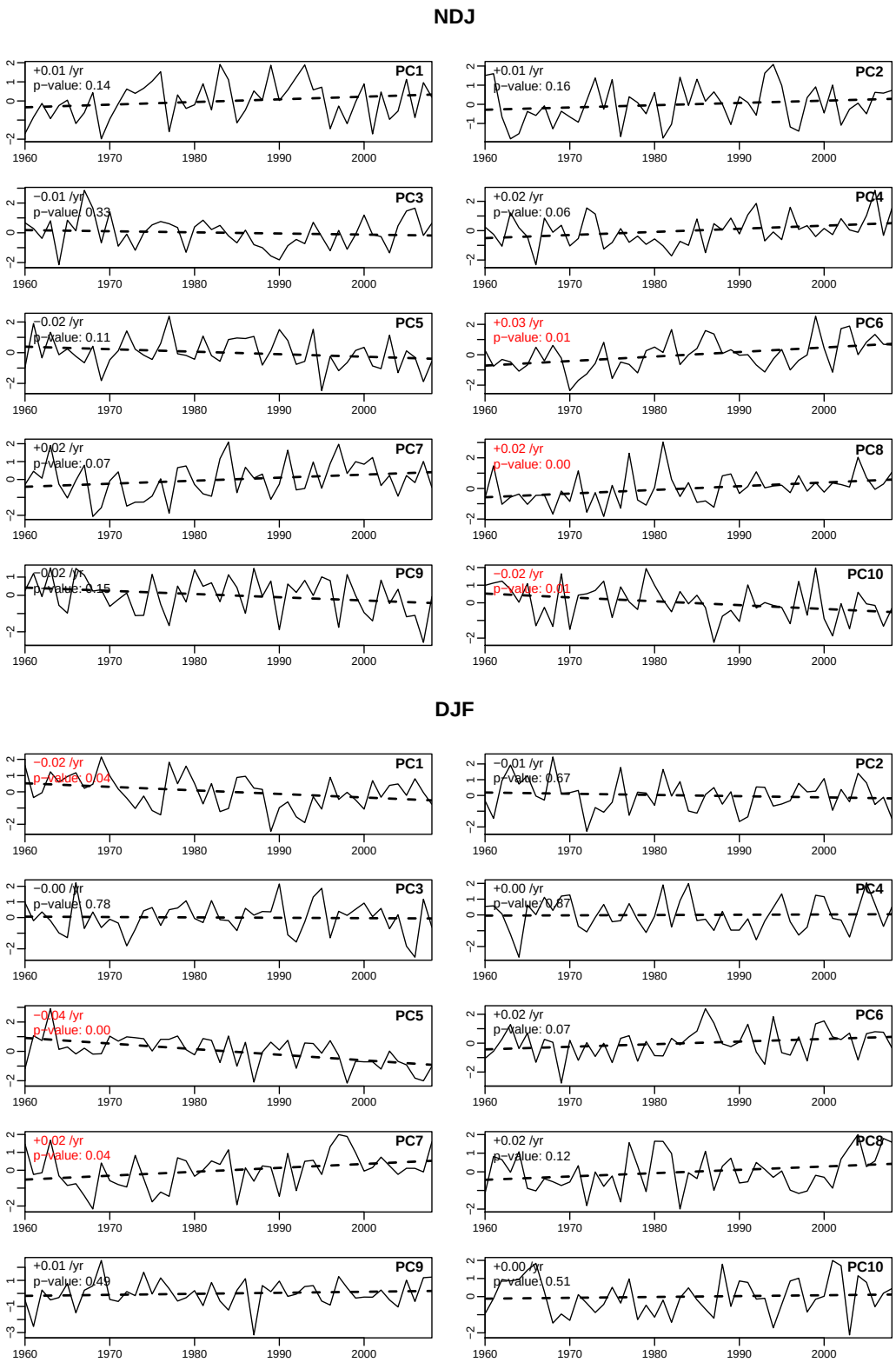

Figure C.6: As in Fig. C.1.